공학박사 학위논문

Therapeutic potential-enhanced mesenchymal stem cell-derived nanovesicles

치료 효능이 증가된 중간엽 줄기세포 유래 나노베지클

2020년 8월

서울대학교 공과대학

화학생물공학부

이 주 로

Therapeutic potential-enhanced mesenchymal stem cell-derived nanovesicles

지도 교수 김 병 수

이 논문을 공학박사 학위논문으로 제출함
2020년 08월

서울대학교 대학원
화학생물공학부
이 주 로

이주로의 공학박사 학위논문을 인준함
2020년 08월

위 원 장 _____ (인)

부위원장 _____ (인)

위 원 _____ (인)

위 원 _____ (인)

위 원 _____ (인)

Abstract

Therapeutic potential-enhanced mesenchymal stem cell-derived nanovesicles

Ju-Ro Lee

School of Chemical and Biological Engineering

The Graduate School

Seoul National University

Due to the safety issues and poor engraftment of mesenchymal stem cell (MSC) implantation, MSC-derived exosomes have been spotlighted as an alternative therapy for wide variety of diseases including myocardial infarction (MI) and spinal cord injury (SCI). Despite of the advantages of exosomes over MSC therapies, there are several limitations for clinical application due to the very small productivity and poor targeting ability to diseased organs after administration. To overcome these obstacles, exosome-mimetic extracellular nanovesicles (NVs) have been

developed as an alternative to conventional exosomes. However, NVs also poorly accumulate in target organs without modification. Here, we developed therapeutic potential-enhanced NVs derived from MSCs that were engineered to possess increased therapeutic and targeting molecules.

First, we developed NVs derived from iron oxide nanoparticles (IONPs)-incorporated MSCs (IONP-MSCs). The retention of injected IONP-MSC-derived NVs (IONP-NVs) within the infarcted heart was dramatically augmented by magnetic guidance. Furthermore, IONPs significantly increased the levels of therapeutic RNAs and proteins in IONP-MSCs as well as IONP-NVs, which can reduce the concern of low exosome-productivity. The injection of IONP-NVs into the infarcted heart and magnetic guidance induced an early shift from the inflammation phase to the reparative phase, reduced apoptosis and fibrosis, and enhanced angiogenesis and cardiac function recovery. This approach can enhance the therapeutic potency of an MSC-derived NV therapy and may pave the way for the clinical application of MI.

Second, we fabricated macrophage membrane-fused-exosome-mimetic nanovesicles (MF-NVs) from macrophage membraned-fused MSCs (MF-MSCs) and confirmed their therapeutic potential in a clinically relevant mouse SCI model (controlled mechanical compression injury model). MF-NVs contained larger quantity of ischemic region-targeting molecules compared to normal MSC-derived nanovesicles. The targeting molecules in MF-NVs, which were derived from macrophage membranes, increased the accumulation of MF-NVs in the injured spinal cord after the *in vivo* systemic injection. Increased accumulation of MF-NVs attenuated apoptosis and inflammation, prevented axonal loss, enhanced blood vessel formation, decreased fibrosis, and consequently improved spinal cord

function. These results present their possibility of clinical application for SCI.

Together, we showed that NVs derived from IONP-MSCs or MF-MSCs contain greater therapeutic molecules or targeting molecules that can facilitate enhanced accumulation in infarcted myocardium or injured spinal cord. Our novel approach to augment therapeutic efficacy of NVs derived from modified MSCs can be a good replacement of conventional MSC or MSC-derived exosome therapies. Our technology can be applied the clinical applications in the future as therapies for acute ischemic/inflammatory diseases.

Keywords: exosome-mimetic extracellular nanovesicles, iron oxide nanoparticles, macrophages, mesenchymal stem cells, myocardial infarction, spinal cord injury

***Student Number*: 2014-21524**

Table of contents

Abstract i

Table of contents iv

List of figures ix

Abbreviations xi

Chapter 1. Research backgrounds and objective 1

1.1. Conventional MSc-based therapies and limitations 3

1.2. Extracellular vesicles: potential therapeutic agent 4

1.2.1 Extracellular vesicles 4

1.2.2. Extracellular vesicles as an alternative to cell-based therapies 6

1.3. Exosome-mimetic extracellular nanovesicles 9

1.4. Modification of extracellular vesicles 11

1.5. Research objective of thesis 12

Chapter 2. Experimental methods 14

2.1. Fabrication and characterization of NVs 15

2.1.1. Preparation of IONP 15

2.1.2. Cell culture 16

2.1.3. Isolation of macrophage membranes and fabrication of MF-MSCs ... 17

2.1.4. Characterization of IONP-MSCs and MF-MSCs 18

2.1.5. Preparation of NVs 19

2.1.6. Characterization of NVs 20

2.2. *In vitro* assays 21

2.2.1. Quantitative PCR and analysis of RNA 21

2.2.2. Evaluation of cellular viability 21

2.2.3. Western blot analysis 22

2.2.4. Flow cytometry 23

2.2.5. Immunocytochemistry 23

2.2.6. *In vitro* cell assay in hypoxic conditions and macrophage polarization by the NV treatment 24

2.2.7. Capillary tube formation 24

2.2.8. Cell migration assay 25

2.2.9. *In vitro* NV binding assay 25

2.3. *In vivo* assays 26

2.3.1. MI model and treatment 26

2.3.2. SCI model and treatment 27

2.3.3. *Ex vivo* biodistribution of NVs 27

2.3.4. MRI 28

2.3.5. Immunohistological assessment *in vivo* 29

2.3.6. Apoptosis assessment *in vivo* 30

2.3.7. Capillary density determination in heart 30

2.3.8. Determination of fibrosis in heart 31

2.3.9. Evaluation of cardiac functions 31

2.3.10. Behavior evaluation 32

2.4. Statistical analysis 32

Chapter 3. Nanovesicles derived from iron oxide nanoparticles-incorporated mesenchymal stem cells for cardiac repair 33

3.1. Introduction 34

3.2. Results and discussion 38

3.2.1. IONPs internalization into MSCs 38

3.2.2. Cellular modification of MSCs by IONPs 40

3.2.3. Production of IONP-NVs from IONP-MSCs 42

3.2.4. Characterization of IONP-NVs 45

3.2.5. Cellular uptake of IONP-NVs *in vitro* 49

3.2.6. Cardioprotective effects of IONP-NVs *in vitro* 52

3.2.7. Antifibrotic effects of IONP-NVs *in vitro* 58

3.2.8. Anti-inflammatory effects of IONP-NVs *in vitro* 60

3.2.9. Proangiogenic effects of IONP-NVs *in vitro* 62

3.2.10. Increased retention of IONPs by magnetic guidance in the infarcted myocardium 65

3.2.11. Cytotoxicity of IONP-NVs with magnetic guidance *in vivo* 68

3.2.12. Attenuation of cell apoptosis and inflammation IONP-NVs with magnetic guidance *in vivo* 72

3.2.13. Increased blood vessel density and improved left ventricular remodeling by IONP-NVs with magnetic guidance *in vivo* 76

3.2.14. Enhanced cardiac function recovery by IONP-NVs with magnetic guidance *in vivo* 79

Chapter 4. Targeted delivery of mesenchymal stem cell-derived nanovesicles for spinal cord injury treatment 82

4.1. Introduction 83

4.2. Results and discussion 87

4.2.1. Production and characterization of MF-MSCs..... 87

4.2.2. Production and characterization of MF-NVs 89

4.2.3. Neuroprotective effects of MF-NVs *in vitro* 92

4.2.4. Anti-inflammatory effects of MF-NVs *in vitro* 94

4.2.5. Proangiogenic effects of MF-NVs *in vitro* 96

4.2.6. Enhanced targeting efficiency of MF-NVs *in vitro* and *in vivo* 98

4.2.7. Reduced glial scar formation and improved function recovery by MF-NVs *in vivo* 100

4.2.8. Enhanced neuroprotection, anti-inflammation, and pro-angiogenesis by MF-NVs *in vivo* 104

Chapter 5. Conclusions 109

References 112

요약 (국문초록) 134

List of figures

Figure 1.1. Biogenesis of extracellular vesicles and their interactions with recipient cells 5

Figure 1.2. Potential clinical applications of EVs 8

Figure. 1.3. Schematic illustration of NV production 10

Figure 3.1. Schematic diagrams for the preparation and intramyocardial injection of IONP-NVs for cardiac repair 37

Figure 3.2. IONPs internalization into MSCs 39

Figure 3.3. Cellular modification of MSCs by IONPs 41

Figure 3.4. Production of IONP-NVs from IONP-MSCs 43

Figure 3.5. Characterization of IONP-NVs 46

Figure 3.6. Cellular uptake of IONP-NVs in vitro 49

Figure 3.7. Cardioprotective effects of IONP-NVs *in vitro* 53

Figure 3.8. Antifibrotic effects of IONP-NVs *in vitro* 59

Figure 3.9. Anti-inflammatory effects of IONP-NVs *in vitro* 61

Figure 3.10. Proangiogenic effects of IONP-NVs *in vitro* 63

Figure 3.11. Increased retention of IONPs by magnetic guidance in the infarcted myocardium 66

Figure 3.12. Cytotoxicity of IONP-NVs with magnetic guidance *in vivo* 69

Figure 3.13. Attenuation of cell apoptosis and inflammation IONP-NVs with magnetic

guidance *in vivo* 73

Figure 3.14. Increased blood vessel density and improved left ventricular remodeling by IONP-NVs with magnetic guidance *in vivo* 77

Figure 3.15. Enhanced cardiac function recovery by IONP-NVs with magnetic guidance *in vivo* 80

Figure 4.1. Schematic diagrams for the fabrication and therapeutic effects of MF-NVs for spinal cord repair 86

Figure 4.2. Production and characterization of MF-MSCs 88

Figure 4.3. Production and characterization of MF-NVs 90

Figure 4.4. Neuroprotective effects of MF-NVs *in vitro* 93

Figure 4.5. Anti-inflammatory effects of MF-NVs *in vitro* 95

Figure 4.6. Proangiogenic effects of MF-NVs *in vitro* 97

Figure 4.7. Enhanced targeting efficiency of MF-NVs in vitro and *in vivo* 99

Figure 4.8. Reduced glial scar formation and improved function recovery by MF-NVs *in vivo* 102

Figure 4.9. Enhanced neuroprotection, anti-inflammation, and proangiogenesis by MF-NVs *in vivo* 106

Abbreviations

AKT	serine/threonine-specific protein kinase
ANOVA	analysis of variance
ANG1	angiopoietin 1
Arg1	arginase 1
BMS	basso mouse scale
BCL-2	B-cell CLL/lymphoma 2
CF	cardiac fibroblast
CM	cardiomyocyte
cTnT	cardiac troponin T
CCK	cell counting kit
Cx43	connexin43
CSPG	chondroitin sulfate proteoglycans
cDNA	complementary DNA
DAPI	4,6-diamidino-2-phenylindole
DLS	dynamic light scattering
EB	ethidium bromide
ECM	extracellular matrix
EDS	energy-dispersive X-ray spectroscopy

ERK1/2	extracellular signal-regulated kinases 1/2
FBS	fetal bovine serum
FDA	fluorescein diacetate
FGF2	fibroblast growth factor 2
GFAP	glial fibrillary acidic protein
HGF	hepatocyte growth factor
HIF1α	hypoxia inducible factor 1 alpha
HUVEC	human umbilical vein endothelial cell
ICP-MS	inductively coupled plasma mass spectrometry
IL	interleukin
IHC	immunohistochemistry
JNK	c-Jun N-terminal kinases
LPS	lipopolysaccharide
MI	myocardial infarction
MRI	magnetic resonance imaging
MSC	mesenchymal stem cell
NF	neurofilament
NOS2	nitric oxide synthase 2
NV	exosome-mimetic nanovesicle

pAKT	phosphorylated serine/threonine-specific protein kinase
PBS	phosphate buffer saline
PCNA	proliferating cell nuclear antigen
PEG	polyethylene glycol
pERK1/2	phosphorylated extracellular signal-regulated kinases 1/2
PFA	paraformaldehyde
PI3K	phosphatidylinositol 3-kinases
pJNK	phosphorylated c-Jun N-terminal kinases
qRT-PCR	quantitative real-time polymerase chain reaction
TEM	transmission electron microscopy
TNFα	tumor necrosis factor alpha
TUNEL	terminal deoxynucleotidyl transferase dUTP nick end labeling
UCB	umbilical cord blood
VEGF	vascular endothelial growth factor
VLA4	very late antigen 4
vWF	von Willebrand factor
STEM	scanning transmission electron microscopy
SCI	spinal cord injury

Chapter 1.

Research backgrounds and objective

1.1. Conventional MSC-based therapies and limitations

Mesenchymal stem cell (MSC)-based therapies for the treatment of various diseases have attracted attention and been considered promising therapies for clinical uses for decades. Due to its therapeutic potential and intrinsic properties, numerous clinical trials[1] that used autologous or allogeneic MSC transplantation including osteoarthritis[2], cardiovascular diseases[3], and spinal cord injury (SCI)[4], are still ongoing. Early studies suggested that transplanted MSCs engraft in damaged tissues and differentiate to specific cell lineages and then subsequently replace the cells in the lesion. However, recent studies have suggested that paracrine factors secreted from MSC play an important role in its therapeutic mechanism, not replacing damaged cells.[5] Despite of the low MSC engraftment in damaged tissue, the obvious therapeutic effects of MSCs strongly support that major therapeutic mechanisms of MSCs are attributed to the paracrine effects. Moreover, the heterogeneity, different origins, and culture procedures of MSCs make their therapeutic results frequently variable.

In spite of accomplished clinical outcomes of MSCs, there are several potential risks of the uses of MSC therapies, such as tumorigenesis, differentiation to other cell lineages, arrythmias, and neuronal damages. In addition, the route of MSC administration has been challenges for clinical applications. Although intravenous administration can be less invasive and easy to inject, there are many obstacles for systemically injected MSCs to elicit clinical outcomes.[6, 7] Moreover, systemically injected MSCs hardly reach the targeting lesion due to the pulmonary entrapment.[8] Systemic injection of MSCs Surgical procedure .

1.2. Extracellular vesicles: potential therapeutic agent

1.2.1. Extracellular vesicles

Extracellular vesicles (EVs) are composed of a lipid bilayer enveloping cytosolic proteins and RNAs, which are derived from various types of cells (Figure 1.1).[9] EVs are secreted from the cells through the budding from the plasma membrane. EVs have a wide range of size (50-1,000 nm in a diameter) and classified by their sizes. They are divided into two main categories, microvesicles and exosomes. Microvesicles are general kind of vesicles with size of 50-1,000 nm and generated outward budding from plasma membrane. Exsomes are specific kind of EVs with size smaller than 150 nm in a diameter and generated inward budding from multivesicular bodies. Both exosomes and microvesicles are involved in intercellular communications. They convey RNAs, proteins, and membranes from donor cells to neighboring cells or distant cells. Their cargos, RNAs and proteins, are active and participate in the regulation of intracellular signaling cascades in the recipient cells.[10, 11] Because RNAs and proteins in microvesicles and exosomes are derived from parent cells, their component are dependent on the characteristics of parent cells. Based on the unique properties of EVs, EVs are largely attributed to the paracrine effects of cell-based therapies. Furthermore, their biocompatibility, low immunogenicity, and relatively free administration route have gained great attention. Thus, EVs have been studied as an alternative to cell-based therapies, "cell-free therapy" for a wide variety of diseases including cancer, immune diseases, cardiovascular diseases, and central nerve system disorder.[12, 13]

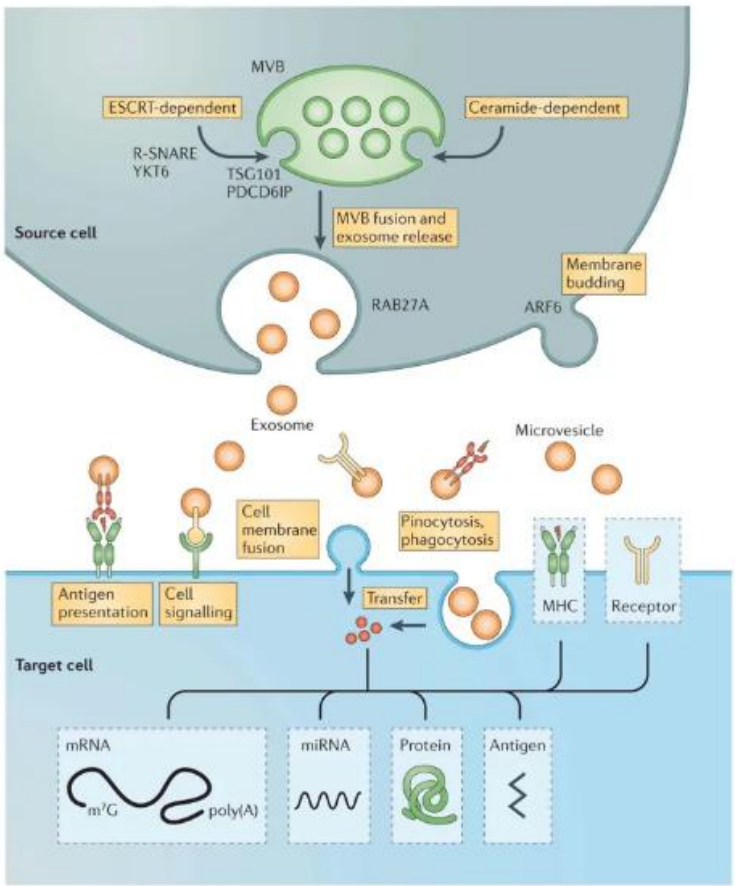

Figure 1.1. Biogenesis of extracellular vesicles and their interactions with recipient cells.[14]

1.2.2. Extracellular vesicles as an alternative to cell-based therapies

In particular, exosomes derived from MSCs are widely studied as a cell-free therapy for various types of diseases *in vitro* or *in vivo* (Figure 1.2). Previous studies reported that exosomes derived from pristine MSCs or GATA-4 overexpressing MSCs exhibited anti-apoptotic effects on cardiomyocyte *in vitro*.[15, 16] MSC-exosomes treatment stimulated Akt pathway in cardiomyocyte, which is involved in the survival under hypoxic and H2O2-induced reactive oxygen species (ROS) condition. MSc-exosomes also showed antifibrotic effects. Treatment of MSC-exosomes reversed epithelial-to-mesenchymal transition and spindle-shaped liver cell line *in vitro*, which indicates that MSC-exosomes can ameliorate the fibrosis. In addition, MSC-exosomes are known to possess immunomodulatory properties. They are involved in immunomodulation in various ways. MSC-exosomes can polarize macrophages inflammatory (M1) phenotype to reparative (M2) phenotype *in vitro*.[17] Also, MSC-exosomes enhanced the production of $CD4^+CD25^+Foxp3^+$ regulatory T cells *in vitro*, which can indirectly exert anti-inflammatory effects.[18] MSC-exosomes are also known to promote angiogenesis of endothelial cells. Tube-like structure formation, migration, and vascular maturation of human umbilical vein endothelial cells (HUVECs) were increased by the stimulation with MSC-exosomes *in vitro*.[19, 20] MSC-exosomes showed protective effects on neuronal cells via PI3K/Akt signaling pathway *in vitro*.[21]

Based on diverse therapeutic abilities of MSC-exosomes, recently, MSC-exosomes have been utilized to pre-clinical studies. MSC-exosomes were successfully attenuated liver fibrosis,[22] accelerated recovery of hindlimb ischemia,[23] and promoted skeletal muscle regeneration.[24] Also, MSC-exosomes

alleviated osteoarthritis[25] and inflammatory arthritis[26] by their immunomodulatory functions. In case of myocardial infarction (MI), MSC-exosomes have showed tremendous outcomes in pre-clinical models. MSC-exosomes suppressed cell death in infarcted myocardium via transferring miRNAs[27] and promoting autophagy[28]. MSC-exosomes also attenuated myocardial ischemia-reperfusion injury through miR-182-mediated regulation of macrophage polarization.[29] Intramyocardial injection of MSC-exosomes improved the microenvironment of infarcted myocardium by promoting angiogenesis.[30] Moreover, MSC-exosomes increased ATP levels and consequent activation of PI3K/Akt pathway, which resulted in prevention of cardiac remodeling.[31] For spinal cord injury (SCI), the intravenous injection of MSC-exosomes suppressed the activation of neurotoxic astrocytes, which led to attenuation of lesion size, promotion of axonal regeneration, and eventual functional behavioral recovery.[32] Also, in rat SCI model, administration of MSC-exosomes relieved spinal cord injury by attenuation of apoptosis, inflammation, and promotion of angiogenesis.[33] Taken together, MSC derived EVs, especially MSC-exosomes, can be future versatile therapies for treating ischemic and inflammatory disease including MI and SCI.

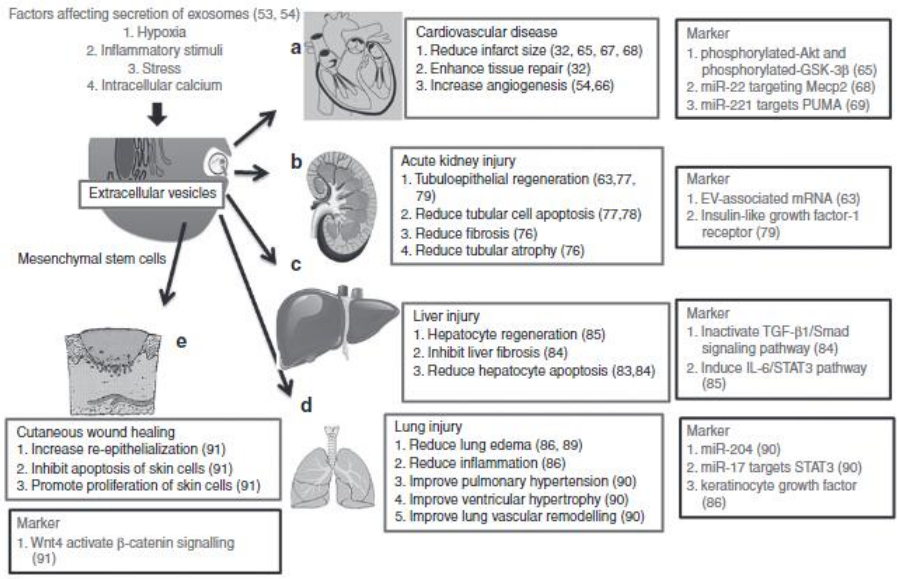

Figure 1.2. Potential clinical applications of EVs.[12]

1.3. Exosome-mimetic extracellular nanovesicles

Despite of MSC-exosomes have great therapeutic potential and the possibility of a replacement of MSC therapy for the treatment of various types of diseases, there are several limitations for their clinical uses. The productivity and the purification of exosomes from MSCs is not feasible for clinical applications due to their low quantities of release and cost-effectiveness. Especially for MSCs, 10^6 MSCs secrete exosomes only 1 to 4 μg per day[34], indicating that it is necessary to prepare large scale of cell culture system for pre-clinical or clinical trials. Because of this need for clinical uses, previous studies suggested exosome-mimetic extracellular nanovesicles (NVs) as a therapeutic replacement of exosomes.[35, 36] They contain cell-derived biomolecules including RNAs and proteins and also can convey the molecules to recipient cells, which is similar to the characteristics of exosomes. NVs are obtained using series of physical extrusion through micro- and nano-sized filter pore (Figure 1.3). Once the cells are subjected to pass the pore, they are split to tiny lipid fragments, and then fragments are immediately assembled to form sphere-shaped particles enclosed by lipid bilayer. Different from exosomes, there is no need to maintain continuous culture system to collect conditioned medium for the fabrication of NVs, which results in significantly higher production yield (up to 250-fold higher). In addition, the quantities of intrinsic biomolecules including RNAs and proteins are higher in NVs compared to exosomes[35], which would be great advantages of NVs for therapeutic potency over exosomes. Therefore, recently, the applications of NVs for various diseases have been gradually increased, including diabetes[36] and liver injury[37].

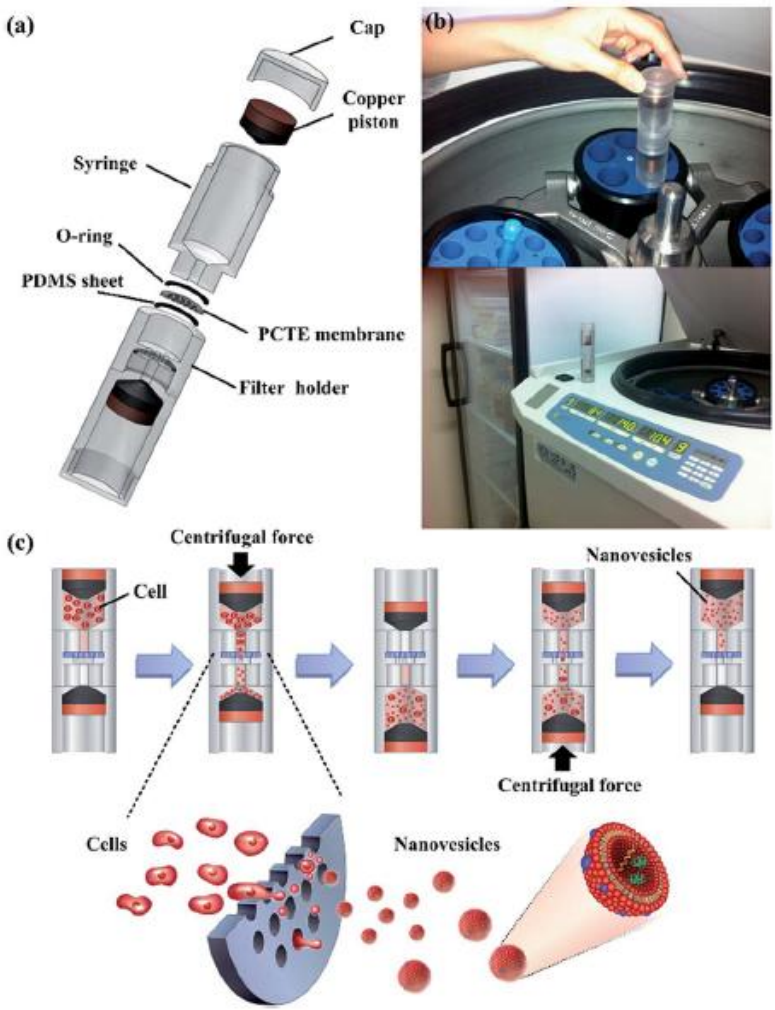

Figure. 1.3. (a) Sectional view of the device. (b) Photograph of the device in operation. (c) Schematic process of nanovesicle generation. After cells were loaded into the syringe, centrifugal force was applied to extrude them. During extrusion, the polycarbonate filter imposes surface tension and generates nanovesicles when they pass through the filter pores.[35]

1.4. Modification of extracellular vesicles

In spite of the advantages of exosomes and NVs over cell-based therapy, the delivery and retention of vesicles to target organs are still remain impediment for their uses. Without modification, they exhibited poor accumulation in target organs when systemically injected.[38, 39] In addition, for MI or SCI treatment, injected exosomes or NVs cannot retained and washed out from infarcted myocardium or spinal cord due to the dynamic microenvironment with fast body fluid. To increase the targeting ability of exosomes, there have been diverse studies to modify the surface of exosomes. To target liver, MSC-exosomes were conjugated with cationized pullulan, which elicited high accumulation in liver.[40] Surface modification of exosomes with antibody facilitated the targeted delivery of exosomes to colorectal cancer site.[41] Binding superparamagnetic nanoparticles with exosomes by conjugation and the application of external magnet dragged them to cancer.[42] Those methods to augment targeting efficiency of exosomes are conducted under chemical reactions that include harsh conditions such as high temperature, pH changes, which would affect the efficacy of exosomes. Thus, biocompatible methods to modify MSC-exosomes or NVs should be developed.

1.5. Research objective of thesis

The research objective in this thesis is the enhancement of the therapeutic efficacy of NVs derived from MSCs for extracellular vesicle therapy to treat acute ischemic/inflammatory diseases, such as myocardial infarction or spinal cord injury. In this thesis, we suggest the therapeutic applications of NVs from therapeutic potential-enhanced MSCs by introducing IONP or macrophage membrane.

Firstly, the chapter 3 reports the therapeutic potential enhanced-NVs using IONPs. Applications of EVs for MI treatment have been studied however, diffusing out of infarcted heart limits the therapeutic potential of EVs. No study has applied IONPs to enhance retention and therapeutic potential of EVs for MI treatment. We developed IONP-incorporated MSC-NVs (IONP-NVs) for MI treatment. The internalization of IONPs not only upregulates therapeutic molecules in IONP-NVs but also facilitates high retention of IONP-NVs in the infarcted heart by external magnetic guidance. The quantities of mRNA and proteins that can contribute to protect cardiac cells, prevent cardiac fibrosis, polarize macrophages pro-inflammatory subtype to anti-inflammatory subtype, and promote vascularization, were increased through iron ion-mediated intracellular ROS signaling cascades in IONP-MSCs. IONP-NVs from IONP-MSCs also contained these therapeutic molecules. In addition, IONPs inside IONP-NVs could be dragged by external magnetic guidance, which facilitated high retention of IONP-NVs in infarcted heart that has dynamic microenvironment. *In vitro*, IONP-NVs showed significantly enhanced antiapoptotic, antifibrotic, anti-inflammatory, and proangiogenic effects on the cells in cardiac microenvironment. *In vivo*, indeed, the injection of IONP-NVs and subsequent magnetic guidance markedly attenuated cell death, fibrosis, and inflammation, and promoted angiogenesis, which ultimately resulted in cardiac

function recovery.

Secondly, the chapter 4 reports the therapeutic potential enhanced-NVs using the macrophage membranes. Low accumulation of systemically administered EVs at diseased organs have been hindered the therapeutic applications. Moreover, modification of EVs with chemicals or nanoparticles can also limit their uses for clinical trials. No study has applied macrophage membranes to improve the targeting efficiency of EVs. We developed macrophage membrane-fused MSC (MF-MSC)-derived NVs (MF-NVs) for SCI treatment. The molecules included in macrophage membrane can bind with inflammatory endothelium. We isolated macrophage membrane and fabricated macrophage membrane-fused MSCs by fusion using PEG. MF-NVs from MF-MSCs also contained the targeting molecules derived from macrophage in their membrane. *In vitro*, MF-NVs exhibited neuroprotective, anti-inflammatory, proangiogenic effects on neuronal cells, macrophages, and endothelial cells. *In vivo*, intravenously injected MF-NVs accumulated in the injured spinal cord. The increased accumulation of MF-NVs in the injured spinal cord prevented of axonal loss, enhanced blood vessel formation, and reduced fibrosis, which consequently resulted in spinal cord function recovery. Ultimately, our approach to enhance targeting efficiency present the possibility of the clinical applications of NVs by using autologous cells from patients.

Chapter 2.

Experimental methods

2.1. Fabrication and characterization of NVs

2.1.1. Preparation of IONPs

IONPs were synthesized by a previously reported method.[43] Two mmol of iron (III) acetylacetonate, 4 mmol of oleic acid, 0.4 g of 4-biphenylcarboxylic acid, and 10 mL of benzyl ether were mixed in a three-neck round-bottomed flask. After degassing, the mixture solution was heated to 290 °C at a heating rate of 20 °C/min with vigorous stirring and aged for 30 minutes. The resulting product was cooled down to room temperature and washed with ethanol for several times. As-synthesized IONPs were dispersed in chloroform to be transferred to water. Three mL of oleic acid-capped IONPs in chloroform (10 mg/mL) was mixed with 60 mg of 1,2-distearoyl-sn-glycero-3-phosphoethanolamine-N-[methoxy(polyethylene glycol)-2000] (DSPE-PEG2000, Avanti Polar Lipids, Inc, Birmingham, AL, USA). The resulting mixture was vigorously sonicated for 5 minutes, and the solvent was evaporated using a rotary evaporator and vacuum oven. After 3 hours, distilled water was added and the mixture was vigorously sonicated to disperse the nanoparticles. The final product was obtained after washing with distilled water and ultracentrifugation several times. To synthesize rhodamine B isothiocyanate (RITC)-labeled IONPs, IONPs were transferred to water with a mixture of amine-functionalized DSPE-PEG2000 and DSPE-PEG2000 (1:10). RITC dissolved in dimethyl formamide was added to the amine-functionalized FIONs. The mixture was shaken for 3 hours, and excessive RITC was removed using PD-10 column chromatography (GE Healthcare, Little Chalfont, UK). The final product was dissolved in distilled water. The concentration and the shape of IONPs were evaluated using Inductively coupled plasma mass spectrometry (ICP-MS) (NexION 350D, PerkinElmer, Waltham, MA, USA), installed at the National

Center for Inter-university Research Facilities (NCIRF) at Seoul National University and transmission electron microscopy (TEM) (JEM-1010, JEOL Ltd., Tokyo, Japan), respectively.

2.1.2. Cell culture

Human bone marrow MSCs were purchased from Lonza (Walkersville, MD, USA) and human umbilical cord blood (UCB)-MSCs were purchased (CEFO, Seoul, South Korea) and cultured according to manufacturer's instructions. Bone marrow MSCs were cultured in Dulbecco's modified Eagle's medium high glucose (Gibco BRL, Gaithersburg, MD, USA) supplemented with 10 % (v/v) fetal bovine serum (Gibco BRL) and 1 % (v/v) penicillin/streptomycin (Gibco BRL). UCB-MSCs were cultured in Dulbecco's modified Eagle's medium low glucose (Gibco BRL) supplemented with 10 % (v/v) fetal bovine serum (FBS) (Gibco BRL) and 1 % (v/v) penicillin/streptomycin (Gibco BRL). MSCs at passage under six were used for the experiments. For osteogenic differentiation of MSCs, we used an osteogenic induction medium containing Dulbecco's modified Eagle's medium high glucose with 10 % (v/v) fetal bovine serum, 1 % (v/v) penicillin/streptomycin, 100 nM dexamethasone (Sigma), 50 mg/L ascorbate-2-phosphate (Sigma), and 10 mM beta-glycerol phosphate (Sigma). For adipogenic differentiation of MSCs, we used an adipogenic induction medium containing Dulbecco's modified Eagle's medium high glucose with 10 % (v/v) fetal bovine serum, 1 % (v/v) penicillin/streptomycin, 500 μM 1-methyl-3-isobutylxanthine (Sigma), 1 μM dexamethasone, 200 μM indomethacin (Sigma), and 10 μg/mL insulin (Gibco BRL). For chondrogenic differentiation of MSCs, we used a chondrogenic induction medium containing Dulbecco's modified Eagle's medium high glucose with 1 % (v/v)

penicillin/streptomycin and 10 ng/mL transforming growth factor β3 after forming pellets. For the preparation of IONP-MSC, IONPs were added to a MSC culture at a concentration of 40 μg/mL. One day after the IONP treatment, IONP-treated MSCs were washed with phosphate buffer saline (PBS, Gibco BRL) three times for the thorough removal of IONPs retained in the culture medium. The cells were cultured for 24 hours in fresh medium, and then analyzed or collected to produce NVs or for the use *in vitro* and *in vivo* experiments. Rat cardiomyocytes (CMs) were purchased from Lonza and cultured in Rat Cardiac Growth Medium (Lonza) on fibronectin-coated culture plates. Rat cardiac fibroblasts (CFs) were purchased from ScienCell (San Diego, CA, USA) and cultured in Fibroblast Medium-2 (ScienCell) on poly-L-lysine-coated culture plates. HUVEC were purchased from Lonza and cultured in Endothelial Cell Growth Media-2 (Lonza) on tissue culture plates. HUVECs at a passage under seven were used for the experiments. RAW 264.7 cell line was purchased from Korean Cell Line Bank (Seoul, South Korea) and cultured in Dulbecco's modified Eagle medium high glucose supplemented with 10 % (v/v) fetal bovine serum (Gibco BRL) and 1 % (v/v) penicillin/streptomycin on tissue culture plates.

2.1.3. Isolation of macrophage membranes and fabrication of MF-MSCs

The plasma membrane of RAW 264.7 cell line was isolated as previously described.[44] Briefly, RAW 264.7 cell line was suspended in a hypotonic buffer, followed by sonication for 5 min and then centrifuged at 10,000 g for 20 min. The pellet was discarded and the supernatant was extruded through 400 nm polycarbonate membrane filter. Then the sample was centrifuged at 25,000 g for 30 min. Approximately, 1×10^9 membrane particles were produced from 1×10^7 cells.

The membranes were stored at - 80 °C before use. Macrophage membrane was fused to MSCs using polyethylene glycol (PEG) as previously described.[45] Briefly, 1×10^6 MSCs and 1×10^{10} membrane particles were mixed in 100 μL of PEG (MW 1500) for 5 min. The mixed sample was then diluted by 5 mL of PBS and followed by centrifugation at 500 g for 5 min to separate free macrophage membranes. MSCs and MF-MSCs were photographed using a fluorescence microscope (Olympus, Tokyo, Japan). To identify the surface marker of MSCs and MF-MSCs, western blot analysis and flow cytometry were used.

2.1.4 Characterization of IONP-MSCs and MF-MSCs

The plasma membranes of MSCs were labeled with DiO. IONPs and macrophage membranes were labeled with RITC. IONP-MSCs and MF-MSCs were fixed with 4 % paraformaldehyde (PFA) for 10 minutes and mounted with a mounting solution containing 4,6-diamidino-2-phenylindole (DAPI) (Vector Laboratories Inc., Burlingame, CA, USA) that stains the nuclei. The samples were photographed using a fluorescence microscope (Olympus, Tokyo, Japan). For the TEM analysis, IONP-MSCs and were fixed using Karnovsky's fixative solution for 2 hours at 4 °C, washed three times with 0.05 M sodium cacodylate buffer, fixed with 1 % osmium tetraoxide for 2 hours at 4 °C, and rinsed twice with distilled water. The samples were stained using 0.5 % uranyl acetate overnight at 4 °C, dehydrated with an ethanol series (30 %, 50 %, 70 %, 80 %, 90 %, and 100 %), infiltrated with propylene oxide, embedded in Spurr's resin, and cut into thin sections with a thickness of 100 nm using an ultramicrotome (Leica, Wetzlar, Germany). The thin sections of IONP-MSCs were collected onto 200-mesh copper grids and imaged using a TEM. To evaluate the contents of IONPs within MSCs, IONP-MSCs were

analyzed using ICP-MS. To identify the surface marker of MSCs and MF-MSCs, western blot analysis and flow cytometry were used.

2.1.5. Preparation of NVs

NVs were prepared from MSCs, IONP-MSCs, and MF-MSCs using a modification of a previously described method.[36] The cells were detached using a cell scraper. The cells were suspended in PBS concentration of at least 1×10^6 cells/mL or placed in – 80 °C before the extrusion. The cells were extruded 5 – 6 times through 10 μm, 5 μm, and 400 nm pore-sized polycarbonate membrane filters (Whatman Inc., Clifton, NJ, USA) with a mini extruder (Avanti Polar Lipids). To separate NVs from free proteins and cellular debris, a gradient solution composed of iodixanol (Axis-Shield PoC AS, Oslo, Norway) was used. One mL of 50 % iodixanol, 2 mL of 10 % iodixanol, and 7 mL of the extruded samples were placed sequentially onto the bottom of an ultracentrifuge tube, and the tube was ultracentrifuged at 100,000 g for 2 hours at 4 °C. Second fraction from the bottom layer (NV, 2.5 mL) of the ultracentrifuge tube was collected, and an additional ultracentrifugation was performed at 100,000 g for 2 hours at 4 °C. The pellet in the tube was resuspended in PBS and filtered with 0.45 μm syringe filter. In case of IONP-NVs, IONP-NVs were further isolated from a mixture of N-NVs and IONP-NVs using magnet. The quantity of proteins of each fraction was determined by using Bradford assay as previously described.[35] The quantity of IONPs of each fraction was measured by using ICP-MS. Approximately, 100-150 μg of NVs were produced from 1×10^6 cells. NVs were stored at – 80 °C prior to use.

2.1.6. Characterization of NVs

To investigate the morphology of NVs, NVs were collected onto 200-mesh copper grids and imaged using a TEM. To further confirm the presence of IONPs in IONP-NVs, scanning transmission electron microscopy (STEM) and energy-dispersive X-ray spectroscopy (EDS)-mapping were performed. The size distribution of NVs was determined using a dynamic light scattering (DLS) (DLS-7000, Otsuka electronics, Osaka, Japan). To investigate *in vitro* cellular uptake of NVs, 10 μg of NVs were treated to CMs, CFs, HUVECs, PC12, and RAW 264.7. To determine intracellular iron content in the cells after the IONP-NV treatment, CMs, CFs, HUVECs, and macrophages were treated with mitomycin C for the inhibition of cell proliferation for 2 hours, and subsequently treated with IONP-NVs (20 μg/mL) for 24 hours. Then the medium was changed with fresh medium. The iron content in the CMs, CFs, HUVECs, and macrophages was analyzed using ICP-MS 1, 5, 10, and 14 days after the IONP-NV treatment.

2.2. *In vitro* assays

2.2.1. Quantitative PCR and analysis of RNA

RNA quantity and expression were evaluated using qRT-PCR. Cell, NV (n=4), and tissue samples (n=5) were lysed using 1 mL of the TRIzol reagent (Invitrogen, Carlsbad, CA, USA), and total RNA was extracted using 200 μL of chloroform. The samples were centrifuged at 10,000 g for 10 minutes at 4 °C. The supernatant was collected, mixed with 80 % (v/v) isopropanol in water, and centrifuged at 10,000 g for 10 minutes at 4 °C. The RNA pellet was rinsed with 75 % (v/v) ethanol, dried, and dissolved in RNase-free water. Complementary DNA was reverse-transcribed from RNA using the AccuPower RT PreMix (Bioneer, Daejeon, South Korea). Gene expressions were evaluated using the StepOnePlus real-time PCR system (Applied Biosystems, Foster city, CA, USA). Glyceraldehyde 3-phosphate dehydrogenase served as the housekeeping genes. Expressions of miRNA and mRNA were analyzed using Affymetrix 4.0 microarray (Thermofisher Scientific) and NOVAseq (Illumina, CA, USA), respectively. A total 343 miRNAs and 227 mRNAs were identified to be differentially included in IONP-NVs versus N-NVs.

2.2.2. Evaluation of cellular viability

Cell viability was determined using the cell counting kit (CCK) assay and fluorescein diacetate (FDA) and ethidium bromide (EB) staining. For the CCK assay, 50 μL of EZ-cytox (Daeillab service, Changwon, South Korea) per well was added to 24 well culture plates and incubated for 2 hours at 37 °C. The absorbance of the solution was measured at 450 nm using a spectrophotometer. For the FDA

and EB staining, 1 mL of FDA (5 μg/mL, Sigma) and EB (10 μg/mL, Sigma) solution was added to each well of 6 well culture plates and incubated 5 minutes at 37 °C. Staining was then photographed with a fluorescence microscope (Olympus).

2.2.3. Western blot analysis

Western blot analysis was used to evaluate the protein expression or quantity within the cell, NV, and tissue samples (n=3). Cell or NV, or tissue samples were lysed by SDS sample buffer (62.5 mM Tris-HCl pH 6.8, 2 % (w/v) of SDS, 10 % (v/v) of glycerol, 50 mM dithiothreitol, and 0.1 % (w/v) bromophenol blue). Proteins were separated by 10 % SDS polyacrylamide gel electrophoresis, and transferred to an Immobilon-P membrane (Millipore Corp., Bedford, MA, USA). For specific protein detection, primary antibodies against β-actin, angiopoietin-1 (ANG1), fibroblast growth factor 2 (FGF2), vascular endothelial growth factor (VEGF), hepatocyte growth factor (HGF), hypoxia-inducible factor 1α (HIF1α), connexin 43 (Cx43), extracellular signal-regulated kinases 1/2 (ERK1/2), phosphorylated extracellular signal-regulated kinases 1/2 (pERK1/2), proliferating cell nuclear antigen (PCNA), CD9, CD68, integrin α4, and integrin β1 (these antibodies were purchased from Abcam, Cambridge, UK) as well as against cJun, pcJun, c-Jun N-terminal kinases (JNK), phosphorylated c-Jun N-terminal kinases (pJNK), Serine/threonine-specific protein kinase (AKT), phosphorylated Serine/threonine-specific protein kinase (pAKT), and Phosphatidylinositol 3-kinases PI3K (these antibodies were purchased from Cell Signaling Technology, MA, USA) were incubated with membranes overnight at 4 °C. The membranes were washed three times and incubated with secondary antibodies conjugated with horseradish peroxidase (Sigma) for 1 hour at room temperature. The blots were developed using

chemiluminescence (LumiGLO, KPL Europe, Guildford, UK). Quantification of the western blots was evaluated using the Image J software.

2.2.4. Flow cytometry

RAW 264.7 cells, MSCs, and MF-MSCs were detached using a cell scraper and Trypsin-EDTA and then made into single-cell suspensions. Cells were stained with antibodies against CD90 and F4/80 which are conjugated with fluorescein isothiocyanate (FITC) and Alexa 647 (Biolegend, San Diego, CA, USA), respectively. Then cells were analyzed by FACS cantoII (BD Bioscience, San Jose, CA, USA).

2.2.5. Immunocytochemistry

The cells (n = 3) were fixed with 4 % paraformaldehyde for 10 min at room temperature and washed in PBS. Primary antibody against Cx43 was used for staining. The samples were then incubated in PBS containing rhodamine RITC-conjugated secondary antibodies (Jackson-Immunoresearch, West Grove, PA, USA) for 1 hr at room temperature. All samples were mounted with mounting solution containing DAPI to stain the nuclei, and photographed using a fluorescent microscope (Olympus, Tokyo, Japan).

2.2.6. *In vitro* cell assay in hypoxic conditions and macrophage polarization by the NV treatment.

To generate hypoxic culture conditions for the CFs, CMs, and HUVECs, the cell culture was carried out in a hypoxic incubator (MCO-18M, Sanyo, Japan) containing 1 % O2 for 6 hours at 37 °C. For PC12 cells and HUVECs for MF-NVs treatment, the cells were co-stimulated by hypoxia and lipopolysaccharide (LPS). To polarize macrophages into M1 phenotype, RAW 264.7 cell line was cultured in the presence of LPS (100 ng/mL, Sigma) for 1 day. After establishing the hypoxic culture or M1 polarization, the cells were co-cultured with MSCs or IONP-MSCs or were treated with IONP (420 ng/mL) or N-NVs or IONP-NVs or MF-NVs (20 μg/mL) for 24 hours. Then the medium was changed with fresh medium. Cells were cultured for 1 day and used for the analysis. To control the equal dose of NVs and the number of MSCs for co-culture, the yield of NVs from MSCs was applied. One hundred fifty μg of NVs were treated against 1×10^6 co-cultured MSCs.

2.2.7. Capillary tube formation

Cell culture plates were coated with Geltrex (Invitrogen) and incubated for 30 minutes at 37 °C to promote gelation. HUVECs underwent hypoxic condition (1 % O2) and were simultaneously co-cultured with MSCs or IONP-MSCs (1.5 105 cells) using transwells (Corning, New York, USA) or treated with IONP (420 ng/mL), N-NVs or IONP-NVs or MF-NVs (20 μg/mL) for 6 hours and be subsequently detached using Trypsin. Then HUVECs were plated at 5×10^4 cells/cm2 on the Geltrex for 6 hours at 37 °C. Capillary tubes were observed using a light microscope. Six random fields were measured for the quantitative analysis.

2.2.8. Cell migration assay

HUVECs were seeded on culture plates, grown until confluence. HUVECs underwent hypoxic condition (1 % O2) and were simultaneously co-cultured with MSCs or IONP-MSCs (1.5×10^5 cells) using transwells (Corning, New York, USA) or treated with IONP (420 ng/mL) N-NVs or IONP-NVs or MF-NVs (20 μg/mL) for 6 hours and then incubated under hypoxic conditions (1 % O2) for 6 hours at 37 °C. Next, a linear gap was created by scratching the surface of the culture plates using a sterile yellow tip. The cells were rinsed three times with PBS to thoroughly remove the detached cells. After 12 hours, five random fields were photographed and quantified using the following equation: [(initial cell-free area – cell-free area at 12 hours) / initial cell-free area] × 100 %. Quantification of the scratched area was evaluated using the Image J software.

2.2.9. *In vitro* NV binding assay

HUVECs were labeled with a fluorescent dye, DiO, for 2 hours prior to exposure to hypoxia. Then HUVECs were cultured under hypoxic condition (1 % O2) in the medium containing 500 μM of H2O2 for 24 hours. The cells were then treated with DiI-labeled N-NVs and MF-NVs in PBS (20 μg/mL) for 5 min at 4 °C to prevent endocytosis of N-NVs and MF-NVs. After NV binding to HUVECs, the cells were washed with PBS 3 times and photographed with a fluorescence microscope (Olympus). Total red fluorescent intensity was measured using Image J software. The fluorescent intensity was divided by HUVEC numbers for the quantification.

2.3. *In vivo* assays

2.3.1. MI model and treatment

The animal studies were approved by The Catholic University of Korea Animal Care and Use Committee and IACUC and Department of Laboratory Animal (DOLA) in Catholic University of Korea, Songeui Campus accredited the Korea Excellence Animal laboratory Facility from Korea Food and Drug Administration in 2017 and acquired AAALAC International full accreditation in 2018. (CUMC-2017-0240-04). Fischer 344 rats (180-200 g, 8-week-old male, Koatec, Korea) were anesthetized with 2 % inhaled isoflurane and intubated via the trachea with an 18G intravenous catheter. The rats were then mechanically ventilated with medical grade oxygen. Animals were placed on a 37°C heating-pad to prevent cooling during the procedure. After shaving the chest, a left thoracotomy was performed. MI was achieved by tying a suture with a sterile polyethylene glycol tubing (22G) that was placed into the left anterior descending (LAD) artery for 1 min, and then, the knot was permanently ligated using 7-0 Prolene suture. One day after the ligation, the rats were anesthetized again using isoflurane inhalation, intubated and mechanically ventilated. The animal chest was re-opened, and IONP (3.15 μg), IONP-MSC (1×10^6 cells), MSC (1×10^6 cells), N-NV (150 μg) or IONP-NV (150 μg) in 100 μL PBS were injected at four different sites in the border zone of the infarcted myocardium. For the IONP-NV + M group, a neodymium magnet (diameter: 15 mm, thickness: 5mm) was immobilized on the heart for 5 minutes just after injection. After closing the chest, the magnet was implanted into the muscle above the heart and removed after 24 hours.

2.3.2. SCI model and treatment

Female 6- to 8-week-old C57BL/6 mice (20–25 g, Koatec Inc, Korea) were deeply anesthetized with an intraperitoneally administered mixture of Zoletil® (50 mg/kg, Virbac Laboratories, France) and Rompun® (10 mg/kg, Bayer, Korea). To induce standing weight compression model of SCI, laminectomy was made at the ninth thoracic vertebral levels (T9) and a stainless steel impounder (weight: 20 g) was loaded to the T10 spinal cord for 30 sec after laminectomy. Following compression lesion, animals were placed on a heating pad to maintain body temperature, and then 0.5mL of 0.9 % sterile saline injected subcutaneously. Manual bladder expression of urine was performed twice daily until a reflex bladder was established. All animal procedures were performed according to the approved protocol by the Institutional Animal Care and Use Committee (IACUC) of CHA University (IACUC180099). The spinal cord-injured mice were randomly assigned into four groups. In the normal group, mice received laminotomy alone. In the no treatment group, SCI mice were injected with 100 μl PBS. In the N-NV group, SCI mice were injected with 25 μg of N-NV in 100 μl PBS. In the MF-NV group, SCI mice were injected with 25 μg of MF-NV in 100 μl PBS. The injection was performed 1 hr and 7 days after injury.

2.3.3. *Ex vivo* biodistribution of NVs

To evaluate the biodistribution of N-NVs, IONP-NVs, tr-MF-NVs, and MF-NVs, the plasma membranes of NVs were labeled with Vivotrack 680 (PerkinElmer, MA, USA) for 2 hours prior to injection. The fluorescent signal of NVs was detected using an *in vivo* imaging system (IVIS spectrum, PerkinElmer) 1 day after the

intramyocardial or intravenous injection. The fluorescent images of organs (lung, liver, kidney, spleen, and heart or spinal cord) were obtained by removing background with no treatment group. Then the fluorescent intensity in the heart or spinal cord was quantified. The relative fluorescent units were quantified by the following equation: [(fluorescent intensity in the heart at 24 hours / initial fluorescent intensity of IONP-MSCs or IONP-NVs) × 100 %] or [(fluorescent intensity in spinal cord/total fluorescent intensity of all organs) × 100 %]. The fluorescent intensities of the spinal cord and other organs were measured using the Living Image 3.1 software.

To further visualize the retention of NVs in the infarcted myocardium, the plasma membranes of NVs were labeled with DiI for 2 hours and injected into the myocardium. After the animals were sacrificed, the heart tissues were fixed with formaldehyde for 24 hours, embedded in paraffin, and sliced into a 4 μm thickness. The tissue sections were photographed using a fluorescent microscope (Olympus) after reducing background fluorescent signals with Dako Antibody Diluent Background Reducing Components (Agilent Technologies). For the detection of IONPs, Prussian blue staining was performed in major organs including lung, heart, kidney, liver, and spleen 1 and 4 weeks after the injection of IONP-NVs. Magnetic guidance was applied for 1 day. Nuclear fast red staining was used for counter-staining.

2.3.4. MRI

Endotracheal intubation was performed with 18-G angio-catheter. The rats were anesthetized with inhaled 2 % isoflurane and then mechanically ventilated with

medical grade oxygen. Subsequently, 0.9 % NaCl solution was perfused for 5 minutes into the right internal jugular vein using a perfusion pump. As the perfusion with 0.9 % NaCl solution started, descending thoracic aorta and inferior vena cava were incised to rapidly clear the blood from the animals. Afterward, 0.9 % NaCl solution was changed to 10 % Multihance (Bracco, Italy) in 4 % PFA solution for perfusion for 10 minutes to fix the heart tissues. The hearts were harvested when the perfusion process was completed. To retain the shape of the harvested tissue, 1.5 % agarose solution was perfused into aorta until the agarose solution was visible from the incised heart region and aorta. MRI was performed with a 9.4T MRI system with 70 mm AD quad volume coil (Agilent Technologies, Santa Clara, CA, USA). Conditions for spin-echo T2-weighted imaging are as follows: repetition time, 3000 ms; echo time, 10 ms; number of excitations, 5; matrix, 256 × 256; slice thickness, 0.5 mm; field of view, 35 mm × 35 mm; scan time, 21 minutes 36 s. For T2 measurements, the Carr-Purcell-Meiboon-Gill pulse sequence was adapted for multiple spin-echo measurements. Thirty-four images were acquired with 34 different echo time values ranging from 8 to 160 ms. T2 relaxation times were obtained from the non-linear least squares fit of the mean pixel values for the multiple spin-echo measurements at each echo time. Relaxivities (R2) were then calculated as an inverse of relaxation time per mM.

2.3.5. Immunohistological assessment *in vivo*

For immunohistochemical analysis, the heart and spinal cord tissues were obtained. Tissue sections were treated with proteinase K for 15 minutes at 37 °C. The non-specific region was blocked with normal goat or horse serum (Sigma). Then the slides were incubated with primary antibodies against cardiac troponin T (cTnT),

Cx43, CD68, CD206, nitric oxide synthase 2 (NOS2), von Willebrand factor (vWF), glial fibrillary acidic protein (GFAP), neurofilament (NF), and chondroitin sulfate proteoglycans (CSPGs) (these antibodies were purchased from Abcam) diluted with Dako Antibody Diluent Background Reducing Components (Agilent Technologies) at 4 °C overnight. The slides were washed three times with PBS, incubated for 1 hour with rhodamine or FITC-conjugated secondary antibodies at room temperature, washed, mounted with a mounting medium (Vector Laboratories Inc.), and photographed using fluorescent microscope (Olympus).

2.3.6. Apoptosis assessment *in vivo*

Deoxynucleotidyl transferase dUTP nick end labeling (TUNEL) assay was performed to detect apoptotic cells with the in situ cell death detection kit (Roche). Briefly, fixed spinal cord sections were permeabilized and incubated with fluorescein TUNEL reaction mixture containing for 60 min at 37°C in dark. After washing with PBS, nuclei were stained with DAPI and the samples were photographed using fluorescent microscope (Olympus).

2.3.7. Capillary density determination in heart

At the time of sacrifice, the hearts were perfused with GFP-conjugated Isolectin B4 from Griffonia simplicifolia for 15 minutes at room temperature. Then, the hearts were fixed in 4 % Paraformaldehyde overnight, embedded in paraffin, and sectioned in 4 μm thick slices. The number of blood vessels were counted in five random microscopic fields using a fluorescence microscope.

2.3.8. Determination of fibrosis in heart

Masson's Trichrome (Sigma) staining was performed to determine the fibrosis area of the MI hearts. Briefly, three tissue sections in each group were fixed in Bouin's solution at 56 °C for 1 hour, stained using Weigert's Iron Hematoxylin Solution for 15 minutes at room temperature, and stained using Biebrich Scarlet-acid Fuchsin solution for 10 minutes at room temperature. Finally, the sections were counterstained with Aniline Blue for 15 minutes followed by incubation in 0.2 % acetic acid for 1 min at room temperature. The collagen fibers appear as blue, and viable myocardium appear as red. The area of fibrosis to the entire left ventricular wall area was quantified with the Image J software.

2.3.9. Evaluation of cardiac functions

The assessment of cardiac functions was performed with echocardiography. The rats were lightly anesthetized with inhaled 2 % isoflurane, and physiological data were recorded with a transthoracic echocardiography system equipped with a 15 MHz L15-7io linear transducer (Affniti 50G, Philips). Different echocardiograms were performed at 1, 2, and 4 weeks after MI. The echocardiography operator was blinded to the group allocation during the experiment. Ejection fraction and fractional shortening, which are indexes of the LV systolic function, were calculated using a previously described method.[46]

2.3.10. Behavior evaluation

Behavioral analysis was conducted by two observers, blinded to the treatment identity. Coordinated motor function was evaluated with the Basso Mouse Scale locomotor rating scale (scored on a 9-point scale).[47] To evaluate functional recovery, ten mice were randomly selected from each group at 0, 1, 7, 14, 21, and 28 days after surgery. The mice were observed continuously from 1 min.

2.4. Statistical analysis

All quantitative data are expressed as the mean ± standard deviation. Two-tailed Student's t-test was used for comparison between two groups. A one-way and two-way analysis of variance (ANOVA) followed by Bonferroni test was used for all statistical analysis. A difference with a P value less than 0.05 was considered statistically significant. All statistical analyses were performed using Prism 7.0 (GraphPad Software Inc.).

Chapter 3.

Nanovesicles derived from iron oxide nanoparticles-incorporated mesenchymal stem cells for cardiac repair

3.1. Introduction

Cardiovascular diseases including MI and their related complications are major causes of death.[48, 49] MI is characterized by the restriction of blood flow in the infarction area and the subsequent death of cardiac cells. The implantation of MSCs can reduce the infarct size, prevent excessive tissue loss, and enhance cardiac function in animal MI models.[50, 51] However, the low survival of implanted MSCs limits their therapeutic potency.[52, 53] In addition, MSC implantation may cause arrhythmias or the differentiation of the MSCs into other types of cells including chondrocytes and osteocytes in the infarcted myocardium or it may trigger tumorigenesis.[54, 55]

It has been revealed that implanted MSCs mediate cardiac repair mainly by secreting paracrine molecules rather than differentiating into cardiac cell lineages.[56] Recent studies have shown that the therapeutic potential of MSCs is largely attributed to exosomes, which are a specific type of extracellular vesicles (EVs) that have diameters of 50-200 nm, contain RNAs and proteins, and are involved in intercellular communications by acting as carriers of bioactive molecules.[57] Due to the enrichment of cardiac repair-favorable molecules in MSC-derived exosomes, they exert a cardiac repair efficacy that is similar to that of implanted MSCs.[30, 58] RNAs and proteins in the exosomes transferred from the parental cells to the recipient cells are functional in the recipient cells and participate in the regulation of intracellular signaling cascades.[10, 11] In addition, MSC-derived exosomes can avoid the low-cell-survival issue, arrhythmia and tumorigenesis risk and the immune response triggered by the MSC implantation therapy. They can also be stored at - 80 °C for a long period. Due to the safety concerns of MSC implantation and the advantages of using exosomes, the

administration of MSC-derived exosomes has emerged as an alternative cell-free therapy for cardiac repair.[59]

Despite the therapeutic potential of exosomes, their use in the clinical applications are not easily feasible because MSCs secrete exosomes in very small quantities. The average exosome yield from 10^6 cells is 1-4 μg per day[34], which cannot easily meet the quantity (100-500 μg per patient) of exosomes required in a clinical trial.[60] Recently, NVs, which have similar size and composition to those of exosomes, have been developed through the serial extrusion of cells through microporous filters.[36, 61] Like exosomes, NVs can also convey the biomolecules of their parental cells to recipient cells. NVs have advantages over exosomes, such as a 250-fold higher production yield and a 2-fold greater quantity of RNAs and proteins.[35] Therefore, in this study, we applied MSC-derived NVs rather than MSC-derived exosomes in terms of clinical scale production, cost effectiveness, and therapeutic potency.

A number of studies have showed that, immediately after cell injection into the infarcted heart, most of the cells diffuse out from the injection area, which would limit their therapeutic potential. Here we found that magnetic guidance of iron oxide nanoparticle (IONP)-incorporated NVs following injection could improve the retention of NVs in the infarcted heart. IONP is slowly ionized and assimilated *in vivo*[62] and the US Food and Drug Administration has approved the clinical usage of IONP (ferumoxytol). In addition to the enhanced retention, we also found that NVs derived from IONP-incorporated MSCs (IONP-NVs) contained much larger quantities of therapeutic molecules for cardiac repair (RNAs and proteins) than normal MSC-derived NVs (N-NVs), which are mediated by intracellular signaling modifications triggered by the ionization of IONPs in IONP-

incorporated MSCs (IONP-MSCs) (Fig. 3.1).[63-68] IONPs not only induced the upregulation of HIF1α-mediated growth factor expression in MSCs, which is similar to hypoxia-induced[68] and heat shock-induced[69] upregulation of HIF1α-mediated growth factor expression in MSCs, but also augmented the retention of NVs in the heart.

Therefore, we hypothesized that IONP-NVs would have stronger therapeutic potential for cardiac repair compared to those of N-NVs through enhanced retention by magnetic guidance and increased quantities of therapeutic molecules in IONP-NVs. In fact, we found that like MSCs, IONP-NVs exhibited anti-apoptotic, anti-fibrotic, anti-inflammatory, and pro-angiogenic effects on CFs, CMs, endothelial cells (ECs), and macrophages, which are the major therapeutic mechanisms of MSCs for cardiac repair *in vitro*. Following the injection of IONP-NVs, the retention of IONP-NVs in the infarcted myocardium was greatly enhanced by the application of a magnetic field for 24 hours. As a result, the IONP-NV injection resulted in reduced apoptosis, inflammation, and infarct size, as well as improved angiogenesis and cardiac function recovery. Overall, our data suggest that IONP-NVs may represent a highly effective and feasible cell-free therapy for MI.

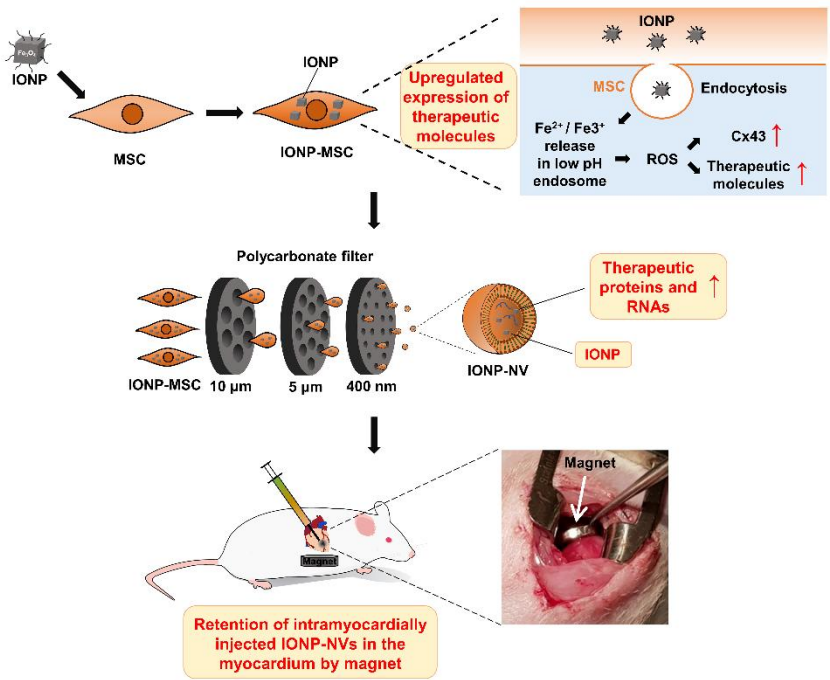

Figure 3.1. Schematic diagrams for the preparation and intramyocardial injection of IONP-NVs for cardiac repair. MSCs modified through the internalization of IONPs exhibited higher expression of therapeutic biomolecules. IONP-NVs were generated from IONP-MSCs by serial extrusion and contained contents similar to those of IONP-MSCs. Magnetic guidance following intramyocardial injection of IONP-NVs can improve cardiac retention of IONP-NVs.

3.2. Results and discussion

3.2.1. IONPs internalization into MSCs

We evaluated the physical and biological characteristics of IONPs. A TEM image shows that IONPs were 20-30 nm in size and had a cubic shape (Fig. 3.2A). In the fluorescent microscope images obtained 24 hours after RITC fluorescent dye-labeled IONP treatment to MSCs, IONPs were well internalized into the cytoplasm of MSCs (Fig. 3.2B). TEM images also showed that the internalized IONPs were retained within intracellular endosomes (Fig. 3.2C). Quantitative evaluation revealed an iron content of 47 pg within one cell (Fig. 3.2D). Quantitative real-time reverse transcription-polymerase chain reaction (qRT-PCR) analyses for apoptosis-related genes and the staining for FDA/EB 2 days after IONP treatment also showed no cytotoxic effects on the viability of MSCs (Fig. 3.2E and F). IONPs did not exhibit cytotoxic effects on MSCs, as evaluated with CCK assay 2, 4, 7, 10, and 14 days after IONP treatment (Fig. 3.2G).

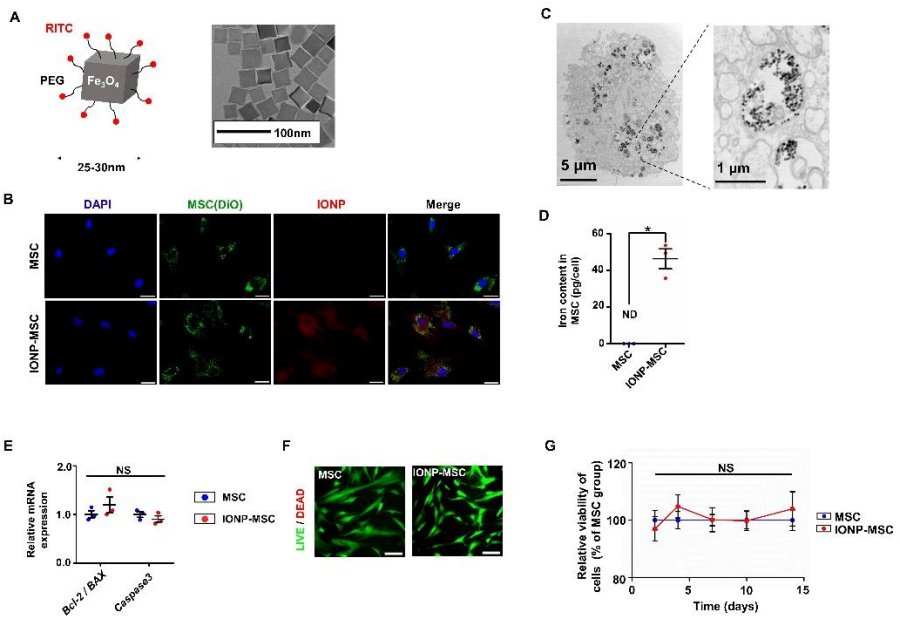

Figure 3.2. IONPs internalization into MSCs. (A) Schematic illustration and TEM image of IONPs. (B) Fluorescent images of IONP (red) uptake by MSCs 24 hours after IONP treatment (green, cell membrane; blue, DAPI). Scale bars, 100 μm. (C) Representative TEM images and a magnification of IONPs in the endosome/lysosome of MSCs. (D) Quantification of iron content in MSC and IONP-MSC, as evaluated by ICP-MS. ND; No detection. (E) Relative mRNA expression of apoptosis-related genes in MSC and IONP-MSC. (F) Representative images of staining for viable and nonviable cells with FDA/EB staining. Scale bars, 100 μm. (G) The cytotoxicity of IONPs 2, 4, 7, 10, and 14 days after IONP treatment to MSCs, as evaluated by CCK assay (n = 4 per group; NS, no significant difference). *$P < 0.05$ by two-tailed t-test. All values are mean ± SD.

3.2.2. Cellular modification of MSCs by IONPs

The IONP treatment stimulated the osteogenic and adipogenic differentiation of MSCs by upregulation of some genes (*ALP, LPL*, and *PPARγ*), but not chondrogenic differentiation (Fig. 3.3A). This result was different from that of a previous study in which IONP loading in MSCs did not stimulate osteogenic and adipogenic differentiation and inhibited chondrogenic differentiation.[70] The inconsistency between two studies could be due to the difference in the IONP dose (47 pg IONPs per cell in the present study versus 10-20 pg IONPs per cell in the previous study).

We determined whether IONPs internalized in MSCs could affect gene expression levels of cardiac repair-related molecules in the MSCs. Interestingly, the IONP uptake significantly increased the expression mRNA and protein levels of cardiac repair-favorable genes including ANG1, FGF2, HGF, VEGF, placental growth factor (PGF), and HIF1α, 2 days after IONP treatment, as evaluated with qRT-PCR and western blot (Fig. 3.3B and C). After cellular uptake, IONPs in the endosomes at a low pH may undergo slow ionization, releasing iron ions into the cytoplasm and generating ROS.[63, 71, 72] The upregulated expression levels of the cardiac repair-favorable genes may be due to the overproduction of ROS that not only activate JNK[64] and cJun,[65] but also upregulate the expression of HIF1.[67, 68] Western blot analysis showed the upregulated expression of HIF1α and activation of JNK and cJun, 2 days after IONP-treatment (Fig. 3.3C).

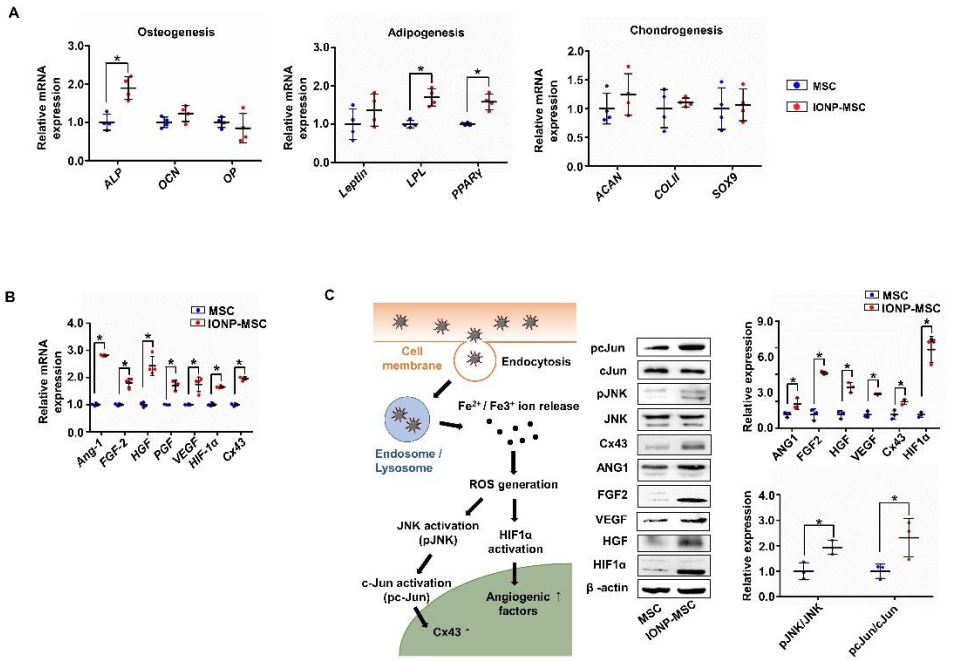

Figure 3.3 Cellular modification of MSCs by IONPs. (A) Relative mRNA expression of osteogenic, adipogenic, and chondrogenic genes in MSCs and IONP-MSCs 2 days after IONP treatment (LPL, lipoprotein lipase; PPARγ, peroxisome proliferator-activated receptor gamma; ALP, alkaline phosphatase; OCN, osteocalcin; OP, osteopontin; ACAN, aggrecan; COLII, collagen type II). (B) Relative mRNA expression levels of various cardiac repair-favorable genes in MSC and IONP-MSC, as evaluated by qRT-PCR (n = 4 per group). (C) Schematic illustration of the IONP-mediated intracellular signaling cascades in MSCs and western blot analysis for the intracellular signaling cascade molecules and associated therapeutic molecules (n = 3 per group). *P < 0.05 by two-tailed t-test. All values are mean ± SD.

3.2.3. Production of IONP-NVs from IONP-MSCs

We have prepared N-NVs and IONP-NVs by serial extrusion of MSCs and IONP-MSCs. The process of IONP-NV preparation and the portion of protein and IONPs of each fraction are shown in Fig. 3.4A. We characterized N-NVs and IONP-NVs. TEM images and DLS analysis revealed that N-NVs and IONP-NVs had spherical shapes and their sizes were similar to the typical size of EVs (Fig. 3.4B (i) and C).[73] TEM and fluorescent confocal images revealed that IONPs were entrapped inside IONP-NVs (Fig. 3.4B). STEM and EDS-mapping images also indicate that IONPs were entrapped in IONP-NVs (Fig. 3.4C). ICP-MS analysis showed an iron content of 21 ng within 1 μg IONP-NVs (Fig. 3.4D).

A

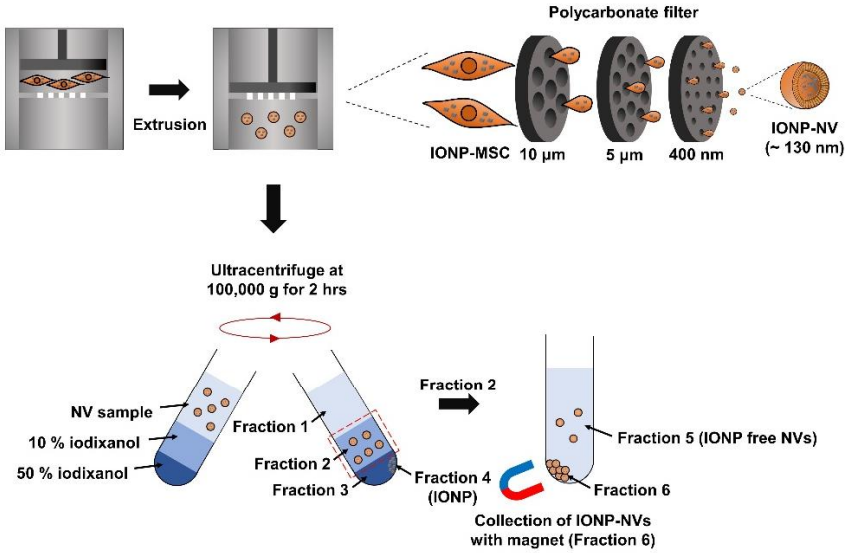

	Protein percentage (%)	IONP percentage (%)
Fraction 1	77.0 ± 1.1	4.0 ± 1.9
Fraction 2	15.5 ± 2.1	13.1 ± 3.8
Fraction 3	3.6 ± 0.4	22.7 ± 1.5
Fraction 4	3.7 ± 0.3	60.2 ±6.0
Total	100	100

	Protein percentage (%)	IONP percentage (%)
Fraction 5	10.5 ± 3.5	8.9 ± 1.7
Fraction 6	89.5 ± 3.5	91.1 ± 1.7
Total	100	100

Figure 3.4 A

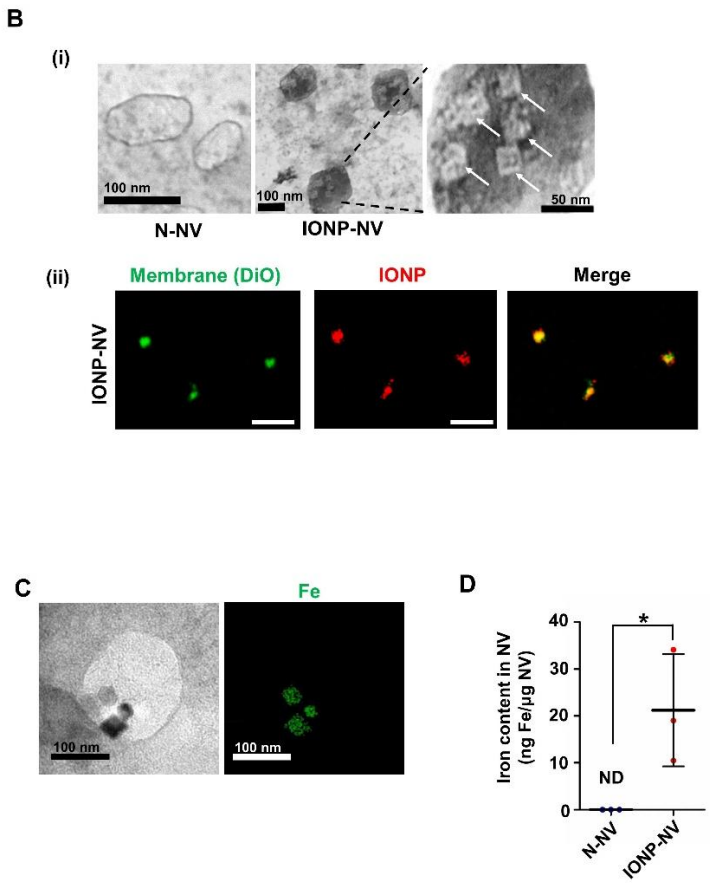

Figure 3.4 Production of IONP-NVs from IONP-MSCs. (A) Schematic diagram of the preparation of IONP-NVs and the quantification of the protein and iron content in each fraction as evaluated by Bradford assay and ICP-MS, respectively. The percentages of protein and iron in each fraction are shown in the table. (B) (i) TEM images of N-NVs and IONP-NVs and (ii) confocal images of IONP-NVs. White arrows indicate IONPs within IONP-NVs. In the fluorescent confocal images, NV lipid layers and IONPs were labeled with DiO (green) and RITC (red), respectively. Scale bars, 1 μm in panel (ii). (C) STEM and EDX-mapping images of IONP-NVs. Green dots indicate Fe (IONP). (D) Iron content in N-NV and IONP-NV, as evaluated by ICP-MS. (ND, no detection). *$P < 0.05$ by two-tailed t-test. All values are mean ± SD.

3.2.4. Characterization of IONP-NVs

The size distributions of N-NVs and IONP-NVs are shown in Fig. 3.5A. To compare the quantities of proteins and RNAs of NVs with those of exosomes, we quantified the amounts of proteins and RNAs in IONP-MSC-derived exosomes and IONP-NVs (Fig. 3.5B). IONP-NVs contain 2.0-2.5 folds larger quantities of proteins and RNAs than IONP-MSC-derived exosomes. To compare the mRNA expression and protein levels in N-NVs and IONP-NVs, qRT-PCR and western blot were performed. The data showed that the mRNA expression and protein levels of ANG1, FGF2, VEGF, PGF, HGF, Cx43, and HIF1α were significantly higher in IONP-NVs compared to N-NVs (Fig. 3.5C and D). Both N-NVs and IONP-NVs contained CD9, a marker for exosome, EV and NV.[36] The levels of cardiac repair-related miRNAs were compared between N-NVs and IONP-NVs using Affymetrix miRNA 4.0 (Fig. 3.5E). Remarkably, many miRNAs known to promote cardiac recovery were increased in IONP-NVs versus N-NVs.

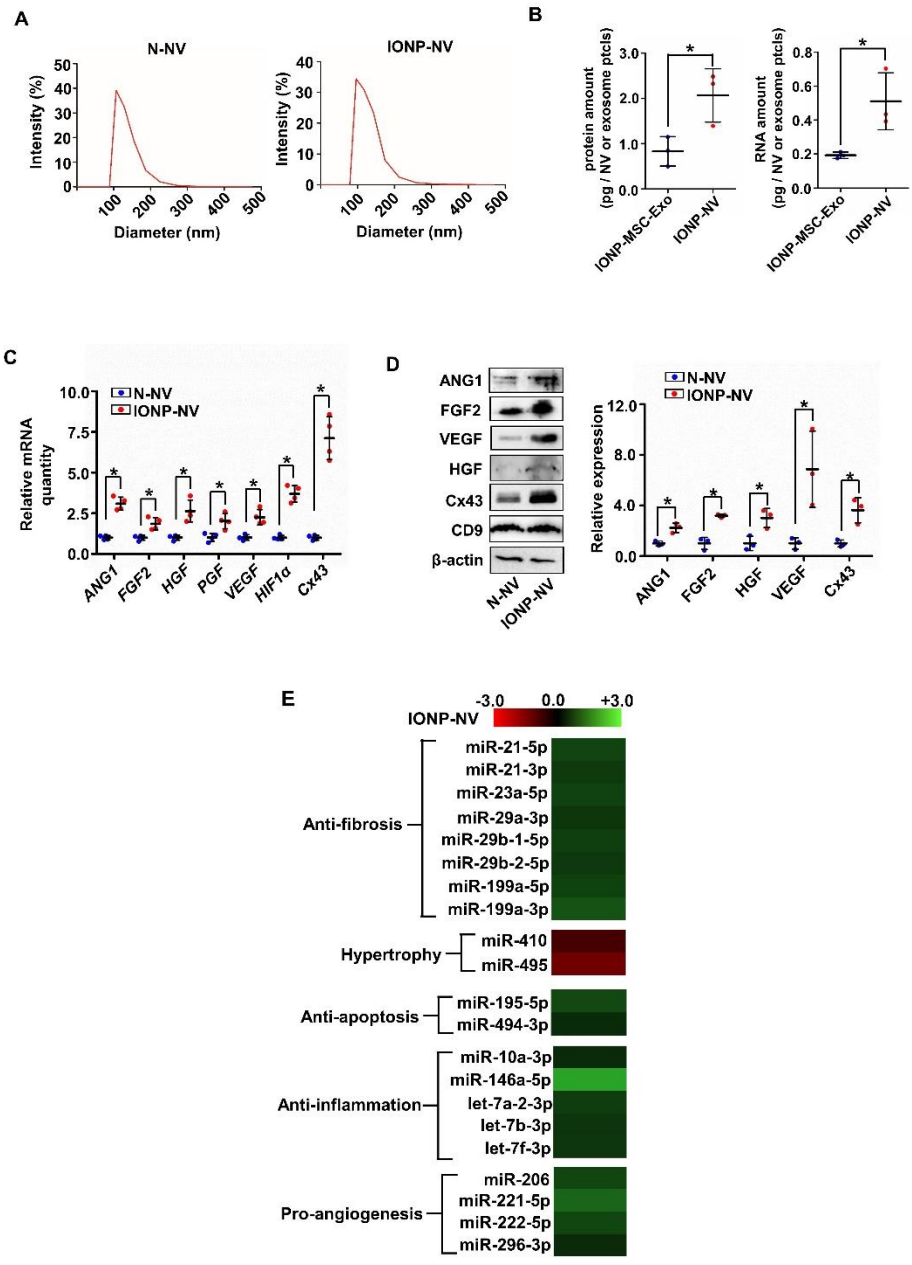
A
N-NV
IONP-NV
Intensity (%)
Diameter (nm)
B
protein amount (pg / NV or exosome ptcls)
RNA amount (pg / NV or exosome ptcls)
IONP-MSC-Exo
IONP-NV
C
Relative mRNA quantity
N-NV
IONP-NV
ANG1
FGF2
HGF
PGF
VEGF
HIF1α
Cx43
D
ANG1
FGF2
VEGF
HGF
Cx43
CD9
β-actin
N-NV
IONP-NV
Relative expression
E
-3.0
0.0
+3.0
IONP-NV
Anti-fibrosis
miR-21-5p
miR-21-3p
miR-23a-5p
miR-29a-3p
miR-29b-1-5p
miR-29b-2-5p
miR-199a-5p
miR-199a-3p
Hypertrophy
miR-410
miR-495
Anti-apoptosis
miR-195-5p
miR-494-3p
Anti-inflammation
miR-10a-3p
miR-146a-5p
let-7a-2-3p
let-7b-3p
let-7f-3p
Pro-angiogenesis
miR-206
miR-221-5p
miR-222-5p
miR-296-3p

Figure 3.5. Characterization of IONP-NVs. (A) Representative size distribution of N-NVs and IONP-NVs derived from MSCs and IONP-MSCs, respectively, as evaluated by DLS. (B) Comparison of the protein and RNA amounts in IONP-NVs and IONP-MSC-derived exosomes. (C) Relative mRNA levels in N-NVs and IONP-NVs, as evaluated by qRT-PCR (n = 4 per group). (D) Representative images of western blots of therapeutic molecules and the marker of EV, CD9 (n = 3 per group). (E) Fold changes in levels of cardiac repair-related miRNA in IONP-NVs compared to N-NVs. All columns represent log2-fold changes. *$P < 0.05$ by two-tailed t-test. All values are mean ± SD.

3.2.5. Cellular uptake of IONP-NVs *in vitro*

To evaluate NV uptake by individual cell levels in cardiac tissue, fluorescent microscopic examination was performed 24 hours after the treatment of CFs, CMs, HUVECs, and macrophages with N-NVs and IONP-NVs *in vitro* (Fig. 3.6A). As shown in Fig. 3.6B, the most of treated IONP-NVs were internalized into the cells *in vitro* within 24 hours after treatment. To evaluate the cytotoxicity of IONPs inside the cells, the viability of CFs, CMs, HUVECs, and macrophages was assessed 2, 5, and 10 days after treatment with IONP or IONP-NV (Fig. 3.6C). IONPs did not affect the cellular viability for a long term. After internalization, the IONPs were slowly ionized and degraded, as the iron content in the cells decreased with time (Fig. 3.6D) and as reported previously.[74]

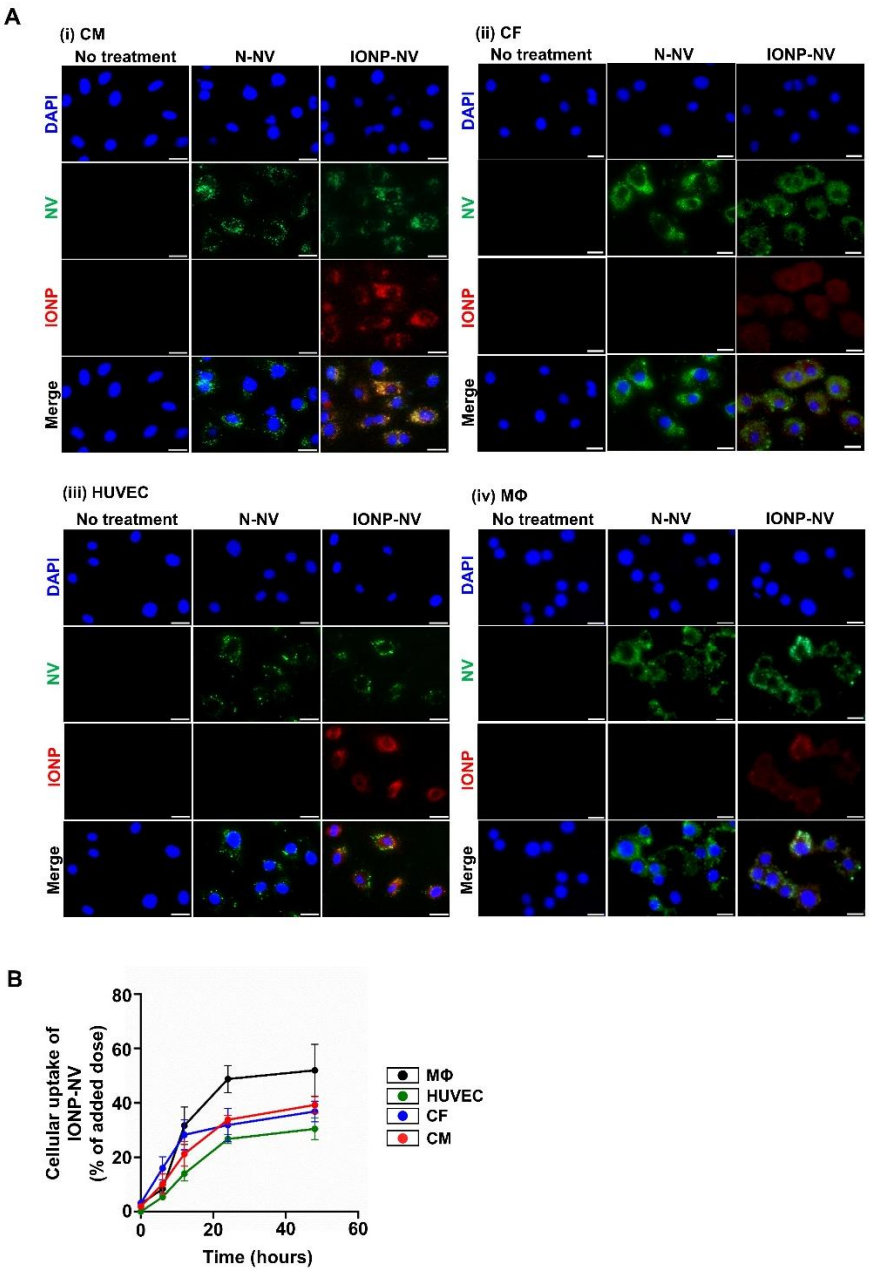
A
(i) CM
No treatment
N-NV
IONP-NV
DAPI
NV
IONP
Merge
(ii) CF
No treatment
N-NV
IONP-NV
DAPI
NV
IONP
Merge
(iii) HUVEC
No treatment
N-NV
IONP-NV
DAPI
NV
IONP
Merge
(iv) MΦ
No treatment
N-NV
IONP-NV
DAPI
NV
IONP
Merge
B
Cellular uptake of IONP-NV (% of added dose)
80
60
40
20
0
0
20
40
60
Time (hours)
MΦ
HUVEC
CF
CM

Figure 3.6 A-B

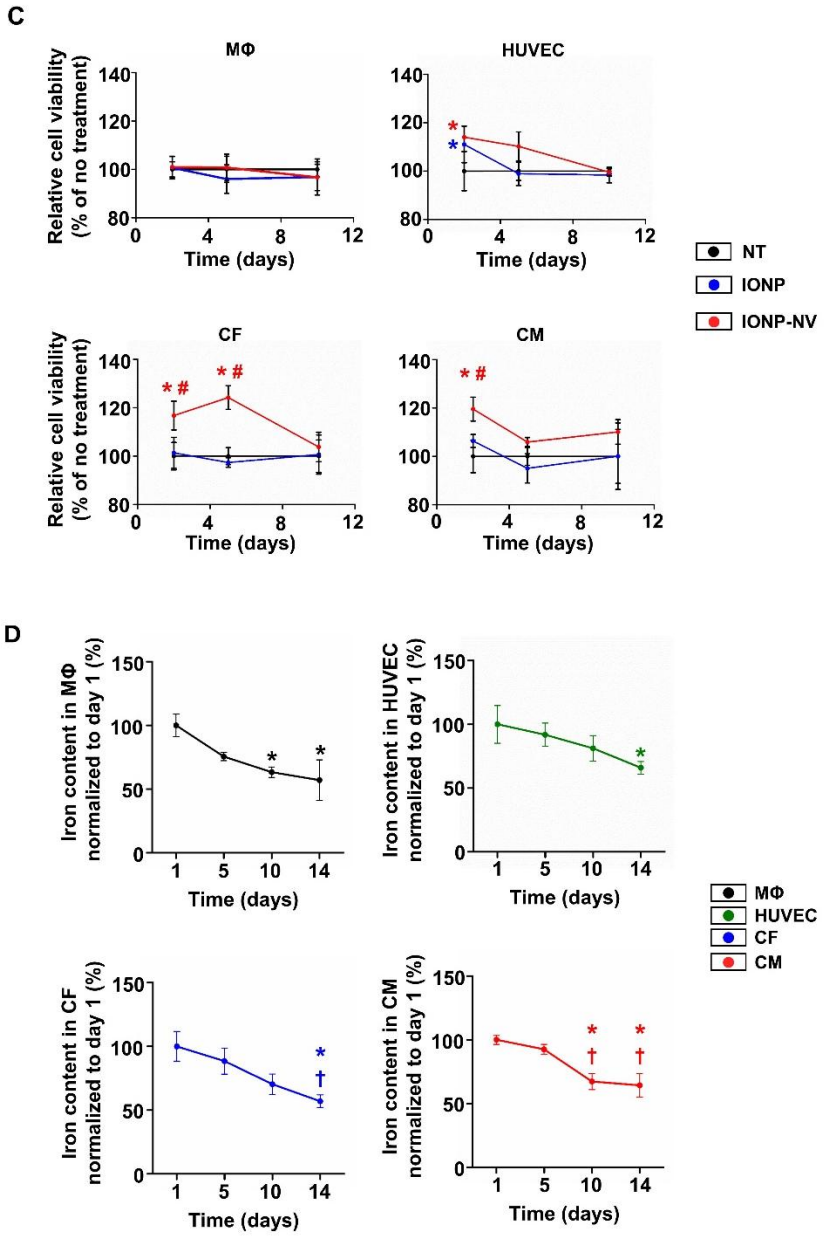

Figure 3.6. Cellular uptake of IONP-NVs *in vitro*. (A) Representative images showing the *in vitro* uptake of N-NVs and IONP-NVs by (i) CMs, (ii) CFs, (iii) HUVECs, and (iv) macrophages (MΦ). (green, NV membrane; red, IONP; blue, DAPI). Scale bars, 100 μm. (B) *In vitro* cellular uptake rate of IONP-NVs as evaluated by ICP-MS. Data

were normalized to iron content of IONP-NV added to the cultures. (C) Relative cell viability as evaluated by the CCK assay 2, 5, and 10 days after treatment with IONPs or IONP-NVs to various cells. *$P < 0.05$ versus NT and #$P < 0.05$ versus IONP by using two-way ANOVA followed by post-hoc Bonferroni test. All data were normalized to NT at day 2. (D) Profiles of intracellular iron content in cells after cellular uptake of IONP-NVs as evaluated by ICP-MS. *$P < 0.05$ versus day 1 and †$P < 0.05$ versus day 5 by one-way ANOVA followed by post-hoc Bonferroni test. All data were normalized to day 1. All values are mean ± SD.

3.2.6. Cardioprotective effects of IONP-NVs *in vitro*

To assess the therapeutic effects of IONP-NV, we used CMs, CFs, HUVECs, and macrophages *in vitro*. To determine whether IONP-NVs possess the therapeutic potential for cardiac repair, we assessed the anti-apoptotic and anti-fibrotic effects of NVs and MSCs on CFs, CMs, and HUVECs *in vitro*. The cells were co-cultured with MSCs or IONP-MSCs, or treated with IONPs, N-NVs or IONP-NVs for 1 day after exposure to a hypoxic condition that mimicked cardiac ischemia (Fig. 3.7A). In the IONP alone group, the quantity of IONPs was equal to that of IONP-NVs (21 ng iron in IONPs/ 1μg NV protein). Both NVs and MSCs showed the cardioprotective effect on the cells after hypoxia (Fig. 3.7B). Gene expression of caspase3 and FDA/EB staining data also showed that NVs and MSCs improved the cell viability and attenuated apoptosis of the cells (Fig. 3.7C and D). Western blot analysis showed that both IONP-NVs and IONP-MSCs exerted the cardioprotective effect via activating AKT/PI3K[31] intracellular signaling cascades (Fig. 3.7E and F). Interestingly, the mRNA expression of Cx43 were upregulated in CFs and CMs under hypoxic condition by NVs and MSCs (Fig. 3.7G). In addition, western blots and immunocytochemistry showed that Cx43 expression in CFs and CMs was upregulated by IONP-NVs and IONP-MSCs (Fig. 3.7H and I) Cx43 is well known to have functions as electrical coupling and intercellular molecule exchange of CFs and CMs. There were several reports that Cx43 expression was decreased in hypoxic condition, which causes arrhythmia and cardiac cell death due to decreased conduction between cells in vtiro and *in vivo*.[75, 76] The data indicate that IONP-NVs can attenuate cell death.

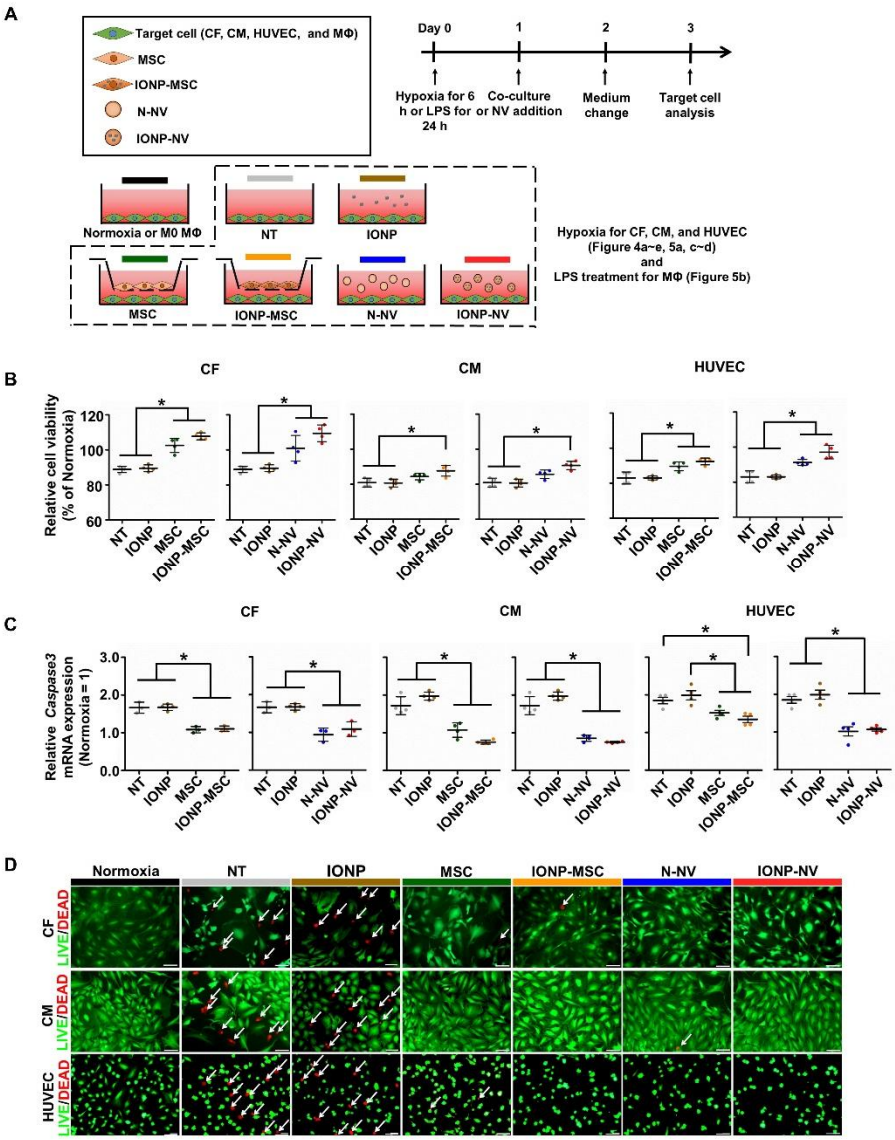
A
Target cell (CF, CM, HUVEC, and MΦ)
MSC
IONP-MSC
N-NV
IONP-NV
Day 0
1
2
3
Hypoxia for 6 h or LPS for 24 h
Co-culture or NV addition
Medium change
Target cell analysis
Normoxia or M0 MΦ
NT
IONP
MSC
IONP-MSC
N-NV
IONP-NV
Hypoxia for CF, CM, and HUVEC (Figure 4a~e, 5a, c~d) and LPS treatment for MΦ (Figure 5b)
B
CF
CM
HUVEC
Relative cell viability (% of Normoxia)
C
Relative Caspase3 mRNA expression (Normoxia = 1)
D
Normoxia
NT
IONP
MSC
IONP-MSC
N-NV
IONP-NV
CF LIVE/DEAD
CM LIVE/DEAD
HUVEC LIVE/DEAD

Figure 3.7 A-D

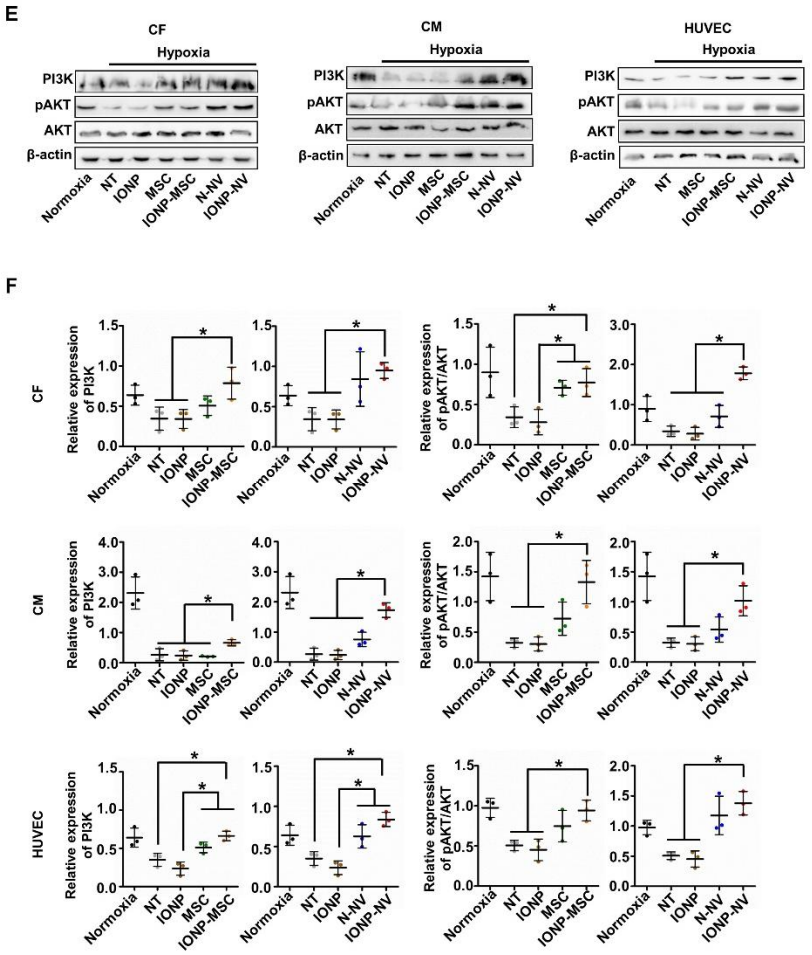
E
CF
CM
HUVEC
Hypoxia
PI3K
pAKT
AKT
β-actin
Normoxia
NT
IONP
MSC
IONP-MSC
N-NV
IONP-NV
F
Relative expression of PI3K
Relative expression of pAKT/AKT

Figure 3.7 E-F

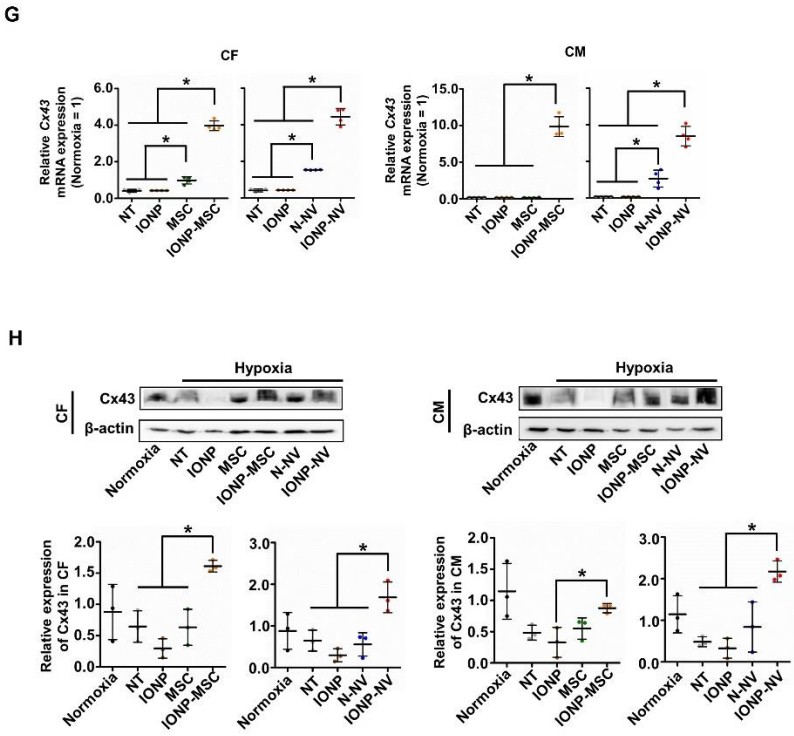
G
CF
CM
Relative Cx43 mRNA expression (Normoxia = 1)
NT
IONP
MSC
IONP-MSC
N-NV
IONP-NV
H
Hypoxia
Cx43
β-actin
Normoxia
Relative expression of Cx43 in CF
Relative expression of Cx43 in CM

Figure 3.7 G-H

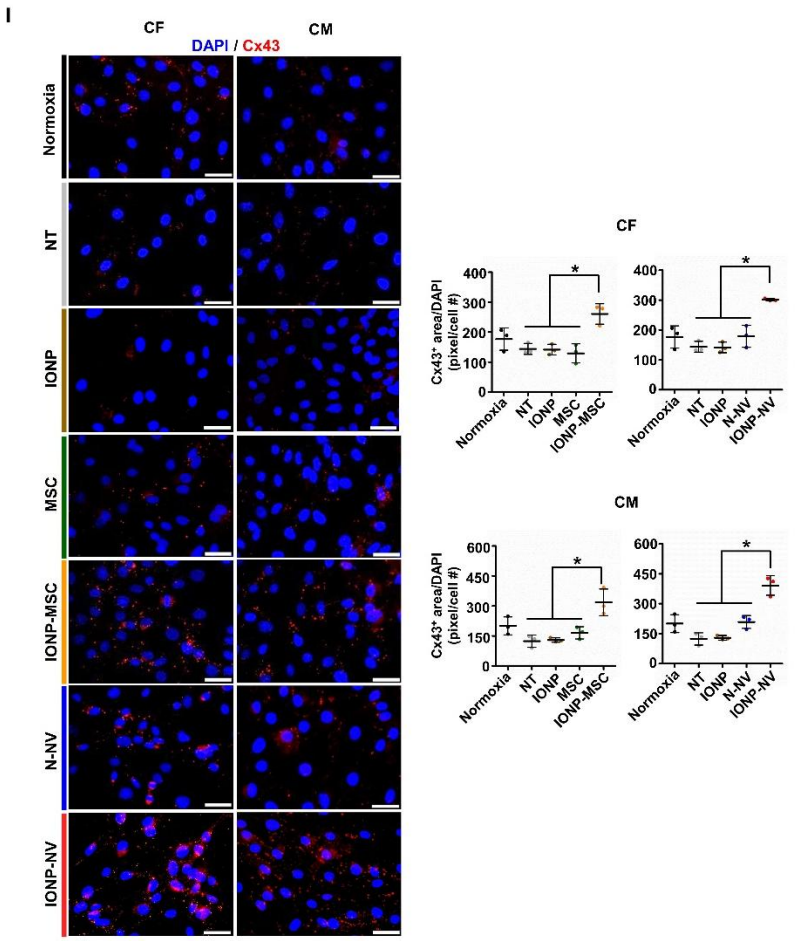

Figure 3.7. Cardioprotective effects of IONP-NVs *in vitro*. (A) Schematic illustration of the *in vitro* cell culture in a hypoxic condition to examine therapeutic effects of IONP-NVs and MSC-secreted paracrine factors *in vitro*. Normoxia or M0 MΦ served as a positive control. NT indicate no treatment. MΦ was used for Fig. 3.9A. (B) Relative cell viability as evaluated by the CCK assay after treatment (n=4 per group). (C) Relative mRNA expression of Caspase3 in CFs, CMs, and HUVECs after treatment, as evaluated by qRT-PCR (n=4 per group). (D) Representative images of viable and nonviable cells stained by FDA/EB after treatment. White arrows indicate dead cells. Scale bars, 100 μm. (E and F) Representative images and the quantification data of western blot analysis for anti-apoptosis-related intracellular signaling cascades in the

CFs, CMs, HUVECs (n=3 per group). (G) Relative mRNA expression of Cx43 in CFs and CMs after treatment, as evaluated by qRT-PCR. (H) Representative images and the quantification data of western blot analysis for Cx43 in CFs and CMs after treatment. (I) Representative images of immunostaining and quantification data for Cx43 (red) in CFs and CMs. Blue indicates DAPI. Scale bars, 50 μm. *$P < 0.05$ by using one-way ANOVA followed by post-hoc Bonferroni test. All data were normalized to normoxia. All values are mean ± SD.

3.2.7. Antifibrotic effects of IONP-NVs *in vitro*

To investigate the antifibrotic effects of NVs and MSCs, gene expression changes in CFs were evaluated using qRT-PCR (Fig. 3.8). NVs and MSCs decreased the expression of the transforming growth factor beta 1 (*Tgfb1*), Alpha-actin 2 (*Acta2*), and matrix metalloproteinase (*Mmp*)-2,9, and increased the tissue inhibitor of metalloproteinase (*Timp*)-1,2, which are the marker of cardiac myofibroblast, within CFs. The data indicate that NVs and MSCs inhibited the differentiation of CFs into cardiac myofibroblasts after hypoxia, which are the major cause of cardiac fibrosis and remodeling. Both IONP-NVs and IONP-MSCs exerted higher antifibrotic effects than those of N-NVs and MSCs, respectively. Taken together, these results demonstrate that IONP-NVs can prevent fibrosis, as MSCs do.

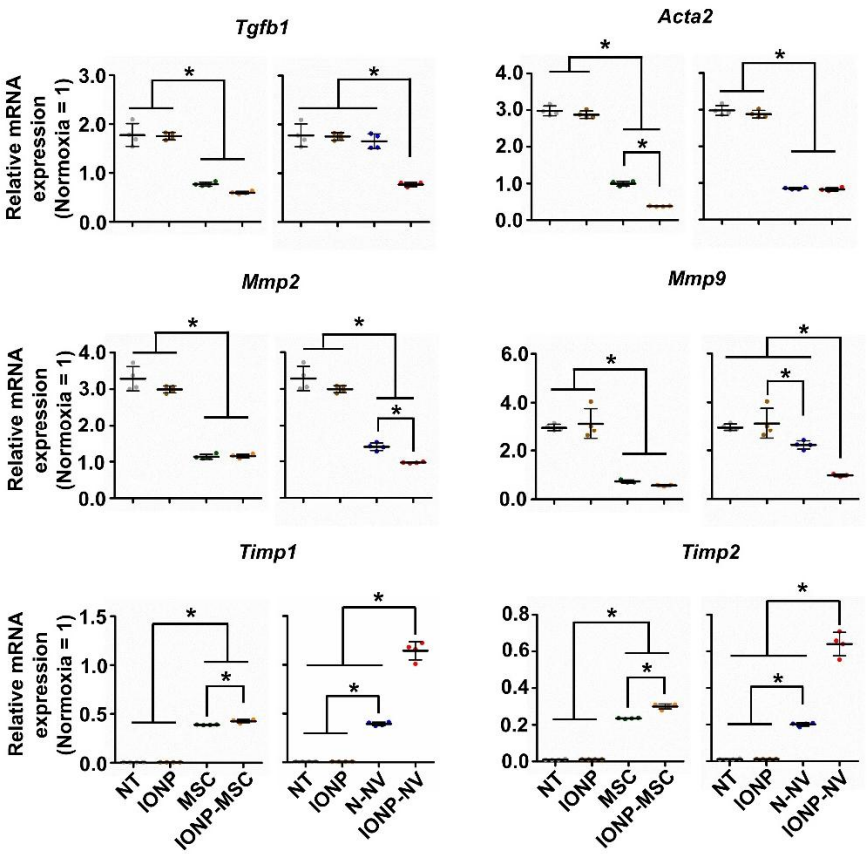

Figure 3.8. Antifibrotic effects of IONP-NVs *in vitro*. Relative mRNA expression levels of cardiac myofibroblast-related genes in CFs after treatment, as evaluated by qRT-PCR (n = 4 per group). NT indicates no treatment. *P < 0.05 by using one-way ANOVA followed by post-hoc Bonferroni test. All values are mean ± SD.

3.2.8. Anti-inflammatory effects of IONP-NVs *in vitro*

We next examined the anti-inflammatory effects of NVs and MSCs on cells, including CFs, CMs, and macrophages *in vitro*. The experimental protocol is described in Fig. 3.7A. We examined the effects of NVs and MSCs on the phenotype change in M1 macrophages. NVs and MSCs downregulated the mRNA expression levels of inflammatory M1 macrophage markers and upregulated those of reparative M2 macrophage markers (Fig. 3.9A). M0 macrophages served as a control. IONP-NVs and IONP-MSCs exerted stronger effects on the M1 macrophage shift to M2 macrophage than N-NVs and MSCs, respectively. In addition, NVs and MSCs decreased the mRNA expression levels of pro-inflammatory cytokines including *Il6* and *Tnfa* in CFs and CMs (Fig. 3.9B). IONP-NVs and IONP-MSCs exerted a higher anti-inflammatory effect on CFs and CMs than N-NVs and MSCs, respectively. Thus, our data indicate that, like MSC implantation, IONP-NV treatment can exert anti-inflammatory effects via polarizing M1 macrophages into M2 phenotype and reducing inflammatory cytokine production of CMs and CFs.

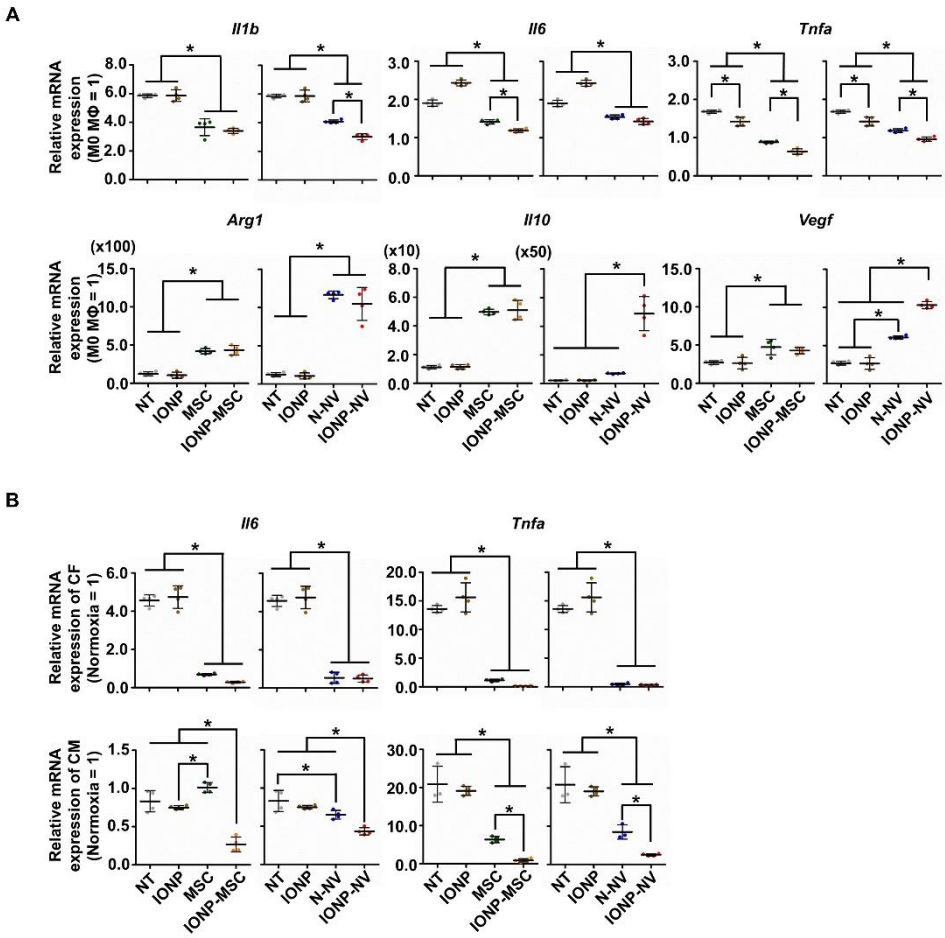

Figure 3.9. Anti-inflammatory effects of IONP-NVs *in vitro*. (A) Macrophage (MΦ) polarization after treatment. Relative mRNA expression levels of the markers of inflammatory M1 macrophages (Il1b, Il6, and Tnfa) and reparative M2 macrophages (Arg1, Il10, and Vegf) in LPS-treated macrophages (M1 MΦ) after treatment, as evaluated by qRT-PCR (n=4 per group). (B) Relative mRNA expression of inflammatory cytokines (Il6 and Tnfa) in CFs and CMs (n=4 per group). NT indicates no treatment. *P < 0.05 by using one-way ANOVA followed by post-hoc Bonferroni test. All data were normalized to normoxia or M0 MΦ. All values are mean ± SD.

3.2.9. Proangiogenic effects of IONP-NVs *in vitro*

We further evaluated the pro-angiogenic effects of NVs and MSCs *in vitro*. NVs and MSCs stimulated the capillary formation of HUVECs cultured under hypoxic conditions (Fig. 3.10A and B). IONP-NVs exerted a higher effect on tube formation compared to N-NVs. The enhanced capillary formation may be mediated via activating ERK and PCNA signaling in HUVECs (Fig. 3.10C), which inhibits p38 that is known to break down capillary tubes [77]. In addition, proliferating HUVECs also increased, which may result in increased capillary tube formation. HUVEC migration was reduced by hypoxia and returned back to normal by NVs and MSCs. IONP-NVs and IONP-MSCs exerted higher effects on the HUVEC migration than N-NVs and MSCs, respectively.

Synthetically, we demonstrated that like MSCs, IONP-NVs exhibit therapeutic effects on CFs, CMs, HUVECs, and macrophages *in vitro*. IONP-NVs not only reduced apoptosis, fibrosis, and inflammation but also increased angiogenesis, which is the major mechanism of MSCs for cardiac repair. Thus, the data suggest that IONP-NVs can be an effective cell-free option that replaces MSC implantation therapy for cardiac repair.

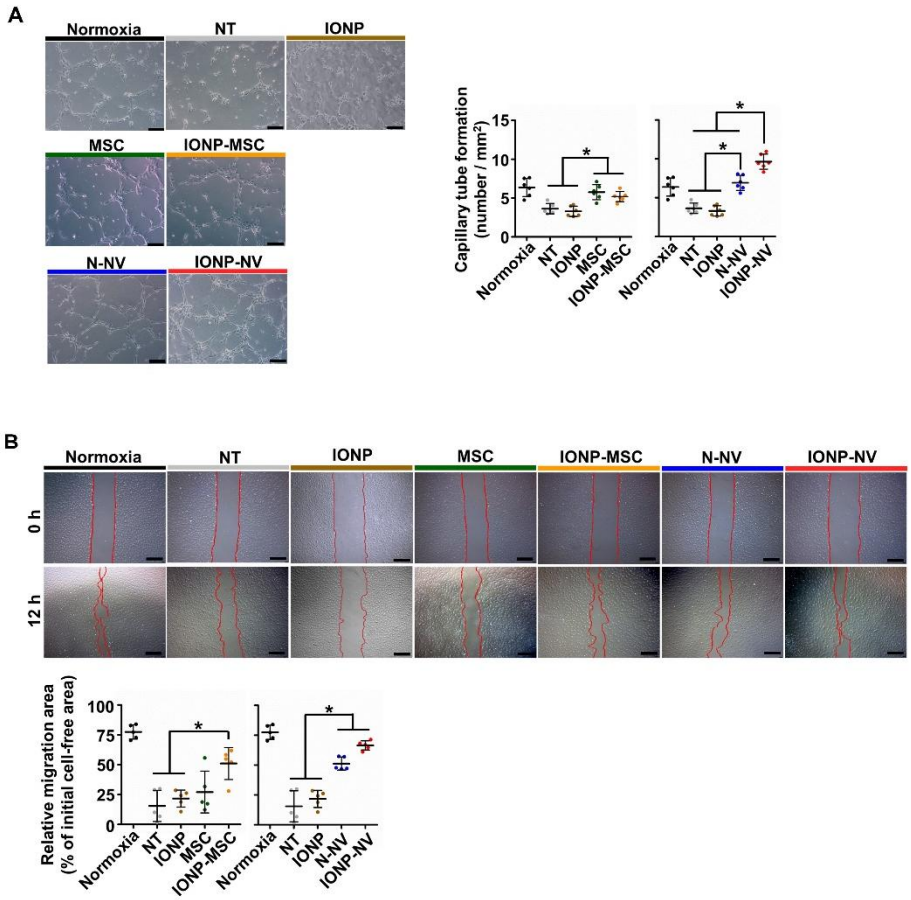

Figure 3.10 A-B

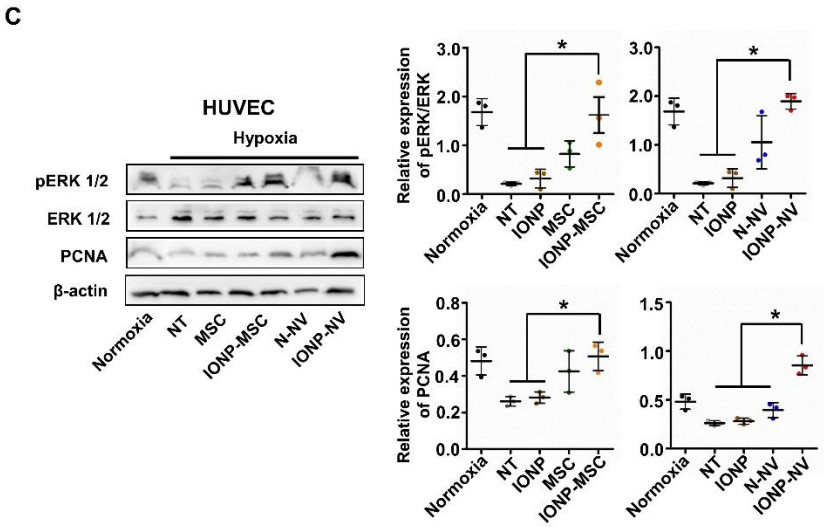

Figure 3.10. Proangiogenic effects of IONP-NVs *in vitro*. (A and B) Capillary tube formation (n = 6 per group) and cell migration (n = 5 per group) of HUVECs after treatment. Red lines indicate borders of the cell-free area. Scale bars, 200 and 500 μm, respectively. (C) Representative images and the quantification data of western blots of HUVECs for PCNA, ERK 1/2, and pERK 1/2 after treatment. NT indicates no treatment. *P < 0.05 by using one-way ANOVA followed by post-hoc Bonferroni test. All data were normalized to normoxia. All values are mean ± SD.

3.2.10. Increased retention of IONPs by magnetic guidance in the infarcted myocardium

To determine whether NVs are superior to MSCs for retention in the myocardium and whether magnetic guidance enhances the retention of IONP-NVs in the myocardium, we intramyocardially injected MSCs, IONP-MSCs, N-NVs, and IONP-NVs both of which were labeled with fluorescent dyes, and magnetic guidance was applied for 24 hours. We injected 10^6 cells of MSCs or 150 μg of NVs, which are correspond to the production yield of NVs from MSCs. The data showed that NVs were superior to MSCs for retention in the myocardium 24 hours after injection (Fig. 3.11A). Furthermore, IONP-NV + M group exhibited the highest retention in the heart. The biodistribution of the MSCs and NVs in other organs of the animals is presented in Fig. 3.11B. In addition, the retention ratio of IONP-NVs with magnetic guidance was gradually decreased in the infarcted heart with the time (Fig. 3.11C). To further assess the increased retention of IONP-NVs by magnetic guidance, we used magnetic resonance imaging (MRI) analysis, as previously described.[78] As shown in Fig. 3.11D, r_2 value of IONP was 163.95 $s^{-1}mM^{-1}$ and the retention of IONP-NVs was significantly augmented by magnetic guidance. Fluorescent images and the quantification data also indicate that IONP-NVs with magnetic guidance exhibited the highest retention in the infarcted myocardium (Fig. 3.11E).

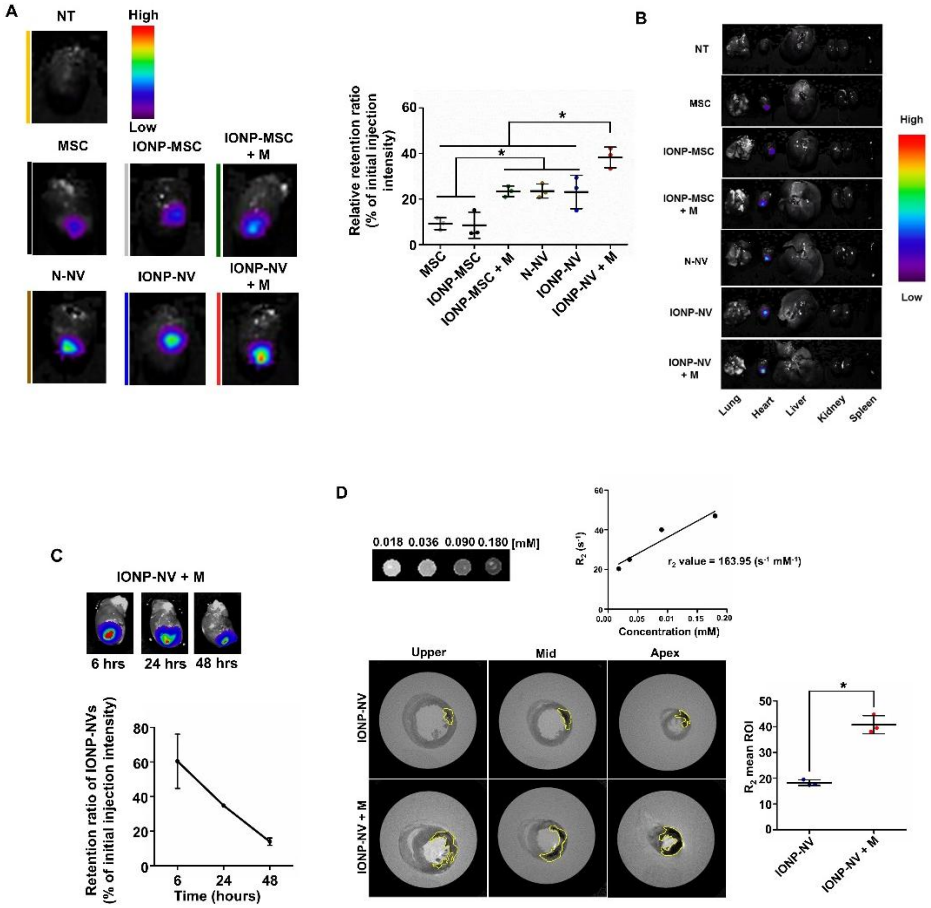

Figure 3.11 A-D

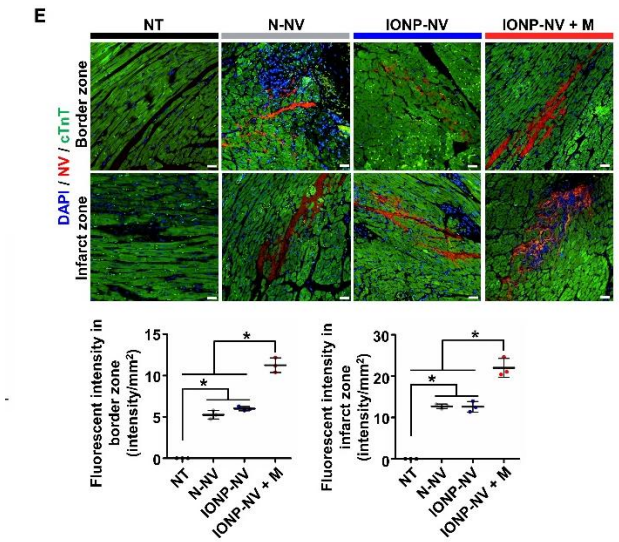

Figure 3.11. Increased retention of IONPs by magnetic guidance in the infarcted myocardium. Fluorescent dye-labeled IONP-MSCs and IONP-NVs were injected into the rat infarcted myocardium. In some groups, magnetic guidance (M) was applied above the hearts for 24 hours after injection. (A) Representative *ex vivo* fluorescent imaging of infarcted hearts and the quantitative data 24 hours after the injection of Vivotrack 680-labeled MSCs, IONP-MSCs, N-NVs, and IONP-NVs (n = 3 animals per group). *P < 0.05 by using one-way ANOVA followed by post-hoc Bonferroni test. (B) Biodistribution of MSCs, IONP-MSCs, N-NVs, and IONP-NVs 24 hours after injection. Fluorescently labeled MSCs, IONP-MSCs, N-NVs, and IONP-NVs were injected into the infarcted myocardium and magnetic guidance (M) was applied for 24 hours or not. (C) The retention ratio of fluorescently labeled IONP-NVs in infarcted heart with magnetic guidance 6, 24, and 48 hours after injection. (D) Representative magnetic resonance images and the quantification of IONP within heart 24 hours after the injection of IONP-NVs (n = 3 animals per group). NT indicates no treatment. The yellow line indicates IONP retention area. *P < 0.05 by using two-tailed t-test. All values are mean ± SD.

3.2.11. Cytotoxicity of IONP-NVs with magnetic guidance *in vivo*

To determine whether IONPs with magnetic guidance exhibit cytotoxic effects *in vivo*, TUNEL assay was performed 24 hours after IONP-NVs injection into the normal hearts (Fig. 3.12A). Magnetic field-applied IONPs did not exhibit the cytotoxic effect on cells *in vivo*. In addition, the levels of hepatic enzymes (aspartate aminotransferase (AST) and alanine aminotransferase (ALT)), blood urea nitrogen (BUN), and creatinine were not significantly different from those of the normal group 1, 3, 7, 14, 21, and 28 days after injection (Fig. 3.12B). Furthermore, to determine whether IONPs remain in heart or travel to other organs, we stained IONPs using Prussian blue staining in major organs 1 and 4 weeks after injection (Fig. 3.12C). IONPs did not detected in organs except heart. Also, IONPs were decreased in the heart with time.

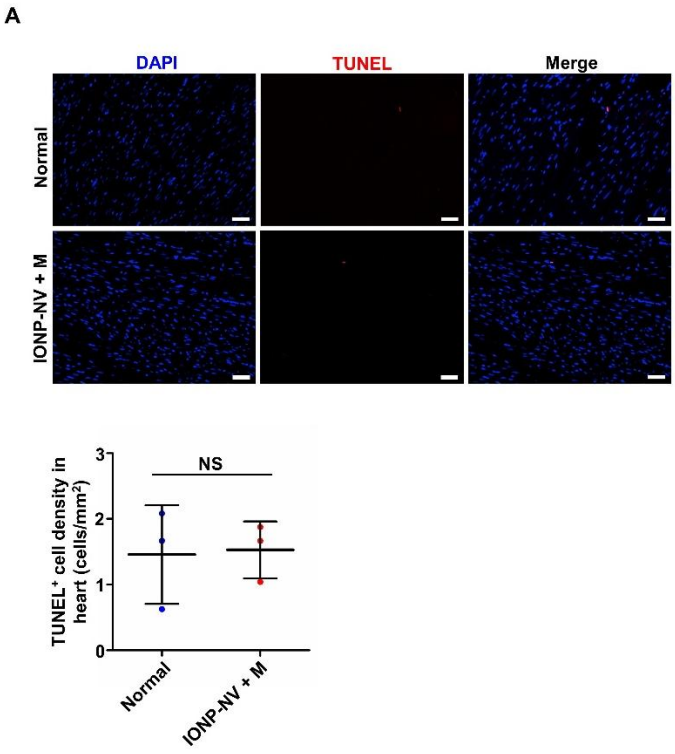
A
DAPI
TUNEL
Merge
Normal
IONP-NV + M
NS
TUNEL+ cell density in heart (cells/mm2)
3
2
1
0
Normal
IONP-NV + M

Figure 3.12 A

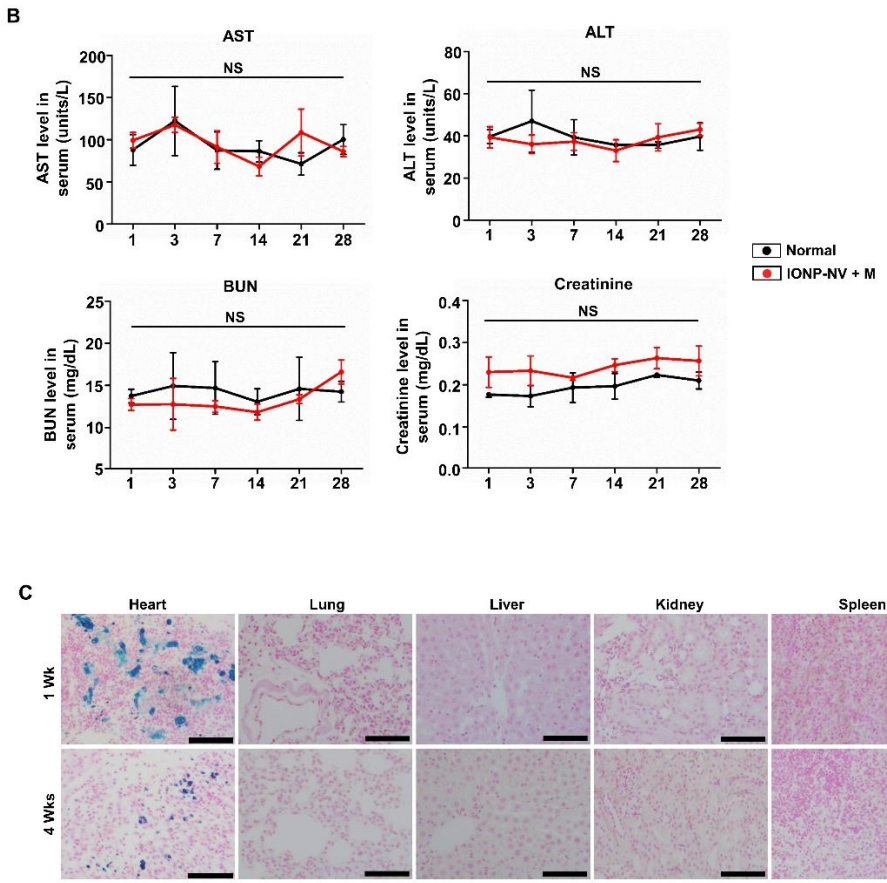

Figure 3.12. Cytotoxicity of IONP-NVs with magnetic guidance *in vivo*. (A) Representative images of TUNEL (red)-positive apoptotic cells in the heart and the quantitative data 24 hours after the injection of IONP-NVs into normal heart (n = 3 animals per group). Scale bars, 50 μm. NS, No significant difference. Two-tailed t-test was used. (B) The levels of creatinine, BUN, AST, and ALT in the serum 1, 3, 7, 14, 21, and 28 days after injection. NS, No significant difference. Two-way ANOVA followed by post-hoc Bonferroni test was used. All values are mean ± SD. (C) The fate of IONPs 1 and 4 weeks after injection. The detection of IONPs in major organs using Prussian blue staining 1 and 4 weeks after injectipon. Magnetic guidance was applied for 1 day.

Blue indicates IONPs. Nuclear fast red staining was used for counter-staining. Scale bars, 100 μm.

3.2.12. Attenuation of cell apoptosis and inflammation IONP-NVs with magnetic guidance *in vivo*

To investigate the antiapoptotic effects of IONP-NVs in the infarcted myocardium, the TUNEL assay was performed 24 hours after injection (Fig. 13A). In the border zone, cell apoptosis was reduced by the injection of either N-NVs or IONP-NVs, and further decreased in the IONP-NV + M group. In the infarct zone, only the IONP-NV + M group exhibited decreased apoptosis. The Cx43 expression in the peri-infarct zone was assessed with immunohistochemistry (Fig. 13B). The IONP-NV + M group exhibited a higher level of Cx43 in the peri-infarct zone compared to the other groups, which may be attributed to the reduction of cell death and arrhythmia at the early stage of infarction.

Next, we examined the anti-inflammatory effects of NVs in the infarcted myocardium through evaluation of macrophage polarization 1 day after injection (Fig. 3.13C). The data showed that only the IONP-NV + M group exhibited upregulated expression levels of reparative M2 macrophage-specific markers (*Cd206*, *Arg1*, and *Il10*). The N-NV, IONP-NV, and IONP-NV + M groups downregulated expression levels of M1 macrophage-specific markers (*Nos2*, *Il1b*, *Il6*). Immunohistochemistry showed that the IONP-NV + M group significantly upregulated CD206 expression and downregulated NOS2 expression in CD68-positive macrophages in the peri-infarct zone (Fig. 3.13D). The data suggest that IONP-NVs can effectively induce early transition of the inflammatory phase to the reparative phase by facilitating the rapid polarization of M1 macrophages into M2 macrophages, which may elicit cardiac repair after MI, as a previous study revealed.[79]

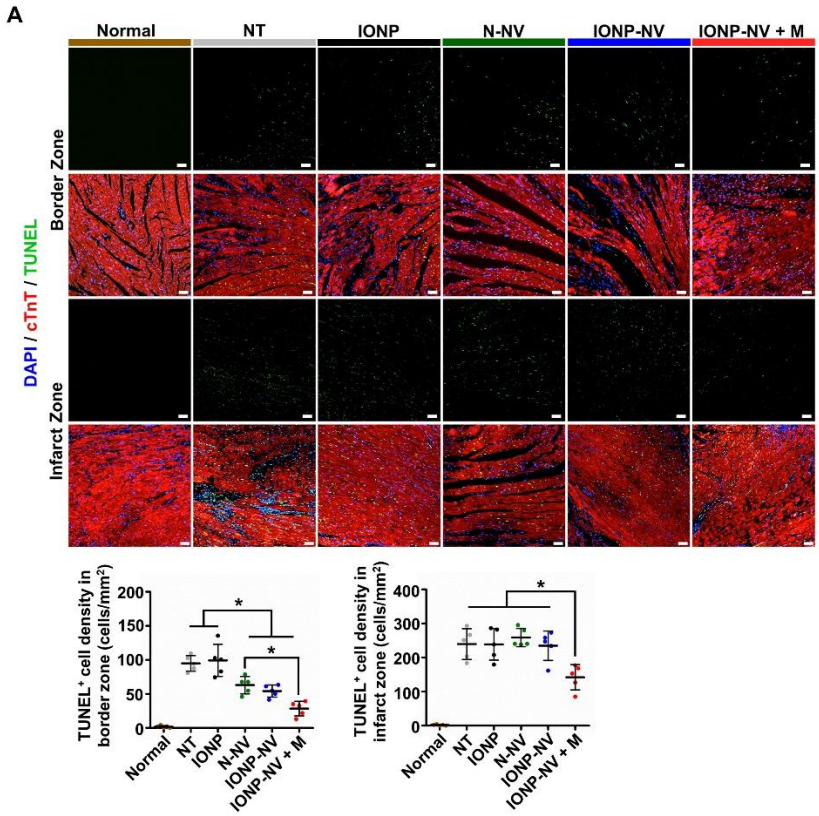
A
Normal
NT
IONP
N-NV
IONP-NV
IONP-NV + M
Border Zone
Infarct Zone
DAPI / cTnT / TUNEL
TUNEL+ cell density in border zone (cells/mm2)
TUNEL+ cell density in infarct zone (cells/mm2)
Normal
NT
IONP
N-NV
IONP-NV
IONP-NV + M

Figure 3.13 A

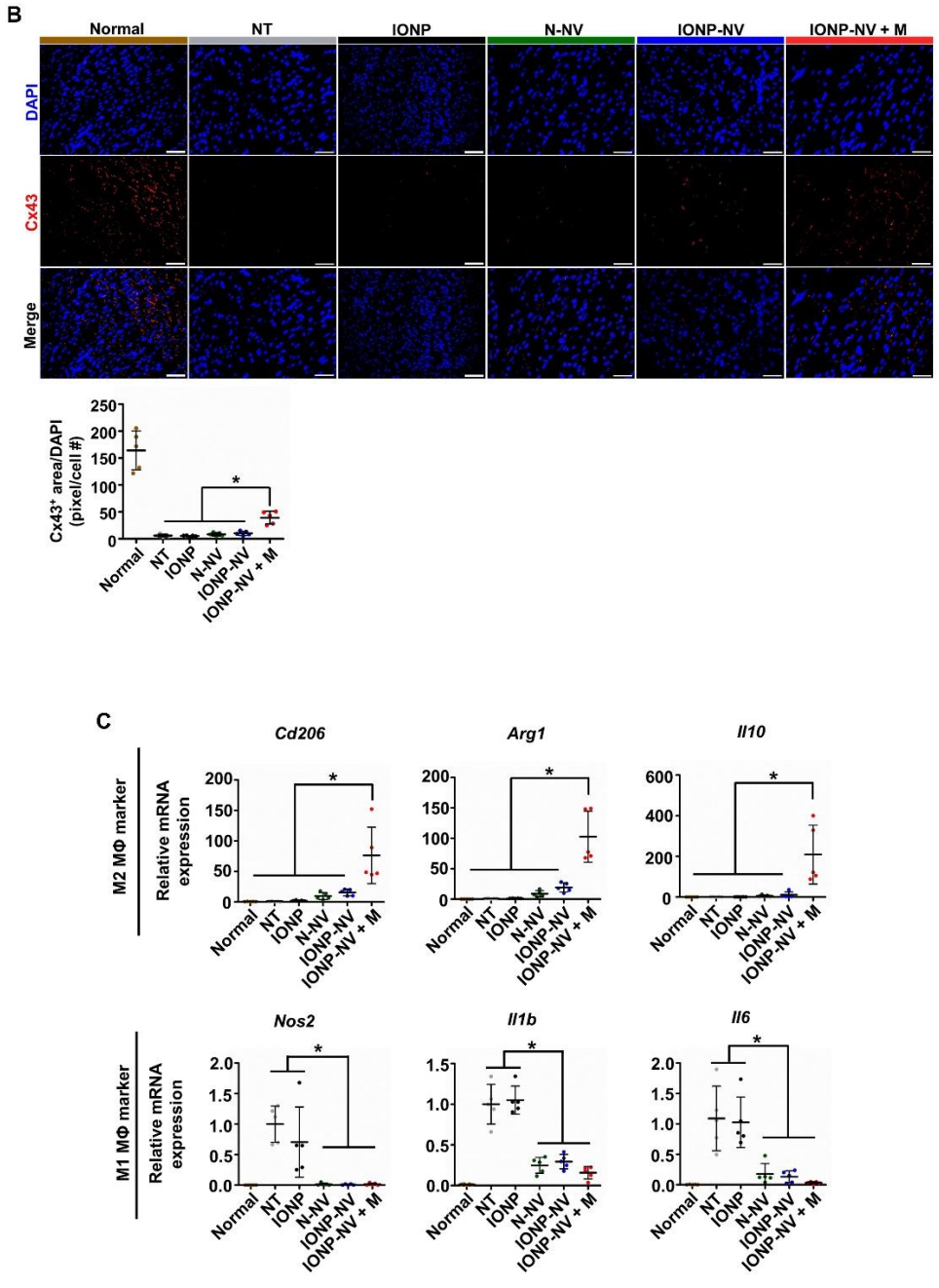

Figure 3.13 B-C

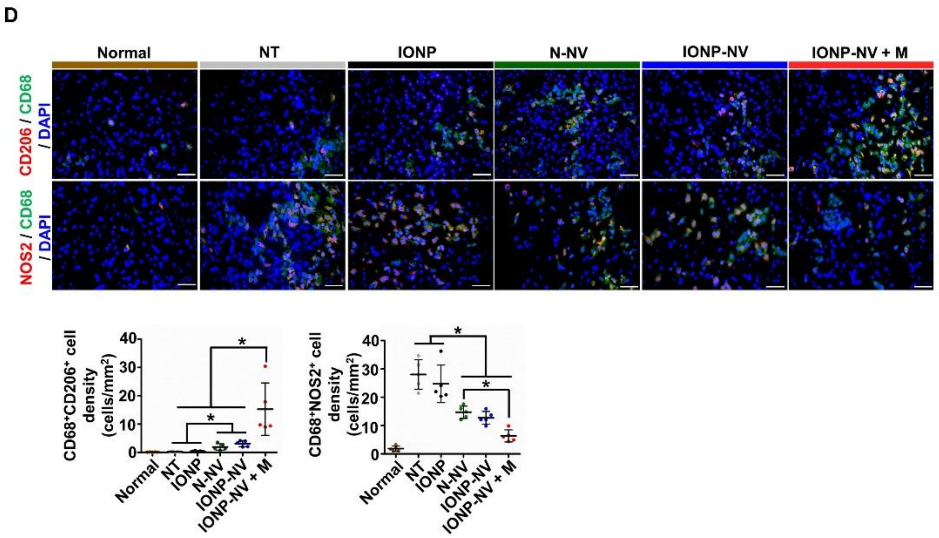

Figure 3.13. Attenuation of cell apoptosis and inflammation IONP-NVs with magnetic guidance *in vivo*. (A) Representative images of TUNEL (green)-positive apoptotic cells and immunostaining for cTnT (CM marker), and the quantitative data 1 day after injection (n = 5 animals per group). Scale bars, 100 μm. (B) Representative images of immunohistochemical staining for Cx43 in the peri-infarct zone and the quantitative data 1 day after injection (n = 5 animals per group). Scale bars, 100 μm. (C) Relative mRNA expression levels of M2 macrophage-specific markers (Cd206, Arg1, and Il10) and M1 macrophage-specific markers (Nos2, Il1b, and Il6) in the infarcted myocardium, as evaluated by qRT-PCR (n = 5 animals per group). (D) Immunohistochemical staining for CD68 (macrophage marker), CD206 (M2 macrophage marker), and NOS2 (M1 macrophage marker) and the quantitative data in the peri-infarct zone 1 day after injection (n = 5 animals per group). Scale bars, 50 μm. NT indicates no treatment. *P < 0.05 by using one-way ANOVA followed by post-hoc Bonferroni test. All values are mean ± SD.

3.2.13. Increased blood vessel density and improved left ventricular remodeling by IONP-NVs with magnetic guidance *in vivo*

To determine whether the NV injection into the infarcted myocardium enhances the blood vessel density, hearts were perfused with isolectin B4 four weeks post-MI (Fig. 3.14A). The IONP-NV + M group exhibited a significant increase in the blood vessel density in both the border zone and infarct zone, compared to the other groups. In addition, IONP-NV also increased the blood vessel density in the border zone and infarct zone as compared to the NT group. This may be attributed to the attenuation of early apoptosis of the ECs (Fig. 3.7B and 3.13A) and the stimulation of migration, proliferation, and tube formation of the ECs (Fig. 3.10A-C).

Four weeks after treatment, heart tissues were stained with Masson's trichrome staining (Fig. 3.14B). The IONP-NV injection and magnetic guidance resulted in a significant decrease in the fibrosis area and scar size and increase in the viable myocardium area and infarcted wall thickness in the infarcted heart (Fig. 3.14C). In addition, IONP-NV also decreased fibrosis area and increased infarcted wall thickness as compared to the NT group and the IONP group.

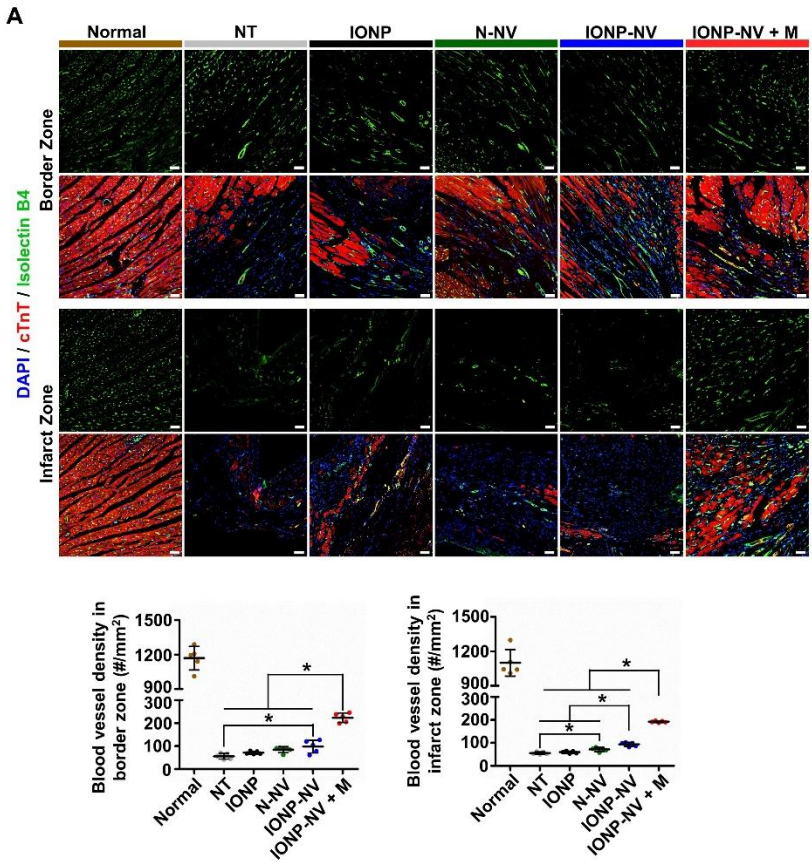
A
Normal
NT
IONP
N-NV
IONP-NV
IONP-NV + M
Border Zone
Infarct Zone
DAPI / cTnT / Isolectin B4
Blood vessel density in border zone (#/mm²)
Blood vessel density in infarct zone (#/mm²)
1500
1200
900
300
200
100
0
*
Normal
NT
IONP
N-NV
IONP-NV
IONP-NV + M

Figure 3.14 A

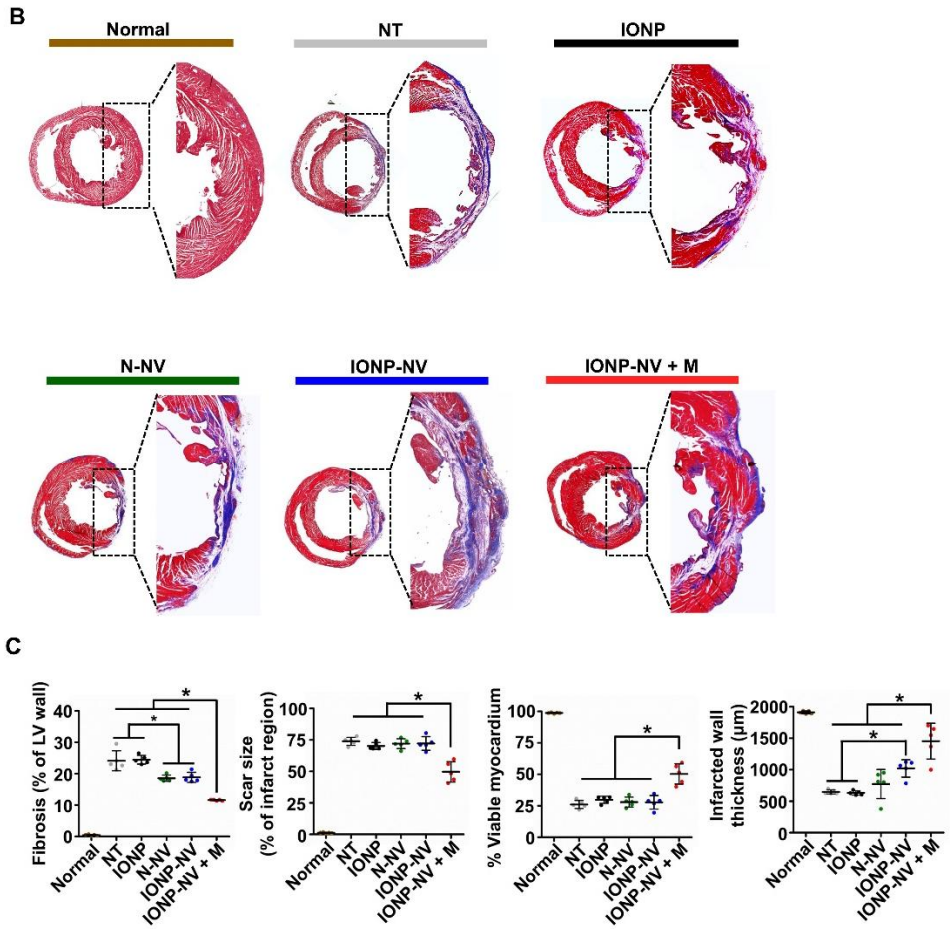

Figure 3.14. Increased blood vessel density and improved left ventricular remodeling by IONP-NVs with magnetic guidance *in vivo*. (A) Representative images of functional blood vessels visualized by perfusion of isolectin B4 and immuostaining for cTnT (CM marker) in the infarct zone and border zone four weeks after injection and the quantitative data (n = 5 animals per group). Scale bars, 50 μm. (B) Representative Masson's trichrome-stained infarcted hearts four weeks after injection (blue, scar tissue; red, viable myocardium). (C) The fibrosis area, scar size, viable myocardium area, and thickness of the LV wall four weeks after injection (n = 5 animals per group). *P < 0.05 by using one-way ANOVA followed by post-hoc Bonferroni test.

3.2.14. Enhanced cardiac function recovery by IONP-NVs with magnetic guidance *in vivo*

To evaluate cardiac functional recovery, transthoracic echocardiography was performed 1, 2, and 4 weeks post-MI (Fig. 3.15A-C). All groups except the IONP-NV + M group showed a significant decrease in the ejection fraction and fractional shortening at 2 and 4 weeks as compared to 1 week. In the IONP-NV + M group, cardiac contractibility, such as ejection fraction and fractional shortening, was preserved or increased during the 4-week follow-up period (Fig. 3.15B and C). Additionally, there was no significant difference in the left ventricular end diastolic dimension (LVIDd) among all groups except for the normal group (Fig. 3.15D). However, the left ventricular end systolic dimension (LVIDs) was significantly lower in the IONP-NV + M group than in the NT group and the IONP group at 4 weeks (Fig. 3.15E). Furthermore, there was no significant difference in the posterior wall thickness among all groups (Fig. 3.15F). However, septal wall thickness was significantly higher in the IONP-NV + M group than in other groups at 4 weeks (Fig. 3.15G). In addition, we further assessed dose-dependent therapeutic effects of IONP-NVs with magnetic guidance (Fig. 3.15H and I). IONP-NVs improved the cardiac functions dose-dependently in 1.0x and 3.0x compared to NT group, but not in 0.3x. The heart functions were not different between 1.0x IONP-NVs and 3.0x IONP-NVs. These data indicate that IONP-NVs with magnetic guidance can prevent adverse left ventricular remodeling and lead to cardiac function preservation, which is likely attributed to the high retention of injected IONP-NVs, attenuation of cell apoptosis, inflammation, and fibrosis, and the enhancement in blood vessel density in the infarcted myocardium (Fig. 5 and 6).

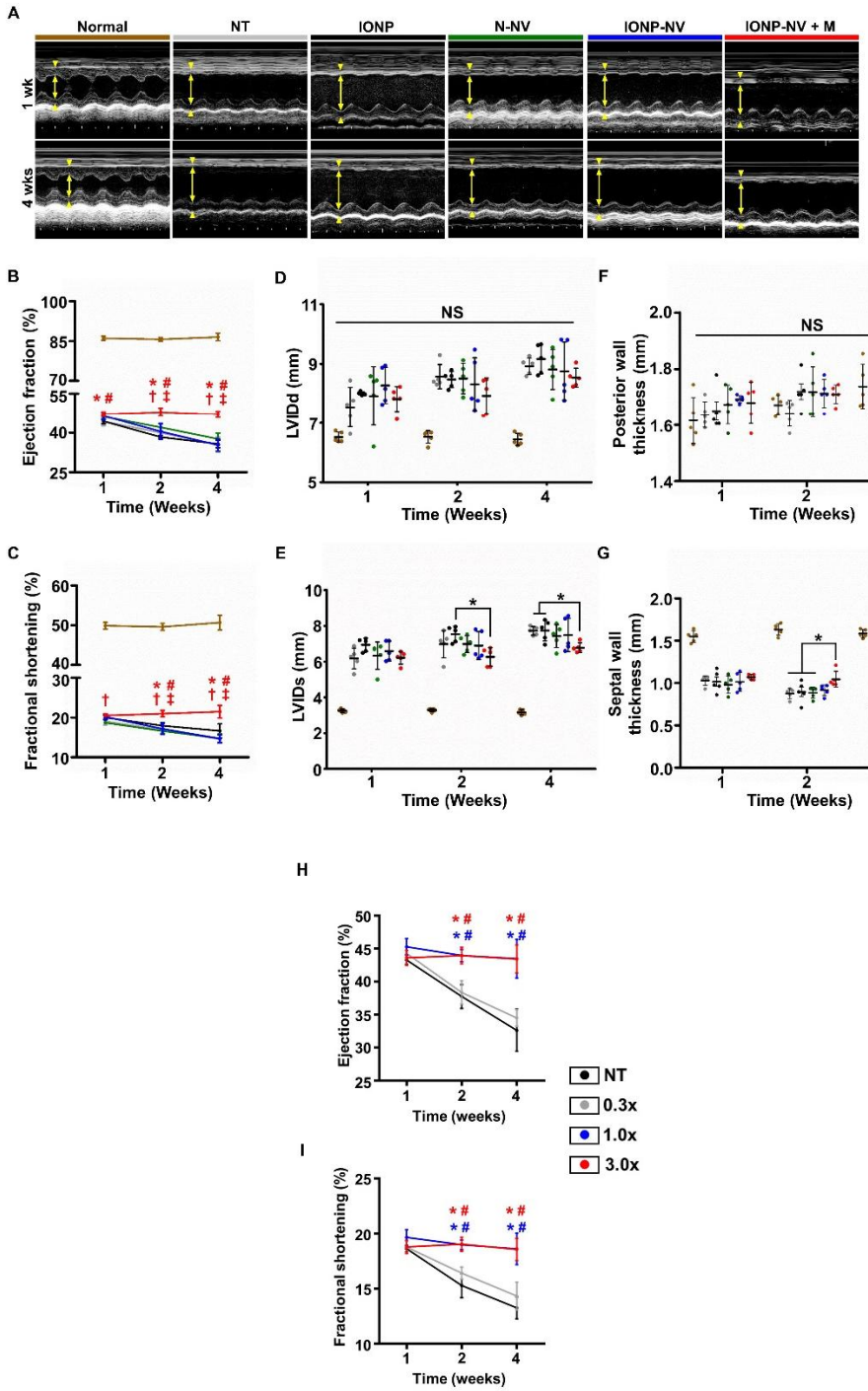
A
Normal
NT
IONP
N-NV
IONP-NV
IONP-NV + M
1 wk
4 wks
B
Ejection fraction (%)
Time (Weeks)
C
Fractional shortening (%)
Time (Weeks)
D
LVIDd (mm)
NS
Time (Weeks)
E
LVIDs (mm)
Time (Weeks)
F
Posterior wall thickness (mm)
NS
Time (Weeks)
G
Septal wall thickness (mm)
Time (Weeks)
H
Ejection fraction (%)
Time (weeks)
NT
0.3x
1.0x
3.0x
I
Fractional shortening (%)
Time (weeks)

Figure 3.15. Enhanced cardiac function recovery by IONP-NVs with magnetic guidance *in vivo*. (A) Representative M-mode images one week and four weeks after treatment. Yellow arrows between wall motion indicate left ventricular dimension. Distance between yellow arrows and arrowheads in upper and lower area indicates left ventricular wall thickness and left ventricular posterior wall thickness, respectively. (B and C) Ejection fraction and fractional shortening at various time points (n = 5 animals per group). *P < 0.05 versus NT, #P < 0.05 versus IONP, †P < 0.05 versus N-NV, and ‡P < 0.05 versus IONP-NV by using two-way ANOVA followed by post-hoc Bonferroni test. (D and E) Left ventricular end diastolic dimension (LVIDd) and left ventricular end systolic dimension (LVIDs) at various time points (n = 5 animals per group). Posterior wall thickness and septal wall thickness at various time points (n = 5 animals per group). *P < 0.05 by using two-way ANOVA followed by post-hoc Bonferroni test. The group names are referred to Fig. 3.14A-C. (H and I) Dose-dependent effects of IONP-NVs on heart functions *in vivo*. Echocardiography was performed 1, 2, and 4 weeks after injection of IONP-NV with magnetic guidance (IONP-NV + M). The dose of 1.0x indicate 150 μg NV per animal. (H) Ejection fraction and (I) fractional shortening (n = 5 animals per group). *P < 0.05 versus NT and #P < 0.05 versus 0.3x by using two-way ANOVA followed by post-hoc Bonferroni test. NT indicates no treatment. All values are mean ± SD.

Chapter 4.

Targeted delivery of mesenchymal stem cell-derived nanovesicles for spinal cord injury treatment

4.1. Introduction

Traumatic spinal cord injury (SCI) is a serious medical condition that causes permanent motor and sensory dysfunction. SCI is a complex dynamic process that initiates a complex cascade of secondary injury mechanisms including hemorrhage, ischemia, apoptosis, inflammation, demyelination, and glial scar formation[80] The inhibitory environment around the axons suppresses the axonal regeneration, and the synaptic plasticity is insufficient for substantial functional improvement. Recently, mesenchymal stem cell (MSC) therapies have emerged for spinal cord repair because of its multifunctional therapeutic abilities for neuroprotection, anti-inflammation, and angiogenesis.[81-89]

However, MSC therapies are limited by several obstacles. Direct injection of MSCs into the injured spinal cord could provide further damage.[8] Also, systemically injected MSCs can rarely reach the lesion site because of the pulmonary entrapment of MSCs.[8] Moreover, the therapeutic efficacy of implanted MSCs can be limited because of the poor survival and the possibility of the differentiation into other cell types including chondrocytes and osteoblasts.[90] To avoid these limitations, MSC-conditioned medium has been suggested as an alternative to the transplantation of MSCs for SCI.[91] Recent studies have revealed that the therapeutic effects of MSCs are mainly attributed to exosomes, which are a type of extracellular vesicles that contain RNAs and proteins and serve as a nanocarrier of the biomolecules between cells.[92, 93] Proteins and RNAs in exosomes are transferred to recipient cells and affect the recipient cells via protein functions and RNA translation.[10, 94] In preclinical studies, MSC-derived exosomes have shown therapeutic potential for numerous diseases including myocardial infarction, ischemic vascular diseases, neurodegenerative diseases, and SCI.[23, 33, 57, 95-98] MSC-

derived exosomes exert therapeutic effects via anti-apoptosis, immunomodulation, anti-inflammation, and angiogenesis, which is similar to the therapeutic effects of MSCs. MSC-derived exosomes have a lower possibility of an immune response.[18] Importantly, MSC-derived exosomes therapies can avoid the major limitations of MSC therapy. MSC-derived exosomes therapies can avoid the problems of poor MSC survival and possible MSC-differentiation into other cell types. Exosomes exhibit less entrapment in the lung following systemic administration due to their small size and can also be stored at - 80 °C, which costs much less than MSC storage at -196 °C. In this context, MSC-derived exosome therapies have emerged as a substitute for MSC therapies.[99]

Although exosomes therapies have shown therapeutic potential, large-scale production of exosomes is a barrier for clinical applications. One million MSCs secrete 1-4 μg of exosomes per day, which can hardly meet the demand for clinical trials.[34, 60] Therefore, to produce sufficient amounts of exosomes from MSCs for clinical applications, cultures of a large number of MSCs and long-term cultures are required. To overcome these obstacles, recent studies have developed NVs. NVs have particle size and component including intracellular RNAs, proteins, and plasma membrane proteins similar to those of exosomes and can transfer biomolecules from parent cells to recipient cells like exosomes.[36, 61] NVs are generated through the serial extrusion of cells via microporous and nanoporous filters, while exosomes are secreted from cells. Importantly, 250-fold larger quantity of NVs can be obtained than exosomes from the same number of cells.[35] Furthermore, each NV contains a 2-fold greater quantity of RNAs and proteins than each exosome.[35] Taken together, NVs would be advantageous over exosomes in terms of production, cost-effectiveness, and therapeutic efficacy. Therefore, in the

present study, we used MSC-derived NVs for SCI treatment rather than MSC-derived exosomes.

Despite the advantages of NVs and exosomes over MSCs therapies, NVs and exosomes do not have the ability to target to diseased organs after systemic injection, which limits the therapeutic efficacy of NV or exosome therapies.[38, 39] To improve the diseased organ-targeting efficiency of NVs, here we fabricated MF-MSCs and then produced MF-NVs through the extrusion of MF-MSCs (Figure 1). Macrophage membranes contain binding molecules such as very late antigen 4 (VLA4) comprising integrin α4 and β1 and the various receptors of inflammatory cytokines. The membrane proteins included in MF-NVs may facilitate the targeting of MF-NVs at the inflammatory tissues and scavenge inflammatory cytokines.[100-102] MF-NVs contain integrin α4 and β1 originated from macrophage membrane and may improve the efficiency of NVs targeting to ischemic and inflammatory organs such as the injured spinal cord. Furthermore, autologous macrophages have been used for large animal model and clinical uses[103, 104], which can facilitate the application of MF-NVs for clinical uses in future. Here, we found that both normal MSC-derived NVs (N-NVs) and MF-NVs exhibited neuroprotective, anti-inflammatory, and angiogenic effects *in vitro*, which are the major therapeutic mechanisms of spinal cord repair. Following the systemic injection into mice with SCI, MF-NVs showed better spinal cord targeting efficiency and therapeutic efficacy than N-NVs.

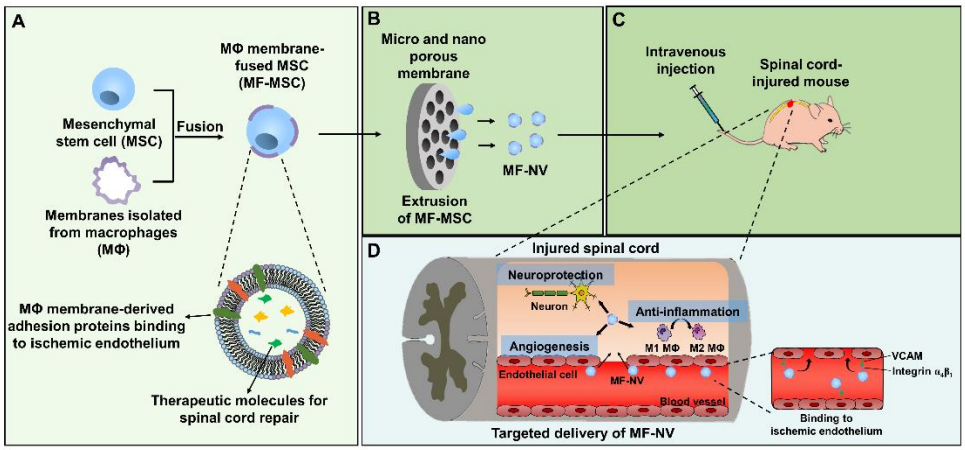

Figure 4.1. Schematic diagrams for the fabrication and therapeutic effects of MF-NVs for spinal cord repair. (A) The preparation of MF-MSC through the fusion of macrophage (MΦ) membranes into MSCs. MF-MSCs contain the membrane proteins of MΦ and the therapeutic molecules. (B) Production of MF-NVs from MF-MSCs by serial extrusion. (C) Intravenous injection of MF-NVs into the spinal cord-injured mouse. (D) The mechanisms of targeting and therapeutic effects of MF-NVs on SCI-injured mice.

4.2. Results and discussion

4.2.1. Production and characterization of MF-MSCs

We first obtained the membranes of macrophages through dissociation and extrusion. The size distribution of macrophage membranes is shown in Fig. 4.1A. We then fused the membranes of macrophages into MSCs using PEG. To determine whether the membranes were integrated into MSCs, we characterized the MF-MSCs. Fluorescent microscopic images showed that DiO-labeled MSCs (green) were decorated with DiI-labeled macrophage membranes (red) (Fig.4.2B). To demonstrate that the overlapping of fluorescent signals was not due to dye transfer, we evaluated the surface markers of MSCs and MF-MSCs using western blot analysis (Fig. 4.2C). MF-MSCs contained CD68, a surface marker of macrophages, indicating that macrophage membranes were integrated into MSCs. Integrin α4 and integrin β1, known as VLA4, were also highly expressed in MF-MSCs than MSCs. VLA4 on the surface of circulating monocytes facilitates monocyte binding to the inflammatory endothelium.[105] The enhanced expression of VLA4 on the membrane of MF-MSCs indicated that MF-MSCs inherit the binding ability of macrophages to the inflammatory sites. Flow cytometry analyses confirmed that a macrophage marker (F4/80) was expressed on MF-MSCs, but not on MSCs (Figure 4.2D). An MSC marker (CD90) was expressed on both MSCs and MF-MSCs.

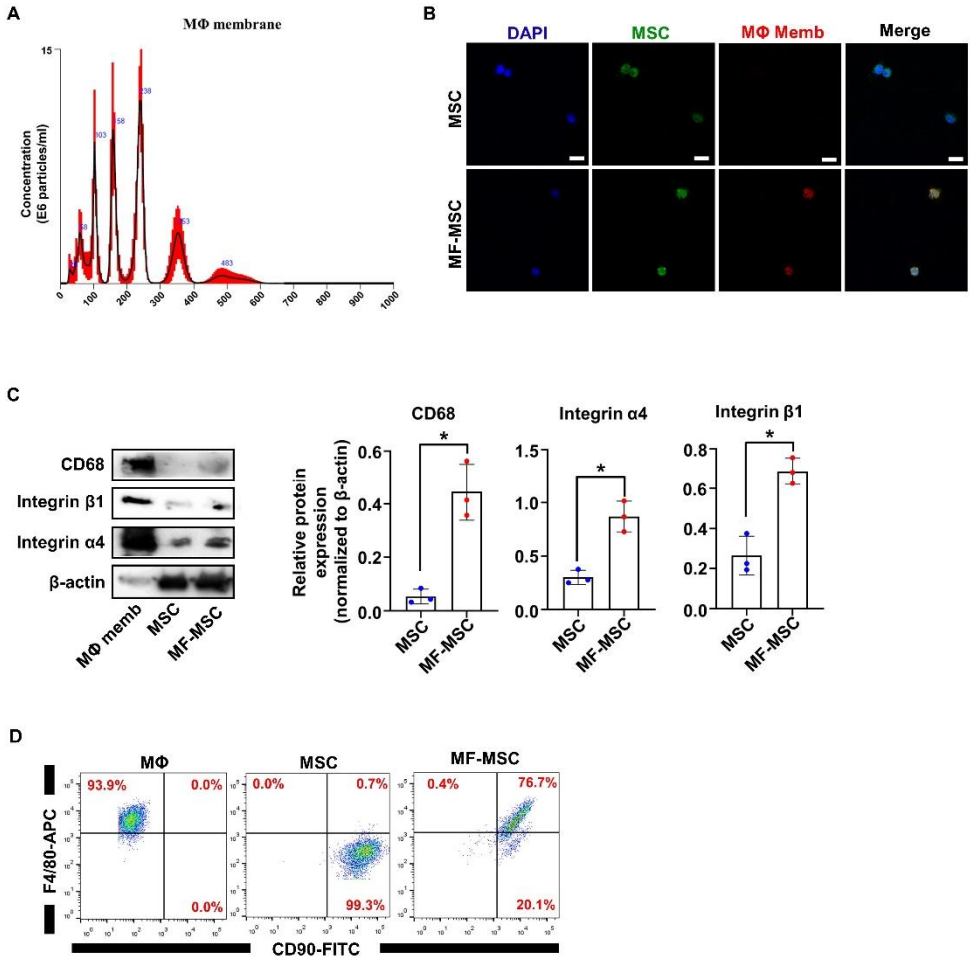

Figure 4.2. Production and characterization of MF-MSCs. (A) Size distribution of MΦ membrane, as evaluated by nanoparticle tracking analysis. (B) Fluorescent confocal images of MSC and MF-MSC after fusion. Scale bars, 25 μm. (C) Representative images of western blots and the quantification data of surface markers of MΦ membrane (CD68, integrin α4 and β1), MSC, and MF-MSC (n = 3 per samples, 20 μg of total proteins). (D) Flow cytometric analysis of MSC (CD90) and MΦ (F4/80) surface marker expressions on MF-MSC (n = 4 per samples). *P < 0.05 by two-tailed t-test. All values are mean ± SD.

4.2.2. Production and characterization of MF-NVs

Next, we prepared N-NVs and MF-NVs by serial extrusion of MSCs and MF-MSCs, respectively, through microporous and nanoporous membranes (Fig. 4.3A). The size distribution of N-NVs and MF-NVs was determined using nanoparticle tracking analysis (Figure 4.3B). N-NVs and MF-NVs showed mean sizes of 238.3 ± 82.2 nm and 233.5 ± 70.3 nm, respectively. The size distributions of NVs were similar to those of NVs in previous studies that exhibited therapeutic effects *in vivo*.[36, 106, 107] TEM images revealed that both N-NVs and MF-NVs had spherical shapes (Fig. 4.3C). Western blot analysis revealed that both N-NVs and MF-NVs contained CD9, a marker for exosomes and NV (Fig. 4.3D). The protein levels of CD68, integrin α4, and integrin β1, which are markers of macrophages, were significantly higher in MF-NVs than in N-NVs. The data indicate that MF-NVs possess similar components with those of MF-MSCs. To evaluate NV uptake by individual cell levels in spinal cord tissues, fluorescent microscopic examination was performed 24 hours after the treatment of HUVECs, PC12 cells, RAW 264.7 cells with N-NVs and MF-NVs for 24 hr (Fig. 4.3E). Fluorescent images showed that NVs were internalized into the cells within 24 hr and uniformly dispersed in the cytoplasm.

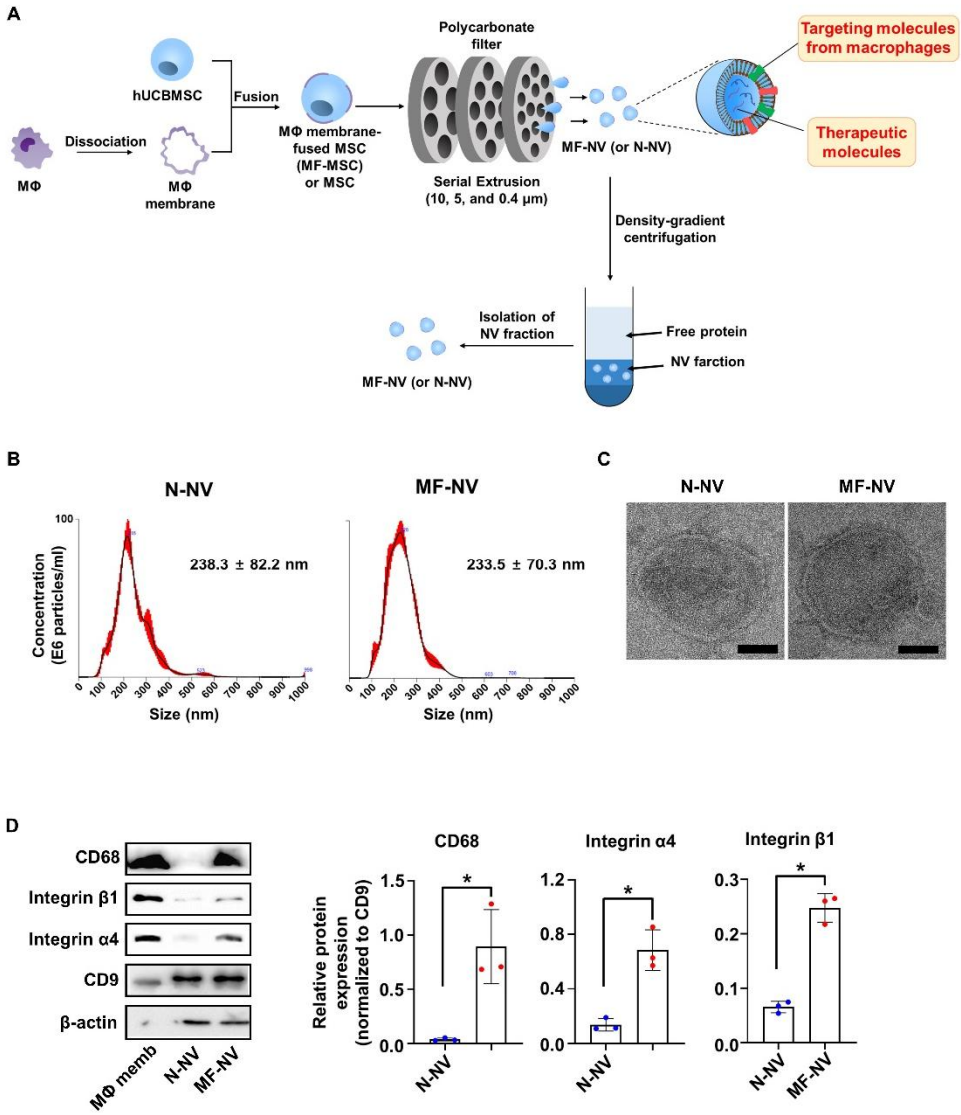
A
hUCBMSC
Fusion
Dissociation
MΦ
MΦ membrane
MΦ membrane-fused MSC (MF-MSC) or MSC
Polycarbonate filter
Serial Extrusion (10, 5, and 0.4 μm)
MF-NV (or N-NV)
Targeting molecules from macrophages
Therapeutic molecules
Density-gradient centrifugation
Free protein
NV farction
Isolation of NV fraction
MF-NV (or N-NV)
B
N-NV
MF-NV
Concentration (E6 particles/ml)
238.3 ± 82.2 nm
233.5 ± 70.3 nm
Size (nm)
C
N-NV
MF-NV
D
CD68
Integrin β1
Integrin α4
CD9
β-actin
MΦ memb
N-NV
MF-NV
Relative protein expression (normalized to CD9)
CD68
Integrin α4
Integrin β1

Figure 4.3 A-D

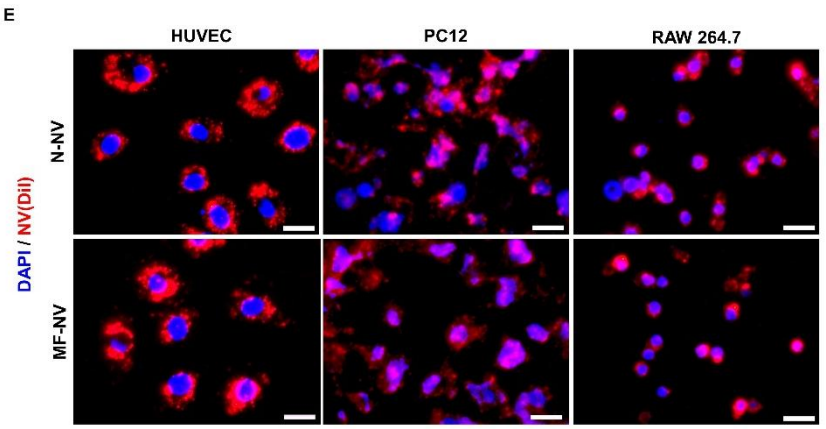

Figure 4.3. Production and characterization of MF-NVs. (A) Schematic diagram of the preparation of MF-NVs. (B) Size distribution of N-NV and MF-NV, as evaluated by nanoparticle tracking analysis (n = 4 per samples). (C) TEM images of N-NV and MF-NV. Scale bars, 50 nm. (D) Representative images and the quantification data of western blots of surface marker of MΦ membrane, N-NV and MF-NV (n = 3 per samples, 20 μg of total proteins). *P < 0.05 by two-tailed t-test. All values are mean ± SD. (E) Representative images showing *in vitro* uptake of DiI-labeled N-NVs and MF-NVs by HUVECs, PC12 cells, and RAW 264.7 cells 24 hours after the treatment. Scale bars, 50 μm.

4.2.3. Neuroprotective effects of MF-NVs *in vitro*

Next, we investigated *in vitro* effects of NVs on various types of cells that can reflect the cell components of spinal cord tissue (neuronal cells, macrophages, and endothelial cells) present in spinal cord under hypoxic and inflammatory (for neuronal and endothelial cells) and inflammatory (for macrophages) conditions. Previous studies have reported that exosomes from MSCs show neuroprotective effects, induce the polarization of macrophages from inflammatory state (M1) to reparative state (M2), and enhance angiogenesis by endothelial cells migration and proliferation.[17, 108, 109] We examined the neuroprotective effects of NVs on neuron-like PC12 cells. PC12 cells were cultured under the ischemic and inflammatory conditions for 24 hrs, because SCI lesions show acute ischemia and inflammation that lead to apoptosis of neurons. Importantly, the treatment with NVs improved the survival of PC12 cells, as evaluated by live/dead staining (Fig. 4.4A) and CCK assay (Fig. 4.4B). NV treatment also increased the expression of an anti-apoptotic gene, Bcl2, and decreased the expression of an apoptotic gene, Bax (Fig. 4.4C). The NV-treated PC12 cells showed increased expression of pAKT and PI3K, which are involved in cell survival (Fig. 4.4D).[110]

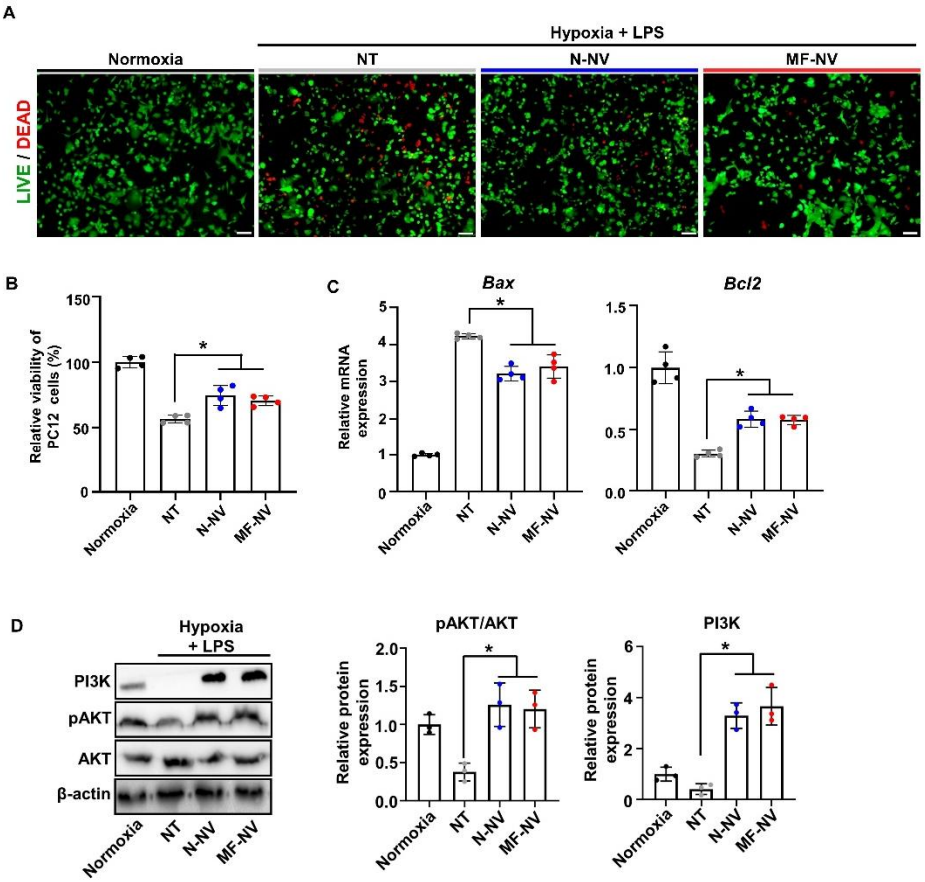

Figure 4.4. Neuroprotective effects of MF-NVs *in vitro*. (A) Representative images of viable and nonviable PC12 cells stained by FDA/EB after treatment. Scale bars, 100 μm. (B) Relative cell viability as evaluated by the CCK assay after the treatment (n = 4 per group). (C) Relative mRNA expression levels of apoptotic (Bax) and anti-apoptotic (Bcl2) genes in PC12 cells after treatment, as evaluated by qRT-PCR (n = 4 per group). (D) Representative images and the quantification data of western blots of PC12 cells for AKT, pAKT, and PI3K after treatment. *P < 0.05 by using one-way ANOVA followed by post-hoc Bonferroni test. All data were normalized to normoxia. All values are mean ± SD. NT indicates no treatment

4.2.4. Anti-inflammatory effects of MF-NVs *in vitro*

Next, we investigated the effects of NVs on the phenotype of macrophages *in vitro*. M1 macrophages are known to be accumulated in inflammatory lesion in the early stage of inflammation. We polarized RAW 264.7 cells, a murine macrophage cell line, into M1 state with LPS for 24 hrs, and treated the cells with NVs. NVs downregulated the LPS-induced expressions of M1 macrophage markers (Il1b, Il6, and Nos2) and upregulated the expressions of M2 macrophage markers (Arg1, Cd206, and Il10), as evaluated by qRT-PCR (Fig. 4.5), indicating that NVs polarized M1 macrophages into M2 macrophages. The transition of inflammatory M1 macrophages into reparative M2 macrophages in the SCI lesion would relieve inflammation, thereby improving spinal cord repair.

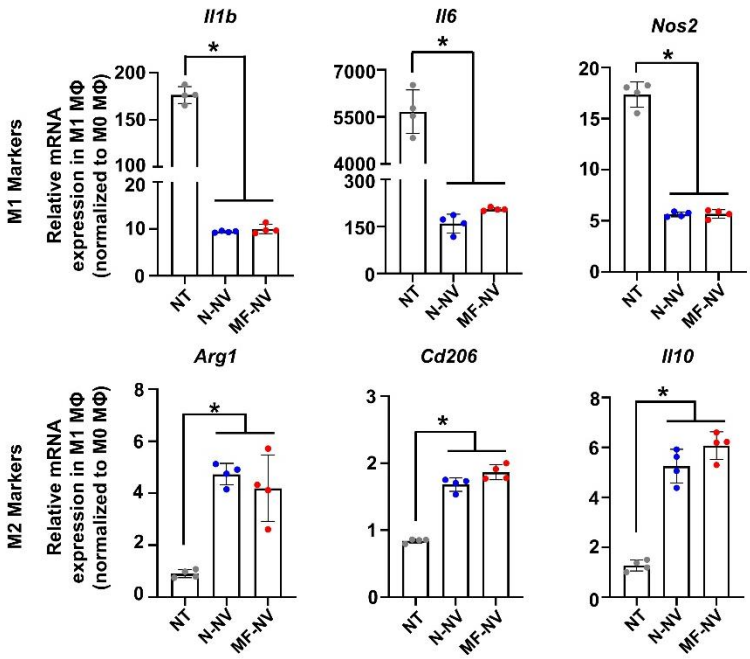

Figure 4.5. Anti-inflammatory effects of MF-NVs *in vitro*. Macrophage polarization after treatment. Relative mRNA expression levels in M1 MΦ of the markers of inflammatory M1 macrophages (Il1b, Il6, and Nos2) and reparative M2 macrophages (Arg1, Cd206, and Il10), as evaluated by qRT-PCR (n = 4 per group). All data were normalized to those of M0 MΦ. NT indicates no treatment. *P < 0.05 by using one-way ANOVA followed by post-hoc Bonferroni test. All values are mean ± SD.

4.2.5. Proangiogenic effects of MF-NVs *in vitro*

Next, we further evaluated the angiogenic effects of NVs on HUVECs. Both N-NVs and MF-NVs stimulated the capillary formation and migration of HUVECs under hypoxic conditions (Fig. 4.6A and B). The angiogenic effects of N-NVs and MF-NVs on HUVECs were mediated via the activation of ERK and PCNA signaling cascades (Fig. 4.6C).[77]

Together, N-NVs and MF-NVs exhibit therapeutic effects via neuroprotection, attenuation of inflammation, and increasing angiogenesis, which are involved in the major mechanisms of spinal cord injury repair.

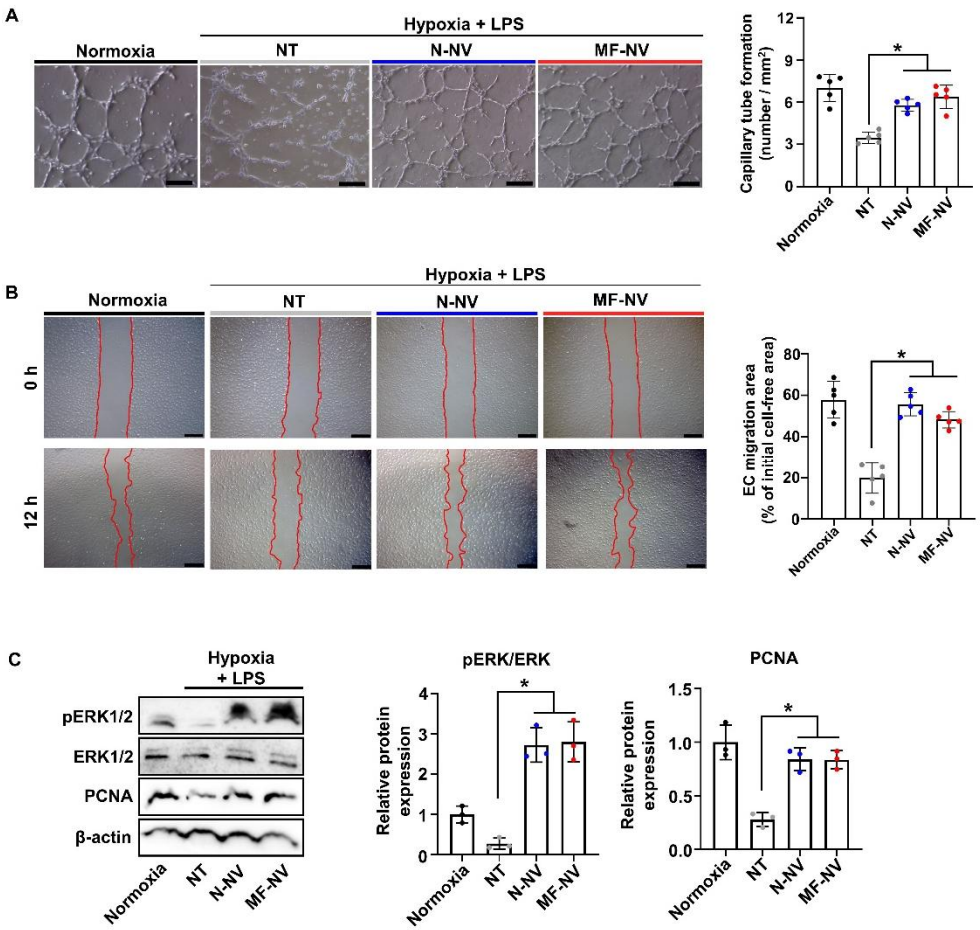

Figure 4.6. Proangiogenic effects of MF-NVs *in vitro*. Representative images and the quantification data of (A) capillary tube formation and (B) cell migration of HUVECs after treatment. Red lines indicate borders of the cell-free area. Scale bars, 100 and 500 μm, respectively. (C) Representative images and the quantification data of western blots of HUVECs for PCNA, ERK 1/2, and pERK 1/2 after treatment. NT indicates no treatment. *P < 0.05 by using one-way ANOVA followed by post-hoc Bonferroni test. All data were normalized to normoxia. All values are mean ± SD.

4.2.6. Enhanced targeting efficiency of MF-NVs *in vitro* and *in vivo*

We investigated the potency of MF-NV targeting to ischemic endothelial cells *in vitro* and injured spinal cord *in vivo*. Prior to NV treatment, HUVECs underwent hypoxia to mimic spinal cord ischemia. DiI-labeled N-NVs and MF-NVs were added to cultures of DiO-labeled HUVECs for 5 min at 4 °C. The data indicate that MF-NVs exhibited augmented adherence to ischemic endothelial cells (Fig. 4.7A). Next, to determine whether the membrane proteins from macrophages affect the spinal cord targeting efficiency of NVs *in vivo*, we treated macrophage membranes with trypsin to denature the membrane proteins prior to fuse. Then we fused the trypsin-treated macrophage membranes into MSCs and then produced NVs (tr-MF-NVs) from the fused MSCs. N-NVs, tr-MF-NVs, and MF-NVs were labeled with fluorescent dyes and systemically injected into SCI mice 1 hr and 7 days post-injury. MF-NV showed and 2.0-fold higher accumulation in the injured spinal cord than N-NV and tr-MF-NV, respectively (Fig. 4.7B). The majority of NVs were accumulated in the liver. However, MF-NVs may not exhibit liver toxicity as a previous study described.[22] Taken together, the data suggest that the macrophage membrane components of MF-NVs contribute to the increased targeting efficiency.

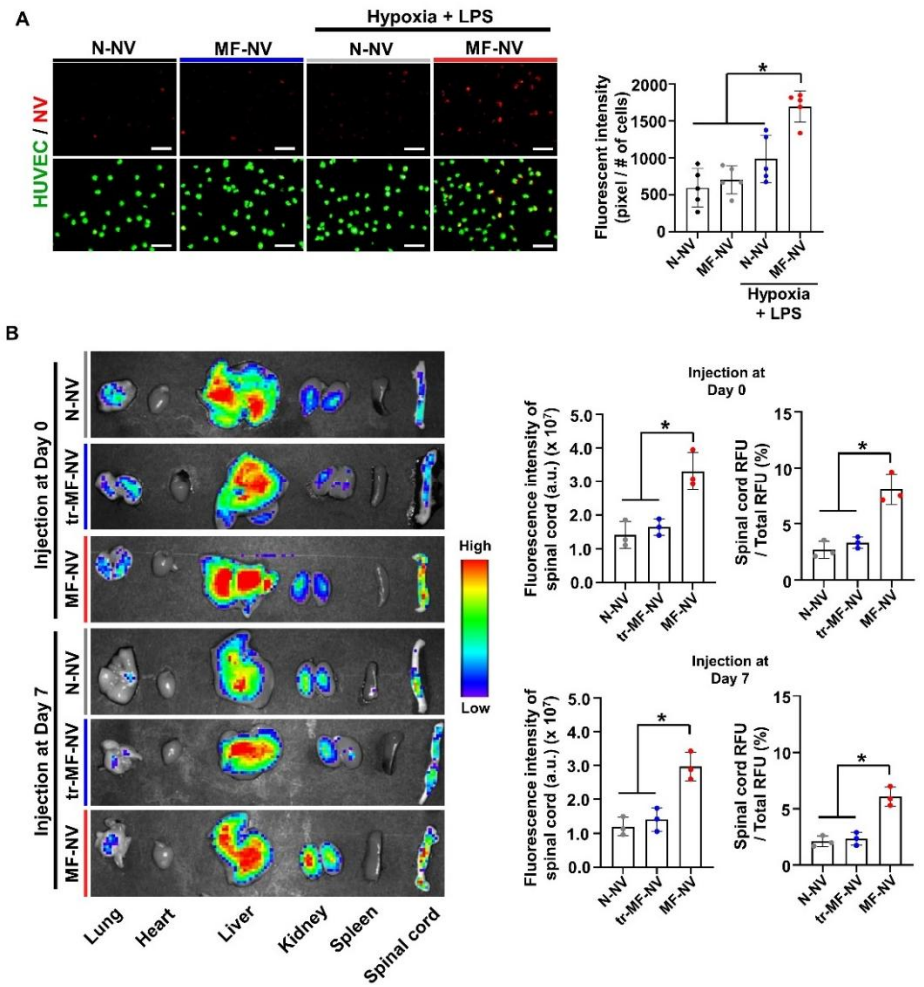

Figure 4.7. Enhanced targeting efficiency of MF-NVs *in vitro* and *in vivo*. (A) Fluorescent images and the quantification data of NV binding to HUVECs *in vitro* (n = 5 per group). Scale bars, 100 μm. *p < 0.05 by using one-way ANOVA followed by post-hoc Bonferroni test. (B) Biodistribution of N-NVs, MF-NVs, and tr-MF-NVs in injured spinal cord 24 hrs after injection 1 hr and 7 days post-injury (n = 3 animals per group). Fluorescently labeled NVs were intravenously injected 1 hr and 7 days after injury. *P < 0.05 by using one-way ANOVA followed by post-hoc Bonferroni test. All values are mean ± SD.

4.2.7. Reduced glial scar formation and improved function recovery by MF-NVs *in vivo*

Morphological observation showed that SCI-induced lesions were markedly reduced by MF-NVs (Fig. 4.8A). After glial scar formation in SCI, axons cannot regenerate beyond the glial scar.[111] To investigate whether MF-NVs attenuate glial scar formation in standing weight compression mice model of SCI, we performed immunohistochemical (IHC) staining. The SCI-induced lesions were stained for NF, a marker for neuron, and GFAP, a marker for astroglia, 28 days post-injury. The no treatment group showed extensive neuronal loss and astrogliosis. MF-NVs showed greater preservation of NF and a significant reduction in GFAP as compared to N-NVs (Fig. 4.8B-D). The glia scar contains extracellular matrix (ECM) deposited by reactive astrocytes in response to SCI. The scar ECM is rich in CSPGs, macromolecules that inhibit axonal growth.[112] IHC staining for CSPGs revealed significantly increased expression of CSPGs in the no treament group day 28 post-injury (Fig. 4.8E and F). By contrast, MF-NV injection significantly reduced CSPGs expression at the lesion 28 days post-injury compared to the no treatment group. These data indicate that MF-NV could play a crucial role in preventing the deposition of CSPGs.

BMS score is commonly used to assess functional recovery following SCI in mice. Before SCI, BMS scores for all mice were 9 points, and the scores on the first postoperative day were 0 (Fig. 4.8G), indicating successful modeling of SCI. After SCI, all mice lost hind limb motor function. Starting from 1 week after injury, the hind limb motor function of the mice gradually recovered till 4 weeks after injury. The scores of the MF-NV injection groups at each time point were significantly higher than those of the other groups. The hind limbs of animals in the MF-NV

injection group showed considerable walking ability, whereas animals in the no treatment group exhibited no movement. These results demonstrated that locomotion function after static compression SCI was improved by injection of MF-NV.

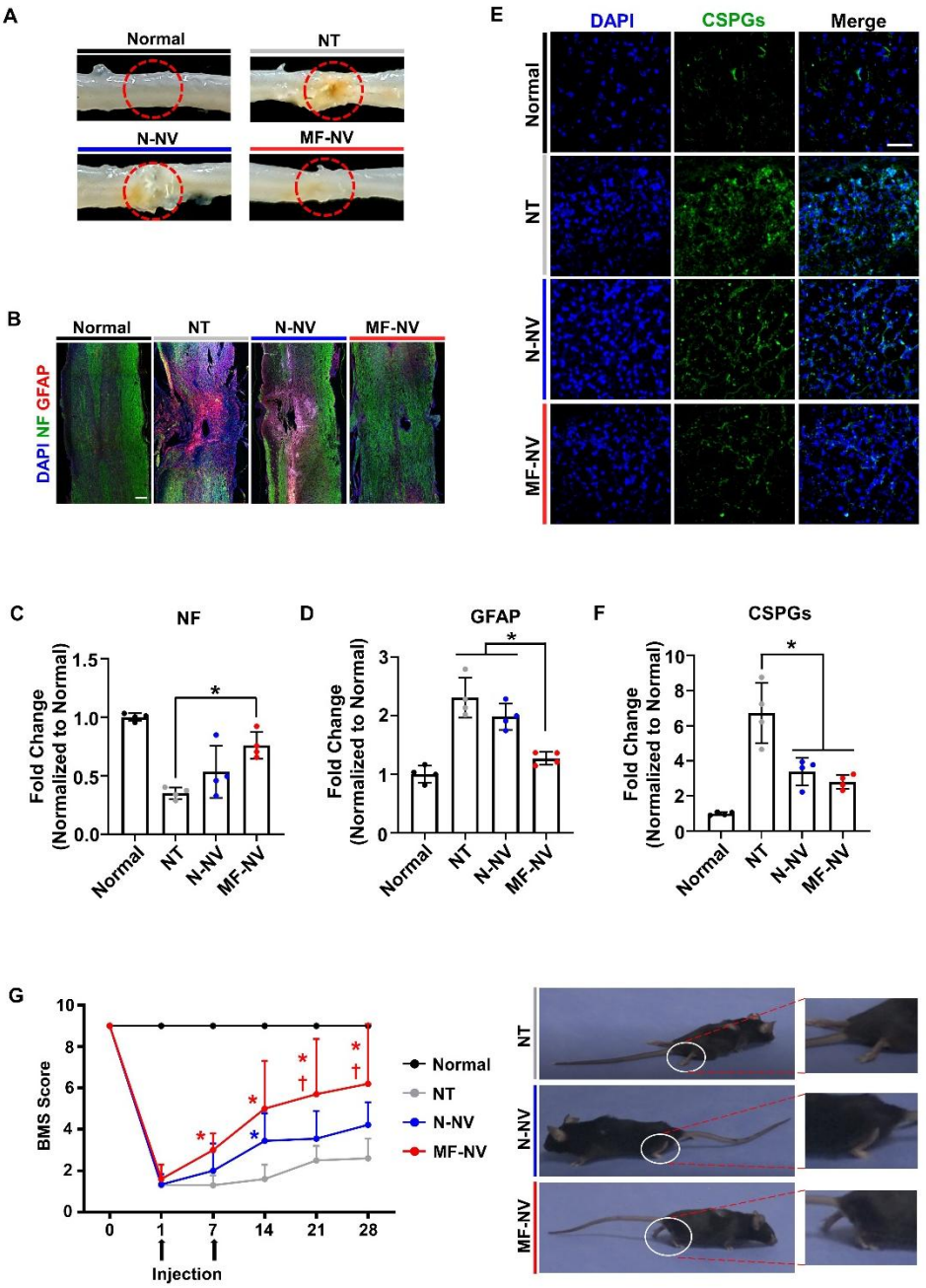

Figure 4.8. Reduced glial scar formation and improved function recovery by MF-NVs *in vivo*. (A) Representative images of spinal cord retrieved 28 days after the NV

injection. The dotted red circles indicate the lesion core. Representative images (B) and the quantification data (C and D) of immunohistochemical staining for neuron (NF, green) and astrogliosis (GFAP, red) in longitudinal sections of spinal cord 28 days post-injury (n = 4 animals per group). Scale bars, 200 μm. Representative images (E) and the quantification data (F) of immunohistochemical staining for glial scar-related component (CSPGs, green) at the lesion core 28 days post-injury (n = 4 animals per group). Scale bars, 20μm. (G) BMS score-based quantitative analysis of time-lapse functional recovery in spinal cord-injured mice and the representative images of injured animals 28 days post-injury (n = 10 animals per group). *P < 0.05 versus NT and †P < 0.05 versus N-NV by using two-way ANOVA followed by post-hoc Bonferroni test. All values are mean ± SD. NT indicates no treatment.

4.2.8. Enhanced neuroprotection, anti-inflammation, and pro-angiogenesis by MF-NVs *in vivo*

In vivo therapeutic mechanisms of MF-NVs were investigated. To evaluate the anti-apoptotic effects of MF-NVs in the injured spinal cord, TUNEL staining assay was performed (Fig. 4.9A and B). The number of TUNEL-positive cells in the spinal cord was significantly increased after SCI. However, the injection of MF-NV decreased apoptotic cells 7 days post-injury.

SCI leads to severe inflammation, microglia and macrophages accumulate at the injured lesion site following trauma to the spinal cord. Indeed, a recent study has described microglial cell and macrophage paradigm associated with SCI. Macrophage activated by microglia can be transformed into M1 (pro-inflammatory) and M2 (anti-inflammatory).[113, 114] The ratio of M1 to M2 macrophages is critical and plays a crucial role in repair following SCI.[39, 115] Mostly, M1 macrophages are considered neurotoxic while M2 macrophages are beneficial after SCI. In addition, M2 activation promotes healing activities of microglia. The microglia secrete neurotrophic factors such as brain-derived neurotrophic factor, neurotrophins, and glial cell–derived neurotrophic factor. Therefore, Strategies to increase M2 cell population and decrease M1 cell population in the injured local microenvironment might enhance tissue repair after SCI.[116, 117] Therefore, we examined the effects of MF-NVs on M1 and M2 phenotype change in injured spinal cords in mice. IHC analysis showed that SCI-induced TNFα expression was significantly reduced 7 days after the injection of MF-NVs (Fig. 4.9 C and D). In addition, the mRNA expression levels of M1 markers—Il1b, Nos2, and Tnfa— decreased and the mRNA expression levels of M2 markers— Arg1, Il10, and Vegf— increased 3 days after injection of MF-NVs (Fig. 4.9E). Taken together, the results suggest that MF-

NVs shift the balance from M1 to M2 macrophages at the lesion site and alter the local microenvironment, which is conducive for SCI repair.

Endothelial cells and blood vessels at the injury site in the spinal cord showed degenerative changes within few hours after injury.[118] Significant decreases in the number of vascular endothelial cells were observed subsequently and might cause necrotic or apoptotic cell death. Therefore, we examined whether MF-NV injection could promote angiogenesis after SCI. MF-NV was administrated 1 hr and 7 days after SCI by injection. Next, IHC staining for vWF of the injured spinal cord was performed 28 days post-injury (Fig. 4.9F and G). Surprisingly, the injection of MF-NV significantly increased vWF in the injured spinal cord, whereas the N-NV group did not. These data indicate that MF-NVs can enhance neuroprotection and angiogenesis, and attenuate inflammation in SCI mice model, which is attributed to the high targeting efficiency of injected MF-NVs.

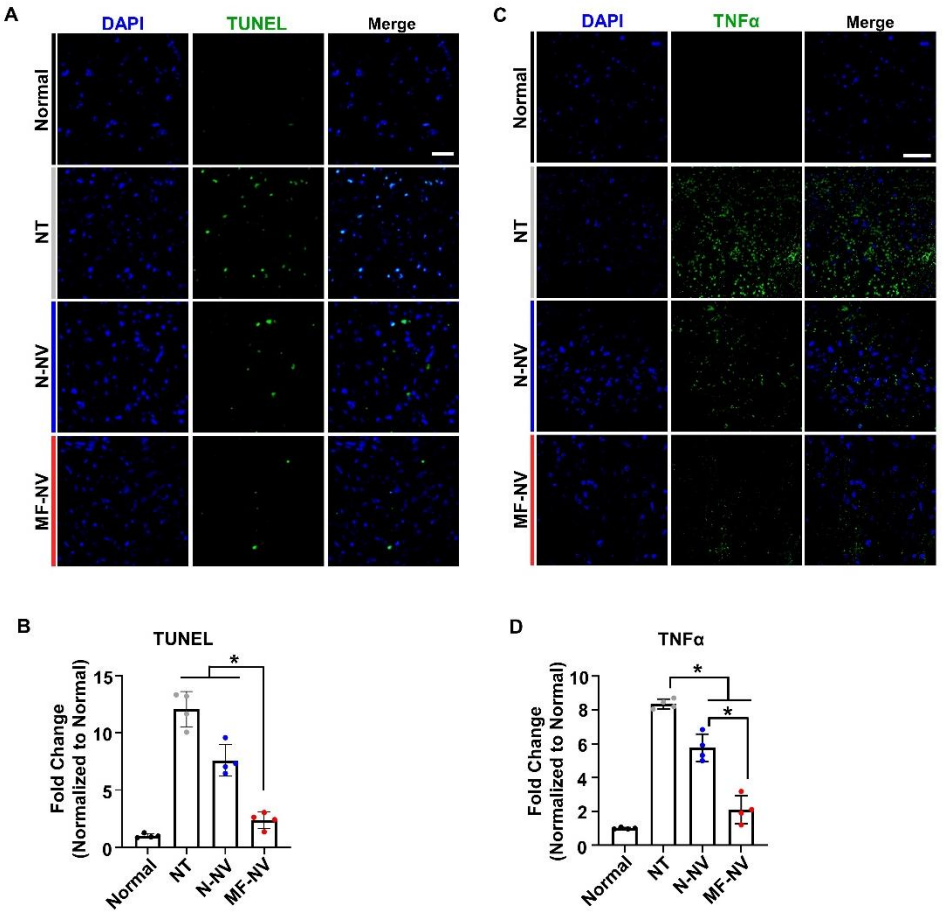
A
DAPI
TUNEL
Merge
Normal
NT
N-NV
MF-NV
C
DAPI
TNFα
Merge
Normal
NT
N-NV
MF-NV
B
TUNEL
Fold Change (Normalized to Normal)
15
10
5
0
*
Normal
NT
N-NV
MF-NV
D
TNFα
Fold Change (Normalized to Normal)
10
8
6
4
2
0
*
*
Normal
NT
N-NV
MF-NV

Figure 4.9 A-D

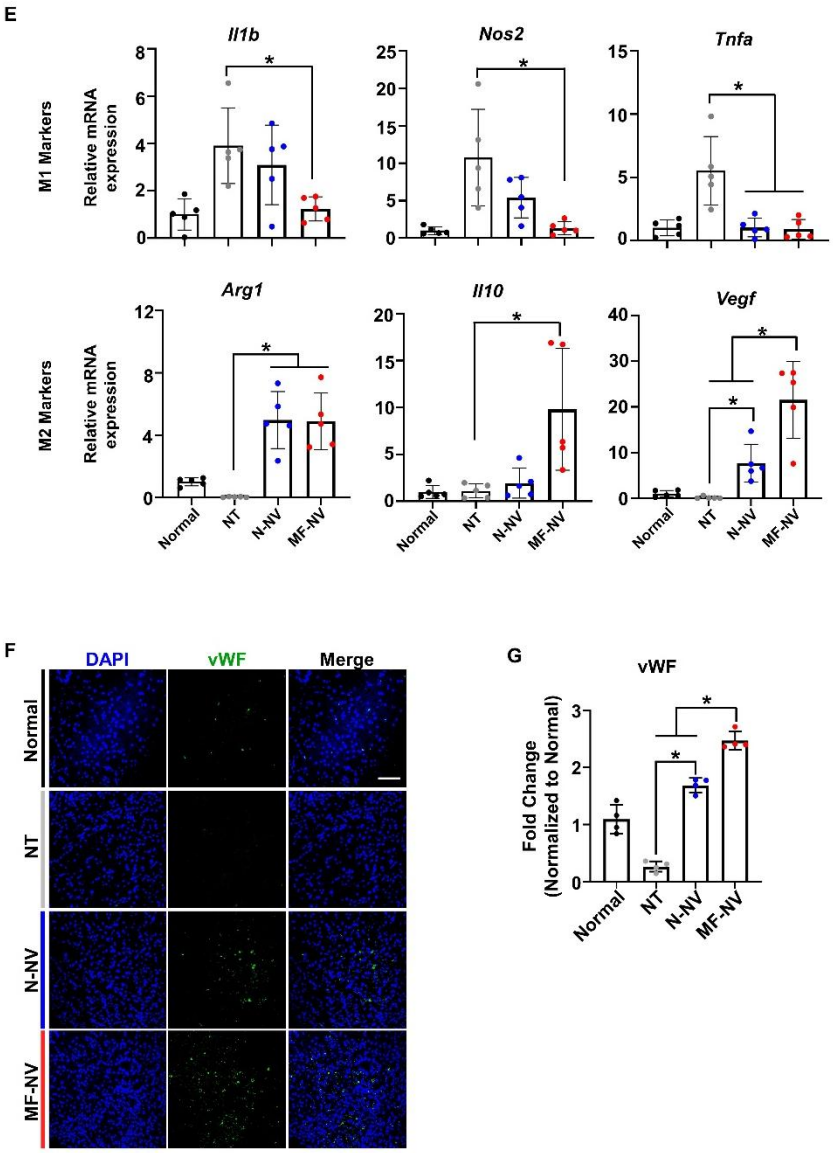

Figure 4.9. Enhanced neuroprotection, anti-inflammation, and proangiogenesis by MF-NVs *in vivo*. Representative images (A) and the quantification data (B) of TUNEL (red)-positive apoptotic cells 7 days post-injury (n = 4 animals per group). Scale bars, 20 μm. Representative images (C) and the quantification data (D) of immunohistochemical staining for TNFα 7 days post-injury (n = 4 animals per group).

Scale bars, 20 μm. (E) Relative mRNA expression levels of M1 macrophage-specific markers (Il1b, Nos2, and Tnfa) and M2 macrophage-specific markers (Il10, Arg1, and Vegf) in the injured spinal cord at 3 days post-injuiry, as evaluated by qRT-PCR (n = 5 animals per group). Representative images (F) and the quantification data (G) of immunohistochemical staining for blood vessels (vWF, green) at the lesion core 28 days post-injury. Scale bars, 20μm. NT indicates no treatment. *$P < 0.05$ by using one-way ANOVA followed by post-hoc Bonferroni test. All values are mean ± SD.

Chapter 5.

Conclusions

These studies present enhancing the cardiomyogenic and skeletal myogenic differentiation efficiency of hMSCs, for treatment of *in vivo* muscle disorders.

In chapter 3, for a NV therapy for MI treatment, we developed therapeutic efficacy-potentiated and cardiac retention-enhanced IONP-NVs from IONP-MSCs for a cell-free therapy for MI. Our data indicate that: (i) biodegradable IONPs increased the levels of cardiac repair-favorable molecules in MSCs without cytotoxicity; (ii) IONP-NVs derived from IONP-MSCs contained higher levels of therapeutic molecules than N-NVs derived from MSCs; (iii) IONP-NVs were efficiently internalized into cardiac resident cells and macrophages and exhibited therapeutic efficacy on damaged cardiac resident cells *in vitro*, which was similar to the therapeutic effects of MSCs, showing the possibility of a cell-free therapy for MI; (iv) In a rat MI model, magnetic guidance enhanced the retention of injected IONP-NVs within the MI injury site; (v) IONP-NV injection to the rat infarcted heart and magnetic guidance facilitated cardiac repair and improved cardiac functional recovery via anti-apoptosis, anti-inflammation, angiogenesis, and anti-fibrosis. IONP-NVs can improve the cardiac repair potency of NVs derived from MSCs. IONPs are biodegradable, nontoxic, and a US Food and Drug Administration-approved material and are assimilated in the body. IONP-NVs may be an effective cell-free therapy that can replace MSC therapy for MI.

In chapter 4, for a NV therapy for SCI treatment, we synthetically fabricated MF-NVs for spinal cord repair. MF-NVs exhibited: (i) neuroprotective effects by reducing apoptosis of neuronal cells; (ii) angiogenic effects by increasing migration and tube formation of endothelial cells; and (iii) anti-inflammatory effects by polarizing M1 to M2 macrophages *in vitro*, which are closely associated with the mechanism of spinal cord repair. Importantly, incorporation of the

macrophage plasma membrane into MSC-derived NVs significantly improved the injured spinal cord-targeting efficiency of MSC-derived NVs and potentiated the therapeutic efficacy of MSC-derived NVs for SCI. Furthermore, the replacement of the cell-line-derived macrophage membranes in the MF-NVs with patient-derived macrophage membranes would increase the possibility of clinical applications of MF-NVs for SCI.

References

1. Squillaro, T.; Peluso, G.; Galderisi, U., Clinical Trials With Mesenchymal Stem Cells: An Update. *Cell Transplant* **2016,** *25* (5), 829-848.

2. Barry, F., MSC Therapy for Osteoarthritis: An Unfinished Story. *J Orthop Res* **2019,** *37* (6), 1229-1235.

3. Lalu, M. M.; McIntyre, L.; Pugliese, C.; Fergusson, D.; Winston, B. W.; Marshall, J. C.; Granton, J.; Stewart, D. J.; Grp, C. C. C. T., Safety of Cell Therapy with Mesenchymal Stromal Cells (SafeCell): A Systematic Review and Meta-Analysis of Clinical Trials. *Plos One* **2012,** *7* (10).

4. Jin, M. C.; Medress, Z. A.; Azad, T. D.; Doulames, V. M.; Veeravagu, A., Stem cell therapies for acute spinal cord injury in humans: a review. *Neurosurg Focus* **2019,** *46* (3).

5. Gnecchi, M.; Danieli, P.; Malpasso, G.; Ciuffreda, M. C., Paracrine Mechanisms of Mesenchymal Stem Cells in Tissue Repair. *Methods Mol Biol* **2016,** *1416*, 123-46.

6. Moll, G.; Rasmusson-Duprez, I.; von Bahr, L.; Connolly-Andersen, A. M.; Elgue, G.; Funke, L.; Hamad, O. A.; Lonnies, H.; Magnusson, P. U.; Sanchez, J.; Teramura, Y.; Nilsson-Ekdahl, K.; Ringden, O.; Korsgren, O.; Nilsson, B.; Le Blanc, K., Are Therapeutic

Human Mesenchymal Stromal Cells Compatible with Human Blood? *Stem Cells* **2012,** *30* (7), 1565-1574.

7. Vassalli, G.; Moccetti, T., Cardiac repair with allogeneic mesenchymal stem cells after myocardial infarction. *Swiss Med Wkly* **2011,** *141*.

8. Willerth, S. M.; Sakiyama-Elbert, S. E., Cell therapy for spinal cord regeneration. *Adv Drug Deliver Rev* **2008,** *60* (2), 263-276.

9. Tkach, M.; Thery, C., Communication by Extracellular Vesicles: Where We Are and Where We Need to Go. *Cell* **2016,** *164* (6), 1226-1232.

10. Valadi, H.; Ekstrom, K.; Bossios, A.; Sjostrand, M.; Lee, J. J.; Lotvall, J. O., Exosome-mediated transfer of mRNAs and microRNAs is a novel mechanism of genetic exchange between cells. *Nat Cell Biol* **2007,** *9* (6), 654-U72.

11. Bang, C.; Thum, T., Exosomes: New players in cell-cell communication. *Int J Biochem Cell B* **2012,** *44* (11), 2060-2064.

12. Rani, S.; Ryan, A. E.; Griffin, M. D.; Ritter, T., Mesenchymal Stem Cell-derived Extracellular Vesicles: Toward Cell-free Therapeutic Applications. *Mol Ther* **2015,** *23* (5), 812-823.

13. Mentkowski, K. I.; Snitzer, J. D.; Rusnak, S.; Lang, J. K., Therapeutic Potential of Engineered Extracellular Vesicles. *Aaps J* **2018,** *20* (3).

14. EL Andaloussi, S.; Maeger, I.; Breakefield, X. O.; Wood, M. J. A., Extracellular vesicles: biology and emerging therapeutic opportunities. *Nat Rev Drug Discov* **2013,** *12* (5), 348-358.

15. Liu, L.; Jin, X.; Hu, C. F.; Li, R.; Zhou, Z. E.; Shen, C. X., Exosomes Derived from Mesenchymal Stem Cells Rescue Myocardial Ischaemia/Reperfusion Injury by Inducing Cardiomyocyte Autophagy Via AMPK and Akt Pathways. *Cell Physiol Biochem* **2017,** *43* (1), 52-68.

16. Yu, B.; Kim, H. W.; Gong, M.; Wang, J. C.; Millard, R. W.; Wang, Y. G.; Ashraf, M.; Xu, M. F., Exosomes secreted from GATA-4 overexpressing mesenchymal stem cells serve as a reservoir of anti-apoptotic microRNAs for cardioprotection. *Int J Cardiol* **2015,** *182*, 349-360.

17. Lo Sicco, C.; Reverberi, D.; Balbi, C.; Ulivi, V.; Principi, E.; Pascucci, L.; Becherini, P.; Bosco, M. C.; Varesio, L.; Franzin, C.; Pozzobon, M.; Cancedda, R.; Tasso, R., Mesenchymal Stem Cell-Derived Extracellular Vesicles as Mediators of Anti-Inflammatory Effects: Endorsement of Macrophage Polarization. *Stem Cell Transl Med* **2017,** *6* (3), 1018-1028.

18. Zhang, B.; Yeo, R. W. Y.; Lai, R. C.; Sim, E. W. K.; Chin, K. C.; Lim, S. K., Mesenchymal stromal cell exosome-enhanced regulatory T-cell production through an antigen-presenting cell-mediated pathway. *Cytotherapy* **2018,** *20* (5), 687-696.

19. Gong, M.; Yu, B.; Wang, J. C.; Wang, Y. G.; Liu, M.; Paul, C.; Millard, R. W.; Xiao, D. S.; Ashraf, M.; Xu, M. F., Mesenchymal stem cells release exosomes that transfer miRNAs to endothelial cells and promote angiogenesis. *Oncotarget* **2017,** *8* (28), 45200-45212.

20. Zhang, B.; Wu, X. D.; Zhang, X.; Sun, Y. X.; Yan, Y. M.; Shi, H.; Zhu, Y. H.; Wu, L. J.; Pan, Z. J.; Zhu, W.; Qian, H.; Xu, W. R., Human Umbilical Cord Mesenchymal Stem Cell Exosomes Enhance Angiogenesis Through the Wnt4/beta-Catenin Pathway. *Stem Cell Transl Med* **2015,** *4* (5), 513-522.

21. Lin, S. S.; Zhu, B.; Guo, Z. K.; Huang, G. Z.; Wang, Z.; Chen, J.; Wei, X. J.; Li, Q., Bone Marrow Mesenchymal Stem Cell-Derived Microvesicles Protect Rat Pheochromocytoma PC12 Cells from Glutamate-Induced Injury via a PI3K/Akt Dependent Pathway. *Neurochem Res* **2014,** *39* (5), 922-931.

22. Li, T. F.; Yan, Y. M.; Wang, B. Y.; Qian, H.; Zhang, X.; Shen, L.; Wang, M.; Zhou, Y.; Zhu, W.; Li, W.; Xu, W. R., Exosomes Derived from Human Umbilical Cord Mesenchymal Stem Cells Alleviate Liver Fibrosis. *Stem Cells Dev* **2013,** *22* (6), 845-854.

23. Gangadaran, P.; Rajendran, R. L.; Lee, H. W.; Kalimuthu, S.; Hong, C. M.; Jeong, S. Y.; Lee, S. W.; Lee, J.; Ahn, B. C., Extracellular vesicles from mesenchymal stem cells activates VEGF receptors and accelerates recovery of hindlimb ischemia. *J Control Release* **2017,** *264*,

112-126.

24. Nakamura, Y.; Miyaki, S.; Ishitobi, H.; Matsuyama, S.; Nakasa, T.; Kamei, N.; Akimoto, T.; Higashi, Y.; Ochi, M., Mesenchymal-stem-cell-derived exosomes accelerate skeletal muscle regeneration. *FEBS Lett* **2015,** *589* (11), 1257-65.

25. Cosenza, S.; Ruiz, M.; Toupet, K.; Jorgensen, C.; Noel, D., Mesenchymal stem cells derived exosomes and microparticles protect cartilage and bone from degradation in osteoarthritis. *Sci Rep-Uk* **2017,** *7*.

26. Cosenza, S.; Toupet, K.; Maumus, M.; Luz-Crawford, P.; Blanc-Brude, O.; Jorgensen, C.; Noel, D., Mesenchymal stem cells-derived exosomes are more immunosuppressive than microparticles in inflammatory arthritis. *Theranostics* **2018,** *8* (5), 1399-1410.

27. Chen, Y.; Zhao, Y.; Chen, W.; Xie, L.; Zhao, Z. A.; Yang, J.; Chen, Y.; Lei, W.; Shen, Z., MicroRNA-133 overexpression promotes the therapeutic efficacy of mesenchymal stem cells on acute myocardial infarction. *Stem Cell Res Ther* **2017,** *8* (1), 268.

28. Zou, L. Y.; Ma, X. K.; Lin, S.; Wu, B. Y.; Chen, Y.; Peng, C. Q., Bone marrow mesenchymal stem cell-derived exosomes protect against myocardial infarction by promoting autophagy. *Exp Ther Med* **2019,** *18* (4), 2574-2582.

29. Zhao, J. X.; Li, X. L.; Hu, J. X.; Chen, F.; Qiao, S. H.; Sun, X.; Gao, L.; Xie, J.; Xu, B., Mesenchymal stromal cell-derived

exosomes attenuatemyocardial ischaemia-reperfusion injury throughmiR-182-regulated macrophage polarization. *Cardiovasc Res* **2019,** *115* (7), 1205-1216.

30. Bian, S. Y.; Zhang, L. P.; Duan, L. F.; Wang, X.; Min, Y.; Yu, H. P., Extracellular vesicles derived from human bone marrow mesenchymal stem cells promote angiogenesis in a rat myocardial infarction model. *J Mol Med* **2014,** *92* (4), 387-397.

31. Arslan, F.; Lai, R. C.; Smeets, M. B.; Akeroyd, L.; Choo, A.; Aguor, E. N. E.; Timmers, L.; van Rijen, H. V.; Doevendans, P. A.; Pasterkamp, G.; Lim, S. K.; de Kleijn, D. P., Mesenchymal stem cell-derived exosomes increase ATP levels, decrease oxidative stress and activate PI3K/Akt pathway to enhance myocardial viability and prevent adverse remodeling after myocardial ischemia/reperfusion injury. *Stem Cell Res* **2013,** *10* (3), 301-312.

32. Liu, W.; Wang, Y. X.; Gong, F. Y.; Rong, Y. L.; Luo, Y. J.; Tang, P. Y.; Zhou, Z.; Zhou, Z. M.; Xu, T.; Jiang, T.; Yang, S. T.; Yin, G. Y.; Chen, J.; Fan, J.; Cai, W. H., Exosomes Derived from Bone Mesenchymal Stem Cells Repair Traumatic Spinal Cord Injury by Suppressing the Activation of A1 Neurotoxic Reactive Astrocytes. *J Neurotraum* **2019,** *36* (3), 469-484.

33. Huang, J. H.; Yin, X. M.; Xu, Y.; Xu, C. C.; Lin, X.; Ye, F. B.; Cao, Y.; Lin, F. Y., Systemic Administration of Exosomes Released

from Mesenchymal Stromal Cells Attenuates Apoptosis, Inflammation, and Promotes Angiogenesis after Spinal Cord Injury in Rats. *J Neurotraum* **2017,** *34* (24), 3388-3396.

34. Katsuda, T.; Tsuchiya, R.; Kosaka, N.; Yoshioka, Y.; Takagaki, K.; Oki, K.; Takeshita, F.; Sakai, Y.; Kuroda, M.; Ochiya, T., Human adipose tissue-derived mesenchymal stem cells secrete functional neprilysin-bound exosomes. *Sci Rep-Uk* **2013,** *3*.

35. Jo, W.; Kim, J.; Yoon, J.; Jeong, D.; Cho, S.; Jeong, H.; Yoon, Y. J.; Kim, S. C.; Gho, Y. S.; Park, J., Large-scale generation of cell-derived nanovesicles. *Nanoscale* **2014,** *6* (20), 12056-12064.

36. Oh, K.; Kim, S. R.; Kim, D. K.; Seo, M. W.; Lee, C.; Lee, H. M.; Oh, J. E.; Choi, E. Y.; Lee, D. S.; Gho, Y. S.; Park, K. S., In Vivo Differentiation of Therapeutic Insulin-Producing Cells from Bone Marrow Cells via Extracellular Vesicle-Mimetic Nanovesicles. *Acs Nano* **2015,** *9* (12), 11718-11727.

37. Wu, J. Y.; Ji, A. L.; Wang, Z. X.; Qiang, G. H.; Qu, Z.; Wu, J. H.; Jiang, C. P., Exosome-Mimetic Nanovesicles from Hepatocytes promote hepatocyte proliferation in vitro and liver regeneration in vivo. *Sci Rep-Uk* **2018,** *8*.

38. Lai, C. P.; Mardini, O.; Ericsson, M.; Prabhakar, S.; Maguire, C. A.; Chen, J. W.; Tannous, B. A.; Breakefield, X. O., Dynamic Biodistribution of Extracellular Vesicles in Vivo Using a

Multimodal Imaging Reporter. *Acs Nano* **2014,** *8* (1), 483-494.

39. Wiklander, O. P. B.; Nordin, J. Z.; O'Loughlin, A.; Gustafsson, Y.; Corso, G.; Mager, I.; Vader, P.; Lee, Y.; Sork, H.; Seow, Y.; Heldring, N.; Alvarez-Erviti, L.; Smith, C. I. E.; Le Blanc, K.; Macchiarini, P.; Jungebluth, P.; Wood, M. J. A.; EL Andaloussi, S., Extracellular vesicle in vivo biodistribution is determined by cell source, route of administration and targeting. *J Extracell Vesicles* **2015,** *4*.

40. Tamura, R.; Uemoto, S.; Tabata, Y., Augmented liver targeting of exosomes by surface modification with cationized pullulan. *Acta Biomater* **2017,** *57*, 274-284.

41. Li, Y.; Gao, Y.; Gong, C. N.; Wang, Z.; Xia, Q. M.; Gu, F. F.; Hu, C. L.; Zhang, L. J.; Guo, H. L.; Gao, S., A33 antibody-functionalized exosomes for targeted delivery of doxorubicin against colorectal cancer. *Nanomed-Nanotechnol* **2018,** *14* (7), 1973-1985.

42. Qi, H. Z.; Liu, C. Y.; Long, L. X.; Ren, Y.; Zhang, S. S.; Chang, X. D.; Qian, X. M.; Jia, H. H.; Zhao, J.; Sun, J. J.; Hou, X.; Yuan, X. B.; Kang, C. S., Blood Exosomes Endowed with Magnetic and Targeting Properties for Cancer Therapy. *Acs Nano* **2016,** *10* (3), 3323-3333.

43. Lee, N.; Choi, Y.; Lee, Y.; Park, M.; Moon, W. K.; Choi, S. H.; Hyeon, T., Water-Dispersible Ferrimagnetic Iron Oxide Nanocubes with Extremely High r(2) Relaxivity for Highly Sensitive in Vivo MRI of Tumors. *Nano Lett* **2012,** *12* (6), 3127-3131.

44. Fang, R. H.; Hu, C. M. J.; Luk, B. T.; Gao, W. W.; Copp, J. A.; Tai, Y. Y.; O'Connor, D. E.; Zhang, L. F., Cancer Cell Membrane-Coated Nanoparticles for Anticancer Vaccination and Drug Delivery. *Nano Lett* **2014,** *14* (4), 2181-2188.

45. Tang, J. N.; Su, T.; Huang, K.; Dinh, P. U.; Wang, Z. G.; Vandergriff, A.; Hensley, M. T.; Cores, J.; Allen, T.; Li, T. S.; Sproul, E.; Mihalko, E.; Lobo, L. J.; Ruterbories, L.; Lynch, A.; Brown, A.; Caranasos, T. G.; Shen, D. L.; Stouffer, G. A.; Gu, Z.; Zhang, J. Y.; Cheng, K., Targeted repair of heart injury by stem cells fused with platelet nanovesicles. *Nat Biomed Eng* **2018,** *2* (1), 17-26.

46. Jang, J.; Park, H. J.; Kim, S. W.; Kim, H.; Park, J. Y.; Na, S. J.; Kim, H. J.; Park, M. N.; Choi, S. H.; Park, S. H.; Kim, S. W.; Kwon, S. M.; Kim, P. J.; Cho, D. W., 3D printed complex tissue construct using stem cell-laden decellularized extracellular matrix bioinks for cardiac repair. *Biomaterials* **2017,** *112*, 264-274.

47. Basso, D. M.; Fisher, L. C.; Anderson, A. J.; Jakeman, L. B.; McTigue, D. M.; Popovich, P. G., Basso mouse scale for locomotion detects differences in recovery after spinal cord in ury in five common mouse strains. *J Neurotraum* **2006,** *23* (5), 635-659.

48. Gaziano, T. A., Cardiovascular disease in the developing world and its cost-effective management. *Circulation* **2005,** *112* (23), 3547-3553.

49. Mozaffarian, Heart Disease and Stroke Statistics-2016 Update: A

Report From the American Heart Association (vol 133, pg e38, 2016). *Circulation* **2016,** *133* (15), E599-E599.

50. Amado, L. C.; Saliaris, A. P.; Schuleri, K. H.; St John, M.; Xie, J. S.; Cattaneo, S.; Durand, D. J.; Fitton, T.; Kuang, J. Q.; Stewart, G.; Lehrke, S.; Baumgartner, W. W.; Martin, B. J.; Heldman, A. W.; Hare, J. M., Cardiac repair with intramyocardial injection of allogeneic mesenchymal stem cells after myocardial infarction. *P Natl Acad Sci USA* **2005,** *102* (32), 11474-11479.

51. Shake, J. G.; Gruber, P. J.; Baumgartner, W. A.; Senechal, G.; Meyers, J.; Redmond, J. M.; Pittenger, M. F.; Martin, B. J., Mesenchymal stem cell implantation in a swine myocardial infarct model: engraftment and functional effects. *Ann Thorac Surg* **2002,** *73* (6), 1919-25; discussion 1926.

52. Delewi, R.; Andriessen, A.; Tijssen, J. G. P.; Zijlstra, F.; Piek, J. J.; Hirsch, A., Impact of intracoronary cell therapy on left ventricular function in the setting of acute myocardial infarction: a meta-analysis of randomised controlled clinical trials. *Heart* **2013,** *99* (4), 225-232.

53. Seif-Naraghi, S. B.; Singelyn, J. M.; Salvatore, M. A.; Osborn, K. G.; Wang, J. J.; Sampat, U.; Kwan, O. L.; Strachan, G. M.; Wong, J.; Schup-Magoffin, P. J.; Braden, R. L.; Bartels, K.; DeQuach, J. A.; Preul, M.; Kinsey, A. M.; DeMaria, A. N.; Dib, N.; Christman, K. L., Safety and Efficacy of an Injectable Extracellular Matrix

Hydrogel for Treating Myocardial Infarction. *Sci Transl Med* **2013,** *5* (173).

54. Beeres, S. L.; Zeppenfeld, K.; Bax, J. J.; Van der Wall, E. E.; Atsma, D. E.; Schalij, M. J., Electrophysiological and arrhythmogenic effects of intramyocardial bone marrow cell injection in patients with chronic ischemic heart disease. *Circulation* **2006,** *114* (18), 606-606.

55. Breitbach, M.; Bostani, T.; Roell, W.; Xia, Y.; Dewald, O.; Nygren, J. M.; Fries, J. W. U.; Tiemann, K.; Bohlen, H.; Hescheler, J.; Welz, A.; Bloch, W.; Jacobsen, S. E. W.; Fleischmann, B. K., Potential risks of bone marrow cell transplantation into infarcted hearts. *Blood* **2007,** *110* (4), 1362-1369.

56. Gnecchi, M.; He, H. M.; Liang, O. D.; Melo, L. G.; Morello, F.; Mu, H.; Noiseux, N.; Zhang, L. N.; Pratt, R. E.; Ingwall, J. S.; Dzau, V. J., Paracrine action accounts for marked protection of ischemic heart by Akt-modified mesenchymal stem cells. *Nat Med* **2005,** *11* (4), 367-368.

57. Lai, R. C.; Arslan, F.; Lee, M. M.; Sze, N. S. K.; Choo, A.; Chen, T. S.; Salto-Tellez, M.; Timmers, L.; Lee, C. N.; El Oakley, R. M.; Pasterkamp, G.; de Kleijn, D. P. V.; Lim, S. K., Exosome secreted by MSC reduces myocardial ischemia/reperfusion injury. *Stem Cell Res* **2010,** *4* (3), 214-222.

58. Teng, X.; Chen, L.; Chen, W.; Yang, J.; Yang, Z.; Shen, Z., Mesenchymal Stem Cell-Derived Exosomes Improve the Microenvironment

of Infarcted Myocardium Contributing to Angiogenesis and Anti-Inflammation. *Cell Physiol Biochem* **2015,** *37* (6), 2415-24.

59. Safari, S.; Malekvandfard, F.; Babashah, S.; Alizadehasl, A.; Sadeghizadeh, M.; Motavaf, M., Mesenchymal stem cell-derived exosomes: A novel potential therapeutic avenue for cardiac regeneration. *Cell Mol Biol* **2016,** *62* (7), 66-73.

60. Dai, S.; Wei, D.; Wu, Z.; Zhou, X.; Wei, X.; Huang, H.; Li, G., Phase I clinical trial of autologous ascites-derived exosomes combined with GM-CSF for colorectal cancer. *Mol Ther* **2008,** *16* (4), 782-790.

61. Jo, W.; Jeong, D.; Kim, J.; Park, J., Self-Renewal of Bone Marrow Stem Cells by Nanovesicles Engineered from Embryonic Stem Cells. *Adv Healthc Mater* **2016,** *5* (24), 3148-3156.

62. Kolosnjaj-Tabi, J.; Lartigue, L.; Javed, Y.; Luciani, N.; Pellegrino, T.; Wilhelm, C.; Alloyeau, D.; Gazeau, F., Biotransformations of magnetic nanoparticles in the body. *Nano Today* **2016,** *11* (3), 280-284.

63. Khan, M. I.; Mohammad, A.; Patil, G.; Naqvi, S. A. H.; Chauhan, L. K. S.; Ahmad, I., Induction of ROS, mitochondrial damage and autophagy in lung epithelial cancer cells by iron oxide nanoparticles. *Biomaterials* **2012,** *33* (5), 1477-1488.

64. Lo, Y. Y. C.; Wong, J. M. S.; Cruz, T. F., Reactive oxygen species mediate cytokine activation of c-jun NH2-terminal kinases. *J Biol Chem*

1996, *271* (26), 15703-15707.

65. Li, L.; Feng, Z. W.; Porter, A. G., JNK-dependent phosphorylation of c-Jun on serine 63 mediates nitric oxide-induced apoptosis of neuroblastoma cells. *J Biol Chem* **2004,** *279* (6), 4058-4065.

66. Bonello, S.; Zahringer, C.; BelAiba, R. S.; Djordjevic, T.; Hess, J.; Michiels, C.; Kietzmann, T.; Gorlach, A., Reactive oxygen species activate the HIF-1 alpha promoter via a functional NF kappa B site. *Arterioscl Throm Vas* **2007,** *27* (4), 755-761.

67. Li, K.; Chi, Y.; Gao, K.; Yan, Q. J.; Matsue, H.; Takeda, M.; Kitamura, M.; Yao, J., Connexin43 Hemichannel-Mediated Regulation of Connexin43. *Plos One* **2013,** *8* (2).

68. Krock, B. L.; Skuli, N.; Simon, M. C., Hypoxia-induced angiogenesis: good and evil. *Genes Cancer* **2011,** *2* (12), 1117-33.

69. Minet, E.; Mottet, D.; Michel, G.; Roland, I.; Raes, M.; Remacle, J.; Michiels, C., Hypoxia-induced activation of HIF-1, role of HIF-1 alpha-Hsp90 interaction. *Febs Letters* **1999,** *460* (2), 251-256.

70. Kostura, L.; Kraitchman, D. L.; Mackay, A. M.; Pittenger, M. F.; Bulte, J. W. M., Feridex labeling of mesenchymal stem cells inhibits chondrogenesis but not adipogenesis or osteogenesis. *Nmr Biomed* **2004,** *17* (7), 513-517.

71. Singh, N.; Jenkins, G. J.; Asadi, R.; Doak, S. H., Potential

toxicity of superparamagnetic iron oxide nanoparticles (SPION). *Nano Rev* **2010,** *1*.

72. Turk, M. J.; Reddy, J. A.; Chmielewski, J. A.; Low, P. S., Characterization of a novel pH-sensitive peptide that enhances drug release from folate-targeted liposomes at endosomal pHs. *Bba-Biomembranes* **2002,** *1559* (1), 56-68.

73. Kordelas, L.; Rebmann, V.; Ludwig, A. K.; Radtke, S.; Ruesing, J.; Doeppner, T. R.; Epple, M.; Horn, P. A.; Beelen, D. W.; Giebel, B., MSC-derived exosomes: a novel tool to treat therapy-refractory graft-versus-host disease. *Leukemia* **2014,** *28* (4), 970-973.

74. Han, J.; Kim, B.; Shin, J. Y.; Ryu, S.; Noh, M.; Woo, J.; Park, J. S.; Lee, Y.; Lee, N.; Hyeon, T.; Choi, D.; Kim, B. S., Iron Oxide Nanoparticle-Mediated Development of Cellular Gap Junction Crosstalk to Improve Mesenchymal Stem Cells' Therapeutic Efficacy for Myocardial Infarction. *Acs Nano* **2015,** *9* (3), 2805-2819.

75. Zeevi-Levin, N.; Barac, Y. D.; Reisner, Y.; Reiter, I.; Yaniv, G.; Meiry, G.; Abassi, Z.; Kostin, S.; Schaper, J.; Rosen, M. R.; Resnick, N.; Binah, O., Gap junctional remodeling by hypoxia in cultured neonatal rat ventricular myocytes. *Cardiovasc Res* **2005,** *66* (1), 64-73.

76. Severs, N. J.; Bruce, A. F.; Dupont, E.; Rothery, S., Remodelling of gap junctions and connexin expression in diseased myocardium. *Cardiovasc Res* **2008,** *80* (1), 9-19.

77. Eguchi, R.; Naitou, H.; Kunimasa, K.; Ayuzawa, R.; Fujimori, Y.; Ohashi, N.; Kaji, K.; Ohta, T., Proteomic analysis of hypoxia-induced tube breakdown of an in vitro capillary model composed of HUVECs: Potential role of p38-regulated reduction of HSP27. *Proteomics* **2008,** *8* (14), 2897-2906.

78. Busato, A.; Bonafede, R.; Bontempi, P.; Scambi, I.; Schiaffino, L.; Benati, D.; Malatesta, M.; Sbarbati, A.; Marzola, P.; Mariotti, R., Magnetic resonance imaging of ultrasmall superparamagnetic iron oxide-labeled exosomes from stem cells: a new method to obtain labeled exosomes. *Int J Nanomed* **2016,** *11*, 2481-2490.

79. Han, J.; Kim, Y. S.; Lim, M. Y.; Kim, H. Y.; Kong, S.; Kang, M.; Choo, Y. W.; Jun, J. H.; Ryu, S.; Jeong, H. Y.; Park, J.; Jeong, G. J.; Lee, J. C.; Eom, G. H.; Ahn, Y.; Kim, B. S., Dual Roles of Graphene Oxide To Attenuate Inflammation and Elicit Timely Polarization of Macrophage Phenotypes for Cardiac Repair. *Acs Nano* **2018,** *12* (2), 1959-1977.

80. McDonald, J. W.; Sadowsky, C., Spinal-cord injury. *Lancet* **2002,** *359* (9304), 417-425.

81. de Almeida, F. M.; Marques, S. A.; Ramalho, B. D.; Massoto, T. B.; Martinez, A. M. B., Chronic spinal cord lesions respond positively to tranplants of mesenchymal stem cells. *Restor Neurol Neuros* **2015,** *33* (1), 43-55.

82. Sasaki, M.; Radtke, C.; Tan, A. M.; Zhao, P.; Hamada, H.; Houkin, K.; Honmou, O.; Kocsis, J. D., BDNF-Hypersecreting Human Mesenchymal Stem Cells Promote Functional Recovery, Axonal Sprouting, and Protection of Corticospinal Neurons after Spinal Cord Injury. *J Neurosci* **2009,** *29* (47), 14932-14941.

83. Spejo, A. B.; Carvalho, J. L.; Goes, A. M.; Oliveira, A. L. R., Neuroprotective Effects of Mesenchymal Stem Cells on Spinal Motoneurons Following Ventral Root Axotomy: Synapse Stability and Axonal Regeneration. *Neuroscience* **2013,** *250*, 715-732.

84. Nakajima, H.; Uchida, K.; Guerrero, A. R.; Watanabe, S.; Sugita, D.; Takeura, N.; Yoshida, A.; Long, G.; Wright, K. T.; Johnson, W. E. B.; Baba, H., Transplantation of Mesenchymal Stem Cells Promotes an Alternative Pathway of Macrophage Activation and Functional Recovery after Spinal Cord Injury. *J Neurotraum* **2012,** *29* (8), 1614-1625.

85. Quertainmont, R.; Cantinieaux, D.; Botman, O.; Sid, S.; Schoenen, J.; Franzen, R., Mesenchymal Stem Cell Graft Improves Recovery after Spinal Cord Injury in Adult Rats through Neurotrophic and Pro-Angiogenic Actions. *Plos One* **2012,** *7* (6).

86. Bhang, S. H.; Lee, Y. E.; Cho, S. W.; Shim, J. W.; Lee, S. H.; Choi, C. Y.; Chang, J. W.; Kim, B. S., Basic fibroblast growth factor promotes bone marrow stromal cell transplantation-mediated neural regeneration in traumatic brain injury. *Biochem Bioph Res Co* **2007,** *359* (1),

40-45.

87. Mun, C. H.; Kang, M. I.; Shin, Y. D.; Kim, Y.; Park, Y. B., The Expression of Immunomodulation-Related Cytokines and Genes of Adipose- and Bone Marrow-Derived Human Mesenchymal Stromal Cells from Early to Late Passages. *Tissue Eng Regen Med* **2018,** *15* (6), 771-779.

88. Kim, J. W.; Ha, K. Y.; Molon, J. N.; Kim, Y. H., Bone Marrow-Derived Mesenchymal Stem Cell Transplantation for Chronic Spinal Cord Injury in Rats Comparative Study Between Intralesional and Intravenous Transplantation. *Spine* **2013,** *38* (17), E1065-E1074.

89. Boido, M.; Garbossa, D.; Fontanella, M.; Ducati, A.; Vercelli, A., Mesenchymal Stem Cell Transplantation Reduces Glial Cyst and Improves Functional Outcome After Spinal Cord Compression. *World Neurosurg* **2014,** *81* (1), 183-190.

90. Casiraghi, F.; Remuzzi, G.; Abbate, M.; Perico, N., Multipotent Mesenchymal Stromal Cell Therapy and Risk of Malignancies. *Stem Cell Rev Rep* **2013,** *9* (1), 65-79.

91. Chudickova, M.; Vackova, I.; Urdzikova, L. M.; Jancova, P.; Kekulova, K.; Rehorova, M.; Turnovcova, K.; Jendelova, P.; Kubinova, S., The Effect of Wharton Jelly-Derived Mesenchymal Stromal Cells and Their Conditioned Media in the Treatment of a Rat Spinal Cord Injury. *Int J Mol Sci* **2019,** *20* (18).

92. Yao, Y.; Huang, J.; Geng, Y. J.; Qian, H. Y.; Wang, F.; Liu,

X. H.; Shang, M. S.; Nie, S. P.; Liu, N. A.; Du, X.; Dong, J. Z.; Ma, C. S., Paracrine Action of Mesenchymal Stem Cells Revealed by Single Cell Gene Profiling in Infarcted Murine Hearts. *Plos One* **2015,** *10* (6).

93. Vizoso, F. J.; Eiro, N.; Cid, S.; Schneider, J.; Perez-Fernandez, R., Mesenchymal Stem Cell Secretome: Toward Cell-Free Therapeutic Strategies in Regenerative Medicine. *Int J Mol Sci* **2017,** *18* (9).

94. Lim, W.; Kim, H. S., Exosomes as Therapeutic Vehicles for Cancer. *Tissue Eng Regen Med* **2019,** *16* (3), 213-223.

95. Sun, G. D.; Li, G. Q.; Li, D. H.; Huang, W. J.; Zhang, R. W.; Zhang, H.; Duan, Y. Y.; Wang, B. C., hucMSC derived exosomes promote functional recovery in spinal cord injury mice via attenuating inflammation. *Mat Sci Eng C-Mater* **2018,** *89*, 194-204.

96. Teng, X. M.; Chen, L.; Chen, W. Q.; Yang, J. J.; Yang, Z. Y.; Shen, Z. Y., Mesenchymal Stem Cell-Derived Exosomes Improve the Microenvironment of Infarcted Myocardium Contributing to Angiogenesis and Anti-Inflammation. *Cell Physiol Biochem* **2015,** *37* (6), 2415-2424.

97. Zhang, K. Y.; Zhao, X. N.; Chen, X. N.; Wei, Y. Z.; Du, W.; Wang, Y. B.; Liu, L. A.; Zhao, W. A.; Han, Z. B.; Kong, D. L.; Zhao, Q.; Guo, Z. K.; Han, Z. C.; Liu, N.; Ma, F. X.; Li, Z. J., Enhanced Therapeutic Effects of Mesenchymal Stem Cell-Derived Exosomes with an Injectable Hydrogel for Hindlimb Ischemia Treatment. *Acs Appl Mater Inter* **2018,** *10* (36), 30081-30091.

98. Xin, H. Q.; Li, Y.; Cui, Y. S.; Yang, J. J.; Zhang, Z. G.; Chopp, M., Systemic administration of exosomes released from mesenchymal stromal cells promote functional recovery and neurovascular plasticity after stroke in rats. *J Cerebr Blood F Met* **2013,** *33* (11), 1711-1715.

99. Ziegler, M.; Haigh, K.; Nguyen, T.; Wang, X. W.; Lim, B.; Yap, M. L.; Eddy, E. M.; Haigh, J. J.; Peter, K., The pulmonary microvasculature entraps induced vascular progenitor cells (iVPCs) systemically delivered after cardiac ischemia-reperfusion injury: Indication for preservation of heart function via paracrine effects beyond engraftment. *Microcirculation* **2019,** *26* (2).

100. Alon, R.; Feigelson, S., From rolling to arrest on blood vessels: leukocyte tap dancing on endothelial integrin ligands and chemokines at sub-second contacts. *Semin Immunol* **2002,** *14* (2), 93-104.

101. Zhang, Q. Z.; Dehaini, D.; Zhang, Y.; Zhou, J. L.; Chen, X. Y.; Zhang, L. F.; Fang, R. H.; Gao, W. W.; Zhang, L. F., Neutrophil membrane-coated nanoparticles inhibit synovial inflammation and alleviate joint damage in inflammatory arthritis. *Nat Nanotechnol* **2018,** *13* (12), 1182-+.

102. Thamphiwatana, S.; Angsantikul, P.; Escajadillo, T.; Zhang, Q. Z.; Olson, J.; Luk, B. T.; Zhang, S.; Fang, R. H.; Gao, W. W.; Nizet, V.; Zhang, L. F., Macrophage-like nanoparticles concurrently

absorbing endotoxins and proinflammatory cytokines for sepsis management. *P Natl Acad Sci USA* **2017,** *114* (43), 11488-11493.

103. Assina, R.; Sankar, T.; Theodore, N.; Javedan, S. P.; Gibson, A. R.; Horn, K. M.; Berens, M.; Sonntag, V. K. H.; Preul, M. C., Activated autologous macrophage implantation in a large-animal model of spinal cord injury. *Neurosurg Focus* **2008,** *25* (5).

104. Knoller, N.; Auerbach, G.; Fulga, V.; Zelig, G.; Attias, J.; Bakimer, R.; Marder, J. B.; Yoles, E.; Belkin, M.; Schwartz, M.; Hadani, M., Clinical experience using incubated autologous macrophages as a treatment for complete spinal cord injury: Phase I study results. *J Neurosurg-Spine* **2005,** *3* (3), 173-181.

105. Beekhuizen, H.; Vanfurth, R., Monocyte Adherence to Human Vascular Endothelium. *J Leukocyte Biol* **1993,** *54* (4), 363-378.

106. Choo, Y. W.; Kang, M.; Kim, H. Y.; Han, J.; Kang, S.; Lee, J. R.; Jeong, G. J.; Kwon, S. P.; Song, S. Y.; Go, S.; Jung, M.; Hong, J.; Kim, B. S., M1 Macrophage-Derived Nanovesicles Potentiate the Anticancer Efficacy of Immune Checkpoint Inhibitors. *Acs Nano* **2018,** *12* (9), 8977-8993.

107. Kim, H. Y.; Kumar, H.; Jo, M. J.; Kim, J.; Yoon, J. K.; Lee, J. R.; Kang, M.; Choo, Y. W.; Song, S. Y.; Kwon, S. P.; Hyeon, T.; Han, I. B.; Kim, B. S., Therapeutic Efficacy-Potentiated and Diseased Organ-Targeting Nanovesicles Derived from Mesenchymal Stem Cells for

Spinal Cord Injury Treatment. *Nano Lett* **2018,** *18* (8), 4965-4975.

108. Li, S. Y.; Qi, Y.; Hu, S. H.; Piao, F. Y.; Guan, H.; Wang, Z. M.; Chen, R. L.; Liu, S., Mesenchymal stem cells-conditioned medium protects PC12 cells against 2,5-hexanedione-induced apoptosis via inhibiting mitochondria-dependent caspase 3 pathway. *Toxicol Ind Health* **2017,** *33* (2), 107-118.

109. Shen, C. Y.; Lie, P. C.; Miao, T. Y.; Yu, M. X.; Lu, Q.; Feng, T.; Li, J. R.; Zu, T. T.; Liu, X. H.; Li, H., Conditioned medium from umbilical cord mesenchymal stem cells induces migration and angiogenesis. *Mol Med Rep* **2015,** *12* (1), 20-30.

110. Xu, X. S.; Chua, C. C.; Gao, F. P.; Chua, K. W.; Wang, H.; Hamdy, R. C.; Chua, B. H. L., Neuroprotective effect of humanin on cerebral ischemia/reperfusion injury is mediated by a PI3K/Akt pathway. *Brain Res* **2008,** *1227*, 12-18.

111. Yuan, Y. M.; He, C., The glial scar in spinal cord injury and repair. *Neurosci Bull* **2013,** *29* (4), 421-435.

112. Cua, R. C.; Lau, L. W.; Keough, M. B.; Midha, R.; Apte, S. S.; Yong, V. W., Overcoming neurite-inhibitory chondroitin sulfate proteoglycans in the astrocyte matrix. *Glia* **2013,** *61* (6), 972-984.

113. Kroner, A.; Greenhalgh, A. D.; Zarruk, J. G.; dos Santos, R. P.; Gaestel, M.; David, S., TNF and Increased Intracellular Iron Alter Macrophage Polarization to a Detrimental M1 Phenotype in the Injured

Spinal Cord. *Neuron* **2014,** *83* (5), 1098-1116.

114. Wang, X.; Cao, K.; Sun, X.; Chen, Y. X.; Duan, Z. X.; Sun, L.; Guo, L.; Bai, P.; Sun, D. M.; Fan, J. Q.; He, X. J.; Young, W.; Ren, Y., Macrophages in Spinal Cord Injury: Phenotypic and Functional Change From Exposure to Myelin Debris. *Glia* **2015,** *63* (4), 635-651.

115. Shin, T.; Ahn, M.; Moon, C.; Kim, S.; Sim, K. B., Alternatively Activated Macrophages in Spinal Cord Injury and Remission: Another Mechanism for Repair? *Mol Neurobiol* **2013,** *47* (3), 1011-1019.

116. Colonna, M.; Butovsky, O., Microglia Function in the Central Nervous System During Health and Neurodegeneration. *Annu Rev Immunol* **2017,** *35*, 441-468.

117. David, S.; Greenhalgh, A. D.; Kroner, A., Macrophage and Microglial Plasticity in the Injured Spinal Cord. *Neuroscience* **2015,** *307*, 311-318.

118. Bethea, J. R.; Castro, M.; Keane, R. W.; Lee, T. T.; Dietrich, W. D.; Yezierski, R. P., Traumatic spinal cord injury induces nuclear factor-kappa B activation. *J Neurosci* **1998,** *18* (9), 3251-3260.

요약 (국문초록)

중간엽 줄기세포 이식의 안전 관련 쟁점과 낮은 이식 생존율로 인해, 중간엽 줄기세포 유래 엑소좀은 심근경색과 척수 손상을 포함한 다양한 질병의 대체 치료제로서 각광받고 있다. 중간엽 줄기세포 유래 엑소좀이 중간엽 줄기세포 치료에 비해 갖는 장점에도 불구하고, 낮은 생산성과 낮은 표적 효능으로 인해 임상 적용에 여러 가지의 제한이 있는 상황이다. 이러한 점들을 극복하기 위해, 엑소좀-모방 나노베지클이 기존 엑소좀의 대체제로서 연구되고 있다. 그러나, 나노베지클 또한 개질 없이 표적 장기에 충분한 양이 축적되지 못한다. 본 연구에서는, 가공을 통해 치료 효능과 표적 물질이 향상된 중간엽 줄기세포로부터 얻은, 치료 효능이 증가된 나노베지클을 개발하였다.

먼저, 우리는 철나노입자가 함유된 중간엽 줄기세포 유래 나노베지클(철나노입자-나노베지클)을 개발하였다. 철나노입자-나노베지클은 경색이 온 심장에서의 잔류량은 자성 유도로 인해 극적으로 증가하였다. 게다가, 철나노입자는 철나노입자를 함유한 중간엽 줄기세포와 철나노입자-나노베지클의 치료성 RNA와 단백질을 증가시켰고, 이는 엑소좀의 낮은 생산성에 대한 우려를 감소시켰다. 철나노입자-나노베지클의 심장으로의 주사와 자성 유도는 염증 단계에서 치료 단계로의 이

른 전환과 세포 사멸 및 섬유화 감소, 그리고 혈관 생성과 심기능 회복 효과를 향상시켰다. 이 접근법은 중간엽 줄기세포 유래 나노베지클 치료법의 치료 효능을 높이고, 심근 경색에 대한 임상적용의 길을 열어줄 것이다.

두 번째로, 우리는 대식 세포 세포막이 융합된 중간엽 줄기세포(대식세포막 융합-중간엽 줄기세포)로부터 대식 세포 세포막이 융합된 엑소좀-모방 나노베지클(대식세포막 융합-나노베지클)을 개발하였고, 이의 치료 효능을 쥐의 척수손상 모델에서 확인하였다. 대식세포막 융합-나노베지클은 일반 중간엽 줄기세포 유래 나노베지클에 비해 허혈성 부위 표적 효능물질을 많이 포함하였다. 대식세포막으로부터 유래된 대식세포막 융합-나노베지클에 포함된 표적 효능물질은 대식세포막 융합-나노베지클을 전신 주사하였을 때 척수로의 축적을 증가시켰다. 대식세포막 융합-나노베지클의 증가된 축적은 세포 사멸과 염증을 감소시켰고, 축삭 손실을 예방, 혈관 형성을 촉진, 섬유화를 감소하였고, 이어서 척수 기능 향상시켰다. 이 결과들은 대식세포막 융합-나노베지클의 임상적용 가능성을 제시한다.

종합하여, 우리는 철나노입자-중간엽줄기세포와 대식세포막 융합-중간엽줄기세포로부터 얻은 나노베지클에서 경색이 온 심장과 다친 척수로의 축적을 증가시켜주는 치료 효능물질 또는 표적 효능물질이

증가한 것을 보여주었다. 개질된 중간엽 줄기세포로부터 유래된 나노베지클의 치료 효능을 높이는 우리의 새로운 접근법은 기존의 중간여 ㅂ 줄기세포 또는 중간엽 줄기세포 유래 엑소좀 치료법의 좋은 대안이 될 것이다. 우리의 기술은 허혈성/염증성 질환에 대한 치료법으로 미래에 임상적용이 가능할 것이다.

주요어: 엑소좀-모방 나노베지클, 철나노입자, 대식세포, 중간엽 줄기세포, 심근경색, 척수 손상

학번: 2014-21524